Artificial Elbow Joint Classification Using Upper Arm Based on Surface-EMG Signal

Jicheng Wang

A Thesis Submitted in Partial Fulfillment of the Requirements for the Degree of Master of Engineering in Electrical Engineering

Prince of Songkla University

2018

Thesis Title	Artificial Elbow Joint Classification Using Upper Arm Based on Surface-EMG Signal
Author	Mr. Jicheng Wang
Major Program	Electrical Engineering

Major Advisor

……

(Dr. Warit Wichakool)

Examining Committee:

……..…Chairperson

(Assoc. Prof. Dr. Pornchai Phukpattaranont)

……..…Committee

(Dr. Rakkrit Duangsoithong)

……..Committee

(Assistant. Prof. Dr. Suparerk Janjarasjitt)

……..Committee

(Dr. Warit Wichakool)

The Graduate School, Prince of Songkla University, has approved this thesis as partial fulfillment of the requirements for the Master of Engineering Degree in Electrical Engineering.

……...

(Prof. Dr. Damrongsak Faroongsarng)

Dean of Graduate School

This is to certify that the work here submitted is the result of the candidate's own investigations. Due acknowledgement has been made of any assistance received.

…...……...……Signature

(Dr. Warit Wichakool)

Major Advisor

……Signature

(Mr. Jicheng Wang)

Candidate

I hereby certify that this work has not been accepted in substance for any degree, and is not being currently submitted in candidature for any degree.

……Signature

(Mr. Jicheng Wang)

Candidate

Thesis Title Artificial Elbow Joint Classification Using Upper Arm Based on Surface-EMG Signal

Author Mr. Jicheng Wang

Major Program Electrical Engineering

Academic Year 2017

ABSTRACT

This thesis proposes a method of elbow joint motions recognition using surface electromyography (sEMG) signal for disable people with below-elbow amputation. It solves the situation that forearm without muscle cannot control forearm pronation. The complete system could be categorised into 4 components: (1) signal measurement, (2) pre-processing, (3) classification and (4) control system. First, the signal measurement includes sEMG data collection and the relationship of motions and muscles. Second, the pre-processing component denoises the sEMG signals by soft threshold method. It reduces not only the electrical noise but also the white Gaussian noise. Third, the classification system recognizes elbow joint motions. Five characteristic features, Mean Absolute Value (MAV), Root Mean Square (RMS), Slope Change (SC), Signal Length (SL) and Zero Crossing (ZC), are extracted from denoised sEMG signals of each channel. The 5 features are used in back propagation neural network (BPNN) for the classifier of 3 channels, which outputs the 99.54% of the elbow joint motions accuracy from 8 healthy subjects. Furthermore, the results of classifier are tested on a subject-by-subject basis. It means that the classification system is a user-

dependent system. It can detect the motions of healthy subject based on his or her own sEMG signals. At the end, the control system is designed in MATLAB and it demonstrates that the recognition results from the classifier is sent to the controller correctly. Moreover, the system is tested when the subjects lifts the weight of 1.5 kg and the accuracy is 96.64% that does not change significantly.

ACKNOWLEDGEMENTS

Firstly, I am very grateful for my parents who gave me support and encouragement all the time when I came across problems and difficulty. Secondly, I would like to thank the Faculty of Engineering, Prince of Songkla University Hatyai campus, Thailand, which gave me so precious an opportunity to learn and study here. I made friends and knew many wise people at this beautiful place. Thirdly, I really would like to thank my supervisor Dr. Warit Wichakool who instructed me and gave me suggestions on my thesis. Then, I would like to thank the staffs of the faculty who always helped me make the document and visa that truly means a lot to me. And then, I would like to express my gratitude towards my friend both in Thailand and China who worked as my experiment subjects. I also appreciate the committee of the research proposal and thesis defense, Assoc. Prof. Dr. Pornchai Phukpattaranont, Dr. Rakkrit Duangsoithong and Assistant. Prof. Dr. Suparerk Janjarasjitt, for giving useful comments and suggestions which without doubt improve my thesis. All in all, thank all the people who helped me when I was in trouble, always supported me and let me not give up. Thank you all!

Jicheng Wang

CONTENTS

CHAPTER 1

Introduction

1.1 Background

According to the World Health Organization, reports show that the population of disable people is over 1 billion in the world, about 15% of the world's population. It increases from the war, population ageing, car accident, occupational injury and a lot of accidents. However, the disable people have less access to health care services [1]. Among disable people, the amount of American people with a major upper-limb loss is approximately 100,000 [2]-[4]. Making the disable people recover their orthobiosis is very beneficial.

Normally, disable people cannot do daily work using forearm if they had a surgery of below-elbow amputation. The problem makes a tough life to disable people. For example, they cannot do sports again and even cannot eat food by themselves. On the other hand, existing artificial prostheses may not solve the problem well. Some prostheses with mechanical component only can provide fixed motion for disable people. In addition, the system needs a long training time and costs relatively high. Therefore, improvements can be done to make artificial prosthesis more friendly and affordable to users.

Nowadays the artificial prosthesis is easy to find. There are many ways to control artificial prostheses. Electroencephalography (EEG), electromyography

(EMG), and electrooculography (EOG) are body signals used for the artificial prosthesis control. Different body signals have both advantages and disadvantages. The EEG signal can predict before limb motion, but require subject-specific training and exhibit decreasing performance as the number of possible targets increase [5]. The EOG can predicts motion before motion starts, but it has low accuracy [5]. The EMG gives high accuracy, but only once the motion has begun [5].

There are other methods for controlling artificial arm, such as sensor technology, camera and video camera. The sensor technology cannot serve for disable people because it becomes difficult for disable people to obtain complex motions with this technology [6]. The camera and video camera technology need professional operation with high cost [6]. Nevertheless, EMG is easier than other methods for disable people.

The EMG is used to evaluate the muscles state and record the electrical signals for the medicine. [7]. In upper-limb prosthetics research, number of research publications have obviously increased in the last ten years. An online search shows that until 2010, the hand prosthesis has about 4000 publications, which are most published on 2001-2010 [8].

Furthermore, the EMG technology is very mature and stable. Cram and Steger provide a device to scan the muscles for EMG in the early 1980s [9]. There are two kinds in EMG: surface-EMG (sEMG) and intramuscular EMG (iEMG). However,

the EMG is limited in the medicine by some US states such as New Jersey and Michigan. [10]-[12]. The sEMG technology is cheaper and safer than iEMG [13], [14]. Since using the iEMG sometimes causes the disable people to have an infection from the electrode of fine wires inserted into muscle. Hence, the sEMG is suitable to use in this thesis.

1.2 Problem statement

Nowadays, many researches are applied to control artificial arm. Some of these researches, however, are not adequate to help disable people who have a surgery of below-elbow amputation. Actually, few researches serve for disable people of below-elbow amputation, because the forearm without muscles cannot activate forearm pronation. In this condition, artificial prostheses that disable people can buy are generally made of the mechanical structure, which are not convenient for the disable people to use in daily life [15]. Hence this thesis uses sEMG to control artificial prostheses. It means that the method of sEMG of the upper arm controlling forearm motions is improved and the feasible motion cases are put forward in this thesis.

This thesis proposes a method of pattern recognition of elbow joint motions using sEMG signal for an artificial arm. The sEMG is a non-invasive, painless means, which helps disable people of below-elbow amputation. The method uses elbow joint of extension motion with high-intensity force to activate artificial arm of forearm pronation in this research. The disable people experience a short delay time before pronation is activated from elbow joint of extension with high-intensity force.

However, this thesis cannot be used to help disable people whose osteotomy sites for metaphyseal and diaphyseal has abnormal muscle of contractility on upper arm [16]. After surgery, disable people whose osteotomy sites for

supracondylar above-elbow amputation or below-elbow amputation needs the rehabilitation training from rehabilitation hospital [17].

CHAPTER 2

Literature review

2.1 The reviews of upper limb prosthesis research

Nowadays, there are many researches about sEMG. Some researches about powered upper limb prosthesis are reviewed, which usually show a part of proportional myoelectrical control [18]-[24]. In addition, the chronological researches on proportional myoelectrical control are shown in Table 2.1 which is in a chronological order to demonstrate how many researches of powered upper limb prosthesis [25]. Moreover, a chronological representation of papers is applied into myoelectrical proportional control for upper limb prostheses [25].

Table 2.1: The chronological researches on proportional myoelectrical control [25]

Years	Research
2017	4
2011-2016	32
2000-2010	9
1990-2000	7
1980-1990	9
1970-1980	7
1960-1970	10

In the development of prosthesis, the multifunction hands is a new control models like targeted muscle reinnervation [26] and implanted electrodes [27]-[30] increase the demand for control systems of prosthesis. It is beneficial for research

and discussion to use common expressions, which are easy to understand. In prosthesis or prosthetic EMG, it has many expressions. Table 2.2 explains the expressions in publications of EMG control models. In Table 2.2, we also give a lot of normally used expressions because some expressions are fuzzy in different areas.

Table 2.2: Common expression in EMG control models

Expression	Description	Examples
User intent	The user intends to exploit a set of motor functions, or to activate motion classes.	Move the leg to walk, move the hand to catch the target.
Intent interpretation	The classifier recognizes the motions to build a classification system.	The layer 4 and 5 of examples 1-3 in Fig. 2.1.
Hybrid prostheses	Prostheses combined with body-powered component and electrical component [31].	The prosthesis of body-powered leg.
Mechanical impedance control	The control system activated with impedance variables.	Impedance control [32].
System training	Training of the prosthesis control system to recognize input signals from the prosthesis user, which is often just referred to as training or supervision in the pattern recognition.	Prosthesis-guided training [33], [34].

To explain the relationship between different terms normally used in prosthesis control, the functionally partitioned model and relevant examples are shown in Fig. 2.1. It has eight layers with an improved version of the model supplied by Losier [35].

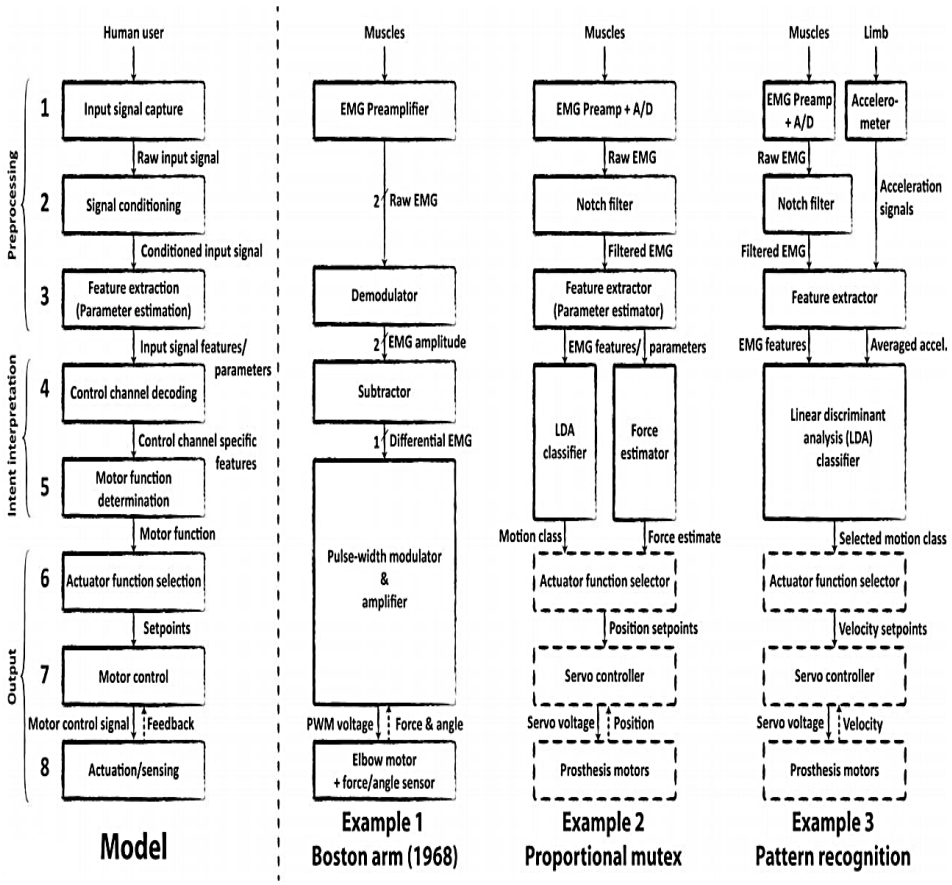

Fig. 2.1 The functionally partitioned model and relevant examples for the prosthesis control [35].

In the left area of Fig. 2.1, the functionally partitioned model has eight layers. The eight layers are [35]:

A. Pre-processing

(1) Input signal capture

(2) Signal conditioning

(3) Feature extraction

B. Intent recognition

(4) Control channel decoding

(5) Motor function determination

C. Output

(6) Actuator function selection

(7) Motor control

(8) Actuation/sensing

The layers show main functions of the control system in this model, but it is not physical software or hardware modules. To put it simply, layers 1-3 are classified into pre-processing; layers 4-5 are classified into intent recognition; layers 6-8 are classified into output.

Moreover, the thesis follows the functionally partitioned model to design the system. In this thesis, the pre-processing system has two systems: the denoised system and feature extraction system, intent recognition is a classification system, output is a control system.

2.2 Examples for the prosthesis control

In the right area of the Fig. 2.1, three examples for the prosthesis control are shown. At the first, the example 1 is a control system of Boston Arm in 1968 [36]. It is a rudiment of control system for the prosthesis arm. It gives the sample to the system development.

Then, the example 2 is a proportional mutex control system. The layers 1-5 correspond to research by Hudgins [37]. The layers 6-8 (dashed lines) are a feasible system in the prosthesis [25]. In addition, the training time in the control system is typically less than 5 minutes for the microcomputer implementation [37]. It used 100 datasets to test the neural network [37]. The control system design is shown in Fig. 2.2. In addition, it has 30 input layer nodes, 8 hidden layer nodes and 4 output layer nodes in the neural network classifier.

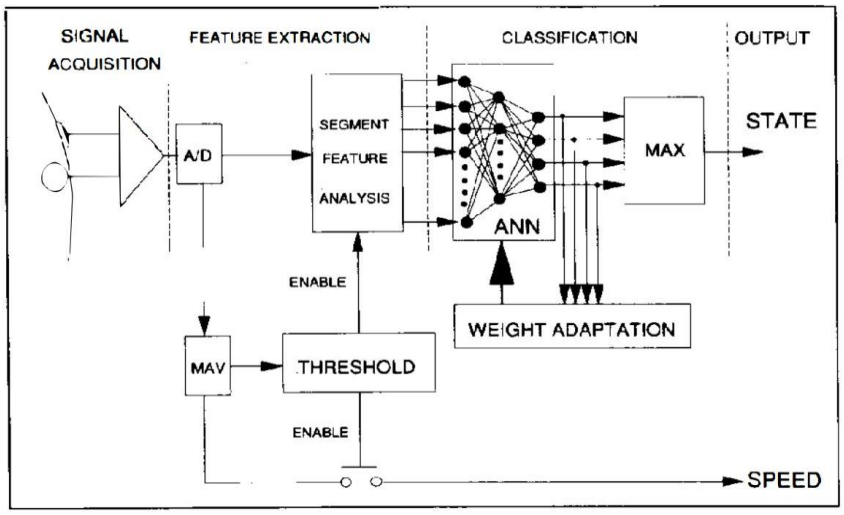

Fig. 2.2 Control system design [37]

At the end, the example 3 is a system of multi-model pattern recognition. The layers 1-5 are shown by Fougner [38]. The dashed lines represent a probable performance of layers 6-8. Moreover, this example improves the classification accuracy for arm motions by accelerometer. The motions are shown in the Fig. 2.3. C1 is wrist flexion. C2 is wrist extension. C3 is pronation. C4 is supination. C5 is open hand. C6 is power grip. C7 is pinch grip. C8 is hand at rest. P1 to P5 are the arm motions. For example, the P3 is straight arm raising up to 45° [38].

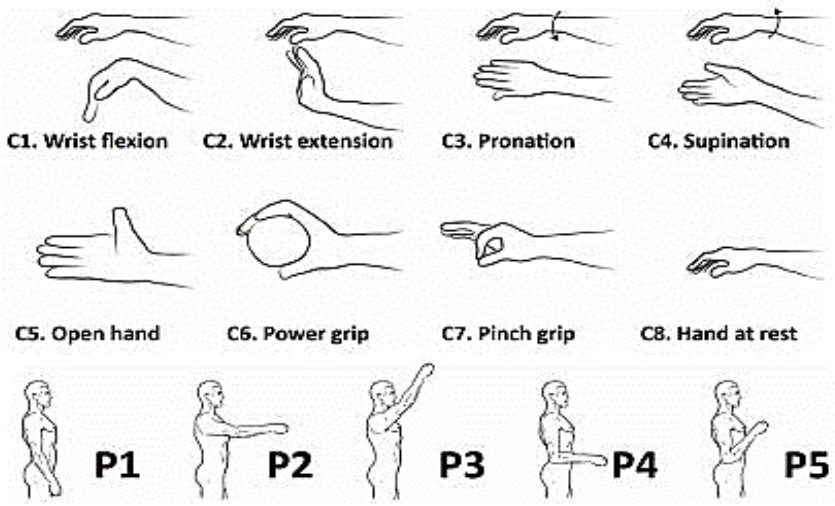

Fig. 2.3 Detected motions by Fougner [38]

The placement of electrodes and sensors are shown in Fig. 2.4. It has 8 channels of EMG on the forearm. The eight channels of EMG are differentially amplified. The system uses remote ac electrode-amplifiers and low pass filter at 500 Hz with a fifth-order Butterworth filter [38]. Six accelerometer channels and eight EMG channels were using a 16-bit analog-to-digital converter [38]. The sampling frequency is 1 kHz.

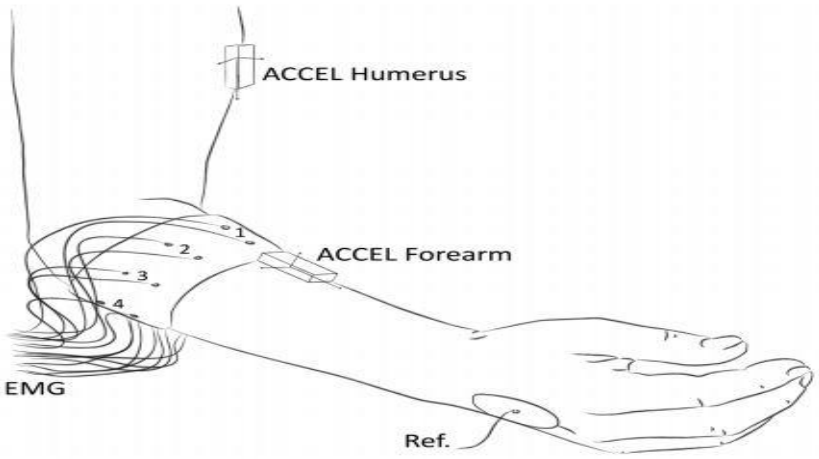

Fig. 2.4 The placement of electrodes and sensors [38]

After the structure of prosthesis control system discussion, the improvement model is produced. As following the improvement model, the Kevin Englehart's model researches about forearm motions [39]. The Kevin Englehart's model uses four channels to get myoelectrical signal (MES). The placements of electrodes are shown in Fig. 2.5. There are 4 channels of electrode on forearm. Kevin Englehart compares two channels and four channels. The result shows that the model of four channels is better than the model of two channels [39]. The four channels have lower error in Kevin Englehart's research.

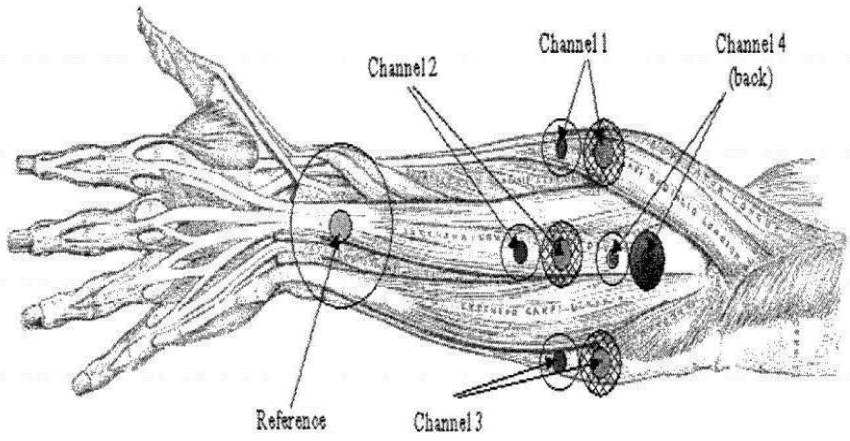

Fig. 2.5 The Kevin Englehart's placements of electrodes [39]

In Kevin Englehart's research, there are 6 classes of motion in the classifier as shown in Fig. 2.6. The 6 classes of motion: (1) hand close, (2) hand open, (3) wrist flexion, (4) wrist extension, (5) ulnar deviation of wrist, (6) radial deviation of wrist.

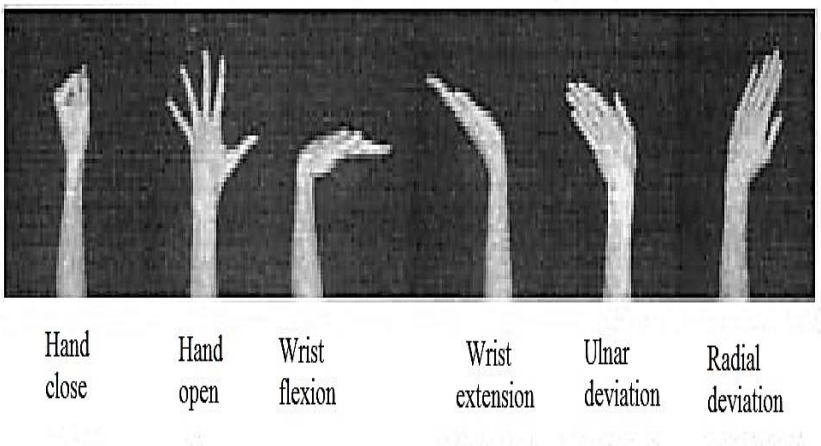

Fig. 2.6 The 6 classes of motion used in the four channels experiments [39]

The signal classification shown in Fig. 2.7 is a multistage process [39]. The first step is the measured signal (each channel of myoelectrical signal). Measured signal sends data to feature extraction. Feature extraction uses 4 algorithms. In this case, feature extraction makes a feature set by time domain feature set (TD), the short-time Fourier transform (STFT), the wavelet transform (WT) and the wavelet packet transform (WPT) coefficients [39]. The dimensionality reduction uses principal components analysis (PCA) for feature set and subject, making a reduced feature set from each channel. Then, the PCA makes a total feature set for six classes of motion.

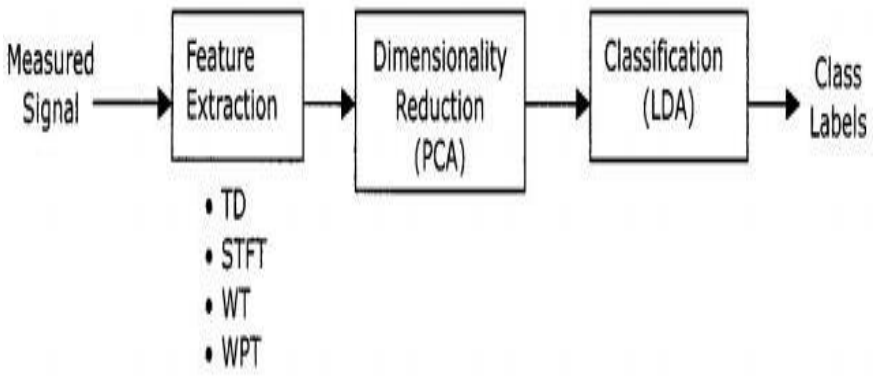

Fig. 2.7 Signal classification [39]

In addition, the 30 features are used in the classification (LDA classifier) [39]. The feature extraction shown in the Fig. 2.7 has 4 algorithms. The time domain feature set (TD) is a set of features for the signal in time domain. In Kevin Englehart's research, they use STFT to analyze localized features in the signal to be examined. The equation is shown in Eq. (2.1),

$$F(f,b) = \int_{-\infty}^{\infty} x(t)h(t-b)e^{-i(2\pi f)t}dt, \tag{2.1}$$

where $h(t-b)$ is the window function as the windowed Fourier transform.

In the wavelet transform, the signal x(t) use a range of dilation parameter a and location parameter b. The wavelet transform function of a continuous signal is shown in Eq. (2.2),

$$T(a,b) = \omega(a) \int_{-\infty}^{\infty} x(t)\Psi^*\left(\frac{t-b}{a}\right)dt, \tag{2.2}$$

where $\omega(a)$ is a weight function.

The last one is the wavelet packet transform (WPT) which is a generalization of the discrete wavelet transform. Wavelet packets involve particular linear combinations of wavelets and the wavelet packet decomposition of a signal is performed in a manner similar to the multiresolution algorithm given earlier for the discrete wavelet transform.

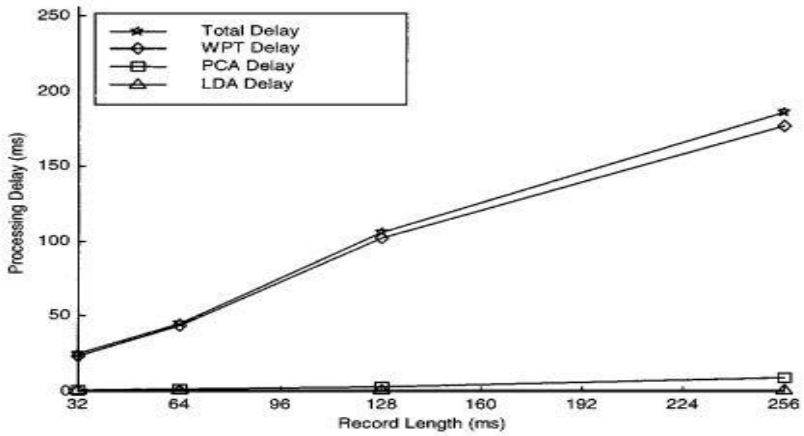

Fig. 2.8 The processing delays use different feature set at record length [39]

In the signal classification, the processing delay uses a 450-MHz Pentium III-based workstation and performed in Matlab [39]. There is a processing delay using different feature sets in Fig. 2.8. Farrell et al. found that human cannot feel a time delay of less than 100 ms [40] and others have advocated that human can accept a delay of up to 300 ms to 400 ms [41]-[43]. In the Fig. 2.8, it is acceptable that the total delay time is 200 ms when the record length is 256 ms [39].

2.3 Summary

Table 2.3: The summary

Literature review	Advantage	Disadvantage
The control system of Boston Arm (1968) [36]	A rudiment of control system for prosthesis arm in 1968s	Low accuracy, not useful for disable people with below-elbow amputation
A proportional mutex control system by Hudgins (1993) [37]	Good accuracy based on neural network	5 mins for training time, not useful for disable people with below-elbow amputation
Kevin Englehart of classifier (2001) [39]	Channel comparison, record length comparison	Not useful for disable people with below-elbow amputation
Losier' model (2009) [35]	A complete system for the prosthesis control	Not useful for disable people with below-elbow amputation
A multi-model pattern recognition method by Fougner (2011) [38]	Good accuracy	Required 8 channels, not useful for disable people with below-elbow amputation

In the Table 2.3, the control system of Boston Arm (1968) [36] creates a new idea for prosthesis arm. A proportional mutex control system of Hudgins (1993) [37] has good accuracy based on neural network. The classifier of Kevin Englehart (2001) [39] compares the numbers of channels and record lengths. Losier' model (2009) [35] builds a complete system for the prosthesis control. A multi-model pattern recognition method by Fougner (2011) [38] has good accuracy. But all of researches in the literature review cannot be directly applied for disable people with a below-elbow amputation. This thesis proposes a new method for artificial elbow joint motions based on sEMG signals of upper arm.

2.4 Objectives

2.4.1. Design a system to solve the problem that the forearm without muscle cannot activate the forearm pronation.

2.4.2. Design a classification system using sEMG signals on upper arm of muscles for artificial arm.

2.4.3. Design a classification system for the elbow joint motions

2.4.2.1. No movement

2.4.2.2. Elbow joint of flexion motion

2.4.2.3. Elbow joint of extension motion

2.4.2.4. Forearm pronation motion

2.4.2.5. Forearm supination motion

2.5 Scope

2.5.1. The thesis investigates of the relationship between muscle and motion.

2.5.2. The thesis designs a classification system for recognition of elbow joint motions.

2.5.3. The system is applied into disable people whose osteotomy sites for supracondylar above-elbow amputation or below-elbow amputation.

2.5.4. The system cannot be used to help disable people whose osteotomy sites for metaphyseal and diaphyseal has abnormal muscle of contractility on upper arm.

2.5.5. The real amputee is not tested in this thesis.

CHAPTER 3

Methodology

3.1 Kinesiology

The 5 detected motions shown in Fig. 3.1 are applied into this thesis: (1) elbow joint of flexion motion, (2) elbow joint of extension motion, (3) forearm pronation motion, (4) forearm supination motion and (5) no movement, which is not shown. In human anatomy, the forearm has two main bones: radius and ulna. In addition, the main bone on the upper arm is humerus shown in Fig. 3.2. The relationship between muscle and kinesiology is shown in Table 3.1.

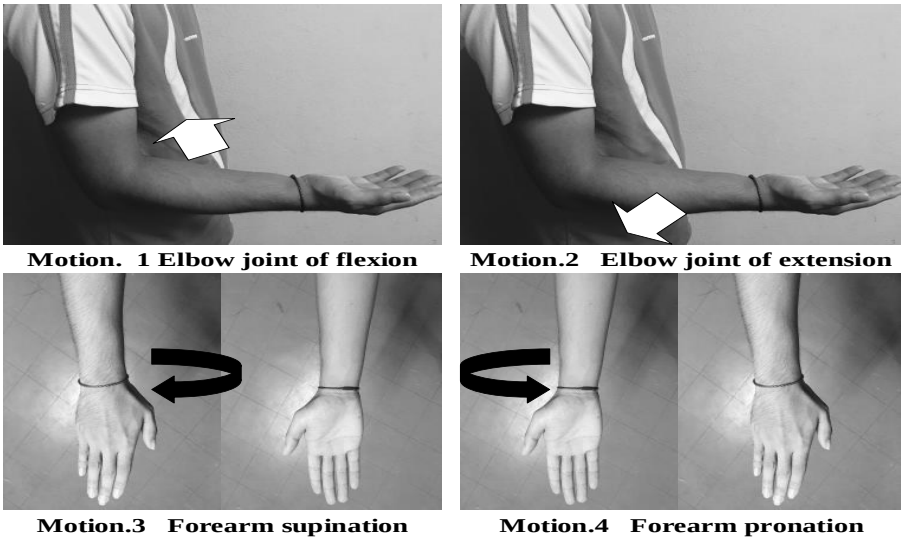

Fig. 3.1 Four targeted motions

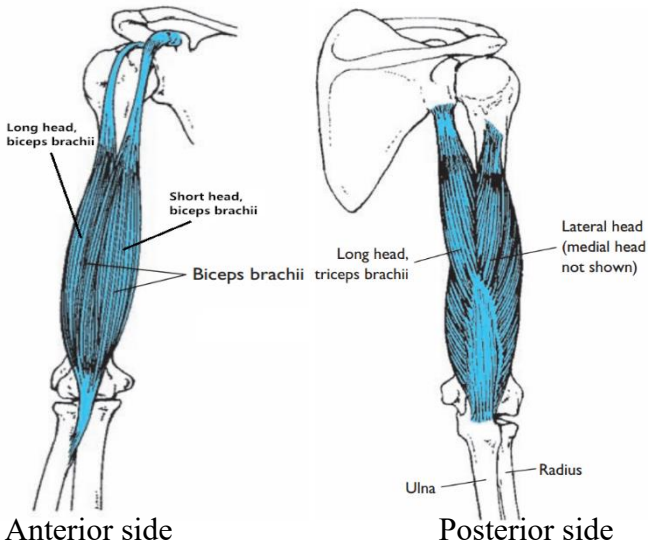

Fig. 3.2 The muscle placements [44]

Table 3.1: The muscle and kinesiology [44]

Muscle	Attachment	Primary action(s)
Biceps	Humerus	Flexion, assists with supination
(Long head)		Flexion, assists with supination
(Short head)		Flexion, assists with supination
Triceps	Humerus	Extension
(Long head)		Extension (sustained force)
(Lateral head)		Extension (occasional high-force)
(Medial head)	Deep muscle	Extension (low-force)
Brachioradialis	Humerus and radius	Flexion, pronation, supination
Brachialis	Humerus (deep muscle)	Flexion
Pronator teres	Radius	Pronation, assists with flexion
Pronator quadratus	Radius and ulna	Pronation
Anconeus	Humerus and ulna	Assists with extension
Supinator	Radius and ulna	Supination

In the Table 3.1, the elbow joint of flexion and extension are shown. The muscle contributes effectively to flexion when the forearm is supinated because it is slightly stretched [44]. The relationship between muscle and elbow joint of flexion and extension is shown in Fig. 3.3. First, the elbow joint of flexion is activated when the biceps of long head contracts. Sometimes, the triceps of long head also contracts to support the elbow joint of flexion when the biceps of long head is not strong enough. Next, the triceps of long head contracts to activate the elbow joint of extension. In addition, the biceps of long head is also contracted to support the elbow joint of extension.

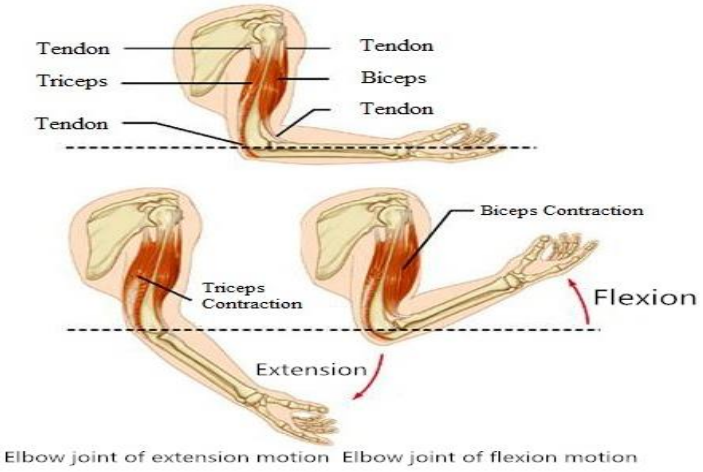

Fig. 3.3 The relationship between muscle and motion [44]

On the other hand, the forearm supination and pronation are activated based on the forearm muscles. The tension in the supinator lessens when the elbow is in the state of flexion, and the biceps assists with supination. The biceps is the primary muscle as a supinator when the elbow is flexed to 90° or less, so that the upper arm

without muscle activates forearm pronation. The contraction of triceps of lateral head can activate the elbow joint of extension motion with high-intensity force. When forearm pronation over 180° is done, the elbow joint of extension with high-intensity force is activated. The users feel a little delay to active forearm pronation. Hence, the triceps of lateral head are used to activate the forearm pronation motion in this thesis.

Therefore, this thesis proposes a new method to classify forearm pronation motion for disable people with below-elbow amputation. Forearm pronation motion is activated by lateral head of triceps using elbow joint of extension motion with high-intensity force to control artificial arm of forearm pronation motion for disable people with below-elbow amputation. In addition, the biceps of long head, the triceps of lateral head and the triceps of long head are used into this thesis for 5 detected motions.

Table 3.2: Primary actions of muscle

Primary Action	Muscle
Elbow joint of flexion	Biceps of long head and triceps of long head
Elbow joint of extension	Biceps of long head and triceps of long head
Forearm supination	Biceps of long head and triceps of lateral head
Forearm pronation	Biceps of long head and triceps of lateral head
No movement	Biceps and triceps

In summary, the forearm pronation motion is activated by all of muscles on radius and ulna. Hence, it is impossible for disable people with below-elbow amputation to use muscle of original function to activate forearm pronation motion. In addition, the five detected motions are based on different muscles. The primary actions of muscle are shown in Table 3.2. The elbow joint of flexion and extension are based on biceps of long head and triceps of long head. On the other hand, the detected muscles of forearm supination and pronation are biceps of long head and triceps of lateral head.

Furthermore, the forearm horizontal abduction and adduction motion are not considered in this thesis because the two motions base on the glenohumeral joint; however, the disable people with below-elbow amputation has full function of muscles on shoulder.

3.2 Experiment

The experiment is performed by 8 healthy subjects shown in Table 3.3. All subjects use their right upper limb in this experiment though two of subjects are left-handed. Every subject performs each motion 30 times, 20 datasets are used to train the classifier and 10 datasets are utilized to test the classification system. The 8 healthy subjects are asked to activate the 5 motions within 3 seconds as shown in Table 3.4.

Table 3.3: Details of 8 healthy subjects

Subject	Gender	Height	Weight	Age	Handedness
1	Female	170cm	55kg	30	L(left)
2	Female	150cm	50kg	23	R(right)
3	Female	163cm	40kg	25	R
4	Female	160cm	49kg	28	R
5	Male	175cm	72kg	25	L
6	Male	170cm	76kg	24	R
7	Male	170cm	65kg	25	R
8	Male	182cm	78kg	26	R

Table 3.4: The experimental setup

Subject	Motion times for training	Motion times for test	Action time for each motion (second)
1~8	20	10	Within 3 seconds

In addition, the onset of 5 motions are activated when it reaches 2 seconds. The motion is terminated when the time reaches 4.5 seconds. The experimental motion timeline is shown in Fig. 3.4.

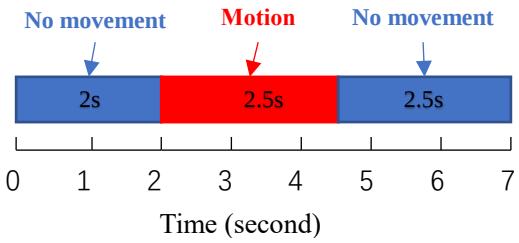

Fig. 3.4 The experimental motion timeline

For human joint, the anatomy is a constraint of inherent attribute from each joint. Range of joint is used for motor of artificial arm in Table 3.5. The range of elbow joint of flexion motion is between 0° and 150° and the range of elbow joint of extension motion also is between 0° and 150°. The range of forearm pronation motion is between 0° and 225° and the range of forearm supination motion is between 0° and 180°. Actually, human attempts to over extend their own forearm that leads the joint to be the hyperextension of about 0° to 5° [45].

Table 3.5: Ranges for each motion

Motion	Onset of motion	Termination of motion
Elbow joint of flexion	0°	150°
Elbow joint of extension	150°	0°
Forearm pronation	0°	225°
Forearm supination	180°	0°

3.3 System

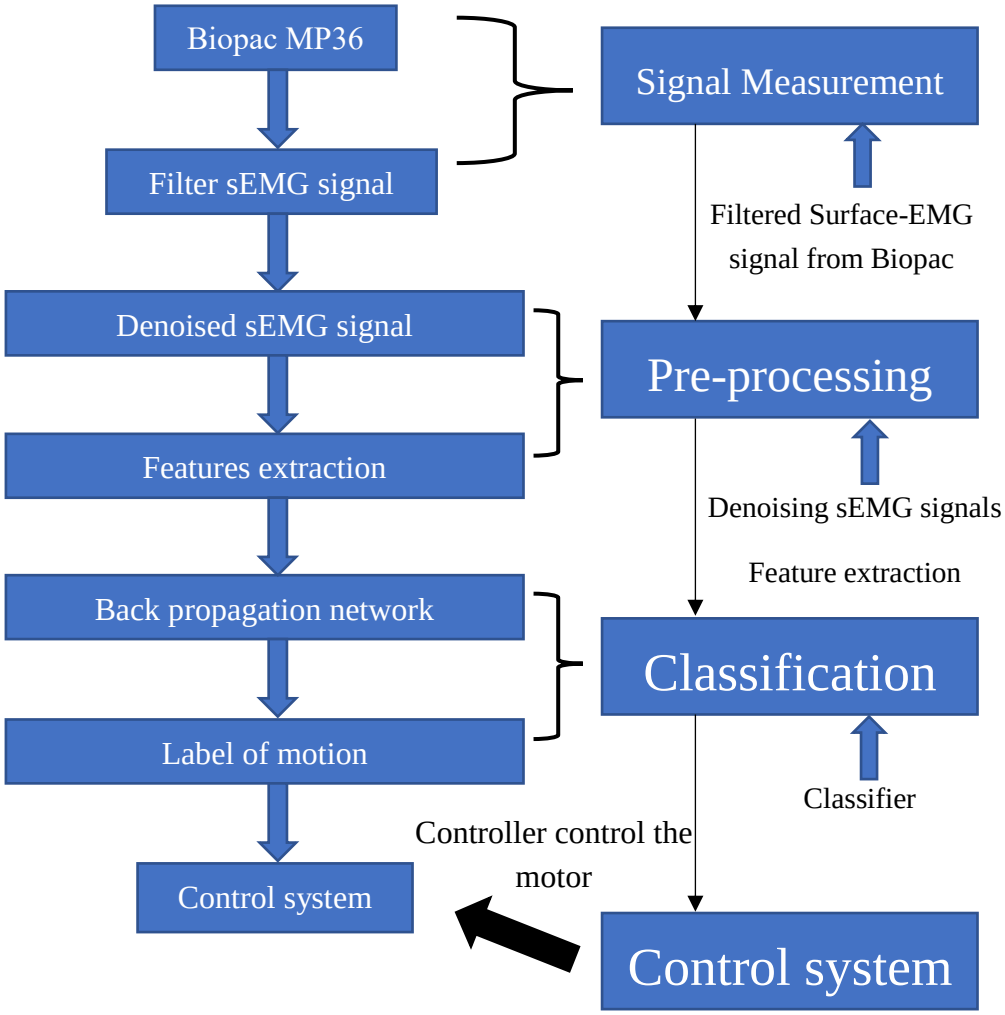

Fig. 3.5 The system structure

In this thesis, the complete system shown in Fig. 3.5 could be categorised into 4 components: (1) signal measurement, (2) pre-processing, (3) classification and (4) artificial robot arm control. First of all, the signal measurement contains data collection. The band-pass filtered is used in this component. Then, the denoised system in the pre-processing component reduces the noise from filtered sEMG signals by soft threshold method. It reduces not only the electrical noise but also the

white Gaussian noise. Next, the classification system is applied to recognize elbow joint motions. In order to design a classification system of high performance, the advisable features are needed to be constructed and selected to reduce the dimension of features. Therefore, five characteristic features, Mean Absolute Value (MAV), Root Mean Square (RMS), Slope Change (SC), Signal Length (SL) and Zero Crossing (ZC), are extracted from denoised sEMG signals of each channel. All five features are applied into back propagation neural network (BPNN) for classifier. Moreover, the results of classifier are tested on a subject-by-subject basis. It means that the classification system is a user-dependent system. It can detect the motions of healthy subject based on his or her own sEMG signals. The final component which is the control system demonstrates the test result on robot arm by Adrunio controller.

3.3.1 Signal measurement

The signal measurement uses electrodes (Red Dot, disposable electrode ECG, 3M health care) shown in Fig. 3.6 (b) and Biopac MP36 Four Channel Data Acquisition System shown in Fig. 3.6 (a). The data collection of sEMG signal uses the Biopac Student Lab (BSL) PRO (Version: 3.73, Build: 08.26.2008).

(a) (b)

Fig. 3.6 Biopac MP36 (a) and Electrode (b)

The BSL system has hardware with built-in general amplifiers to record condition of electrical signals from the heart, muscle, nerve, brain, eye, respiratory system, and tissue preparations. The system receives the signals from electrodes and transducers [46].

The sampling frequency is 1 kHz in the Biopac MP36. A band-pass filter that begins from 30 Hz to 500 Hz cuts noise from the raw sEMG signal because the frequency band for sEMG signals on the muscles of upper arm is 30 Hz to 500 Hz [14]. The raw sEMG signal is shown in Fig. 3.7 (a) and the filtered sEMG signal is shown in

Fig. 3.7 (b). In Fig. 3.7 (a), the raw sEMG signal has a floating sEMG signal component that can cause motion detection error. Hence, the filtered sEMG signal shown in Fig. 3.7 (b) is better than the raw sEMG signal shown in Fig. 3.7 (a) for motion detection.

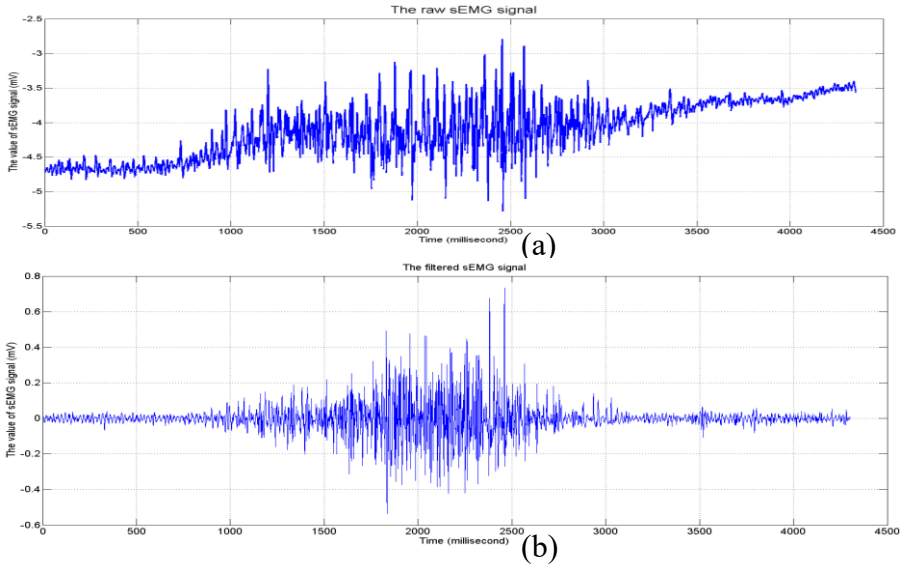

Fig. 3.7 The raw sEMG signal (a) and the filtered sEMG signal (b)

In frequency domain, the raw sEMG signal and filtered sEMG signal are transformed by fast fourier transform (FFT) $X_{fft}(k)$ shown in Eq. (3.1)

$$X_{fft}(k) = \sum_{j=0}^{N-1} x(j)\, W_N^{\mathrm{jk}}, \tag{3.1}$$

where k=0,…,N-1 and W_N is N_{th} root of unity, it is calculated by Eq. (3.2) and

$$W_N = e^{(-2\pi i)/N}, \tag{3.2}$$

where N is length of signal.

In Fig. 3.8, the magnitude of filtered sEMG signal in the frequency domain is reduced by the band pass filter. It means that the band pass filter reduces not

only the magnitude outside of the pass band of 30 Hz to 500 Hz, but also the magnitude within the pass band. In addition, the reduced magnitude outside of the pass band is bigger than inside. Moreover, the electrical noise of filtered sEMG signal shown in Fig. 3.8 (b) is less than the electrical noise of the raw sEMG signal shown in Fig. 3.8 (a) at 50 Hz. It means that the electrical noise is reduced by band-pass filter. In conclusion, the band pass filter remove noise outside of the pass band of 30 Hz to 500 Hz that is not the sEMG signals on the muscle of upper arm. The filtered sEMG signal is better than the raw sEMG signal for motion detection and interference of electrical noise.

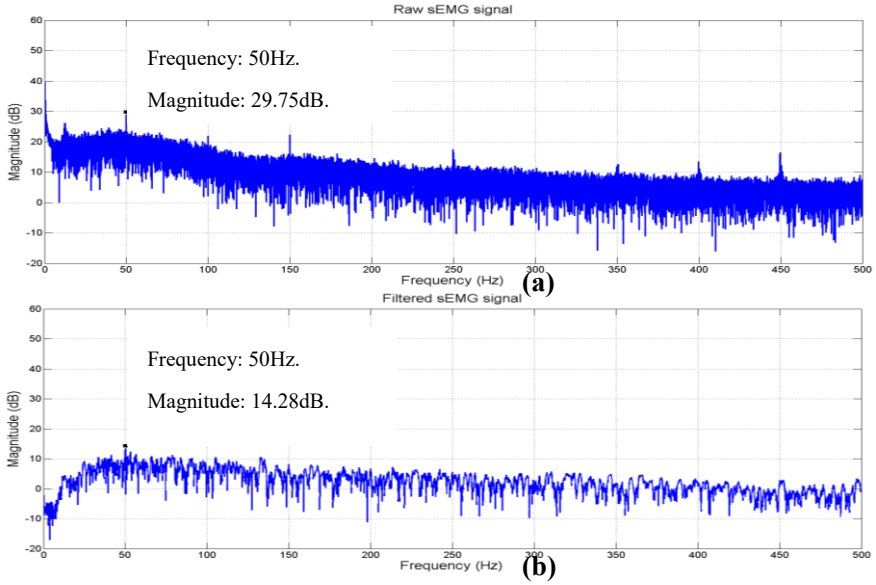

Fig. 3.8 In frequency domain, the raw sEMG signal (a) and the filtered sEMG signal (b)

3.3.2 Electrode placements

In the signal measurement, the biceps of long head, the triceps of lateral head and the triceps of long head are used into this thesis for four detected motions, so that the sEMG signals of 3 channels are collected to detect and classify the four motions. Three electrode placements are shown in Fig. 3.9. The channel 1 (ch.1) is biceps of long head. The channel 2 (ch.2) is triceps of lateral head. The channel 3 (ch.3) is triceps of long head. There is a common ground for all channels.

Fig. 3.9 The electrode placements

The complete signal measurement system is shown in Fig. 3.10. After the filtered sEMG signals collection, the filtered sEMG signal data are sent to the next component for pre-processing.

Fig. 3.10 The complete signal measurement system

3.3.3 Sampling windows

The filtered sEMG signal is partitioned into different window sizes for features extraction in classification system. It means that the system processes data based on a window basis. So that the window sizes are compared in the thesis, including 1024 samples, 512 samples, 256 samples and 128 samples. The window sizes bigger than 1024 samples are not considered, because the approximately acceptable delay is 300 milliseconds to 400 milliseconds [26]. In addition, the sampling frequency is 1000 Hz for collection sEMG signal. The window size of 1024 and 512 samples would take 1024 milliseconds and 512 milliseconds. Therefore, the sampling time over 1 second is not suitable to use. An example of forearm pronation for sampling window size of 256 samples is shown in Fig. 3.11.

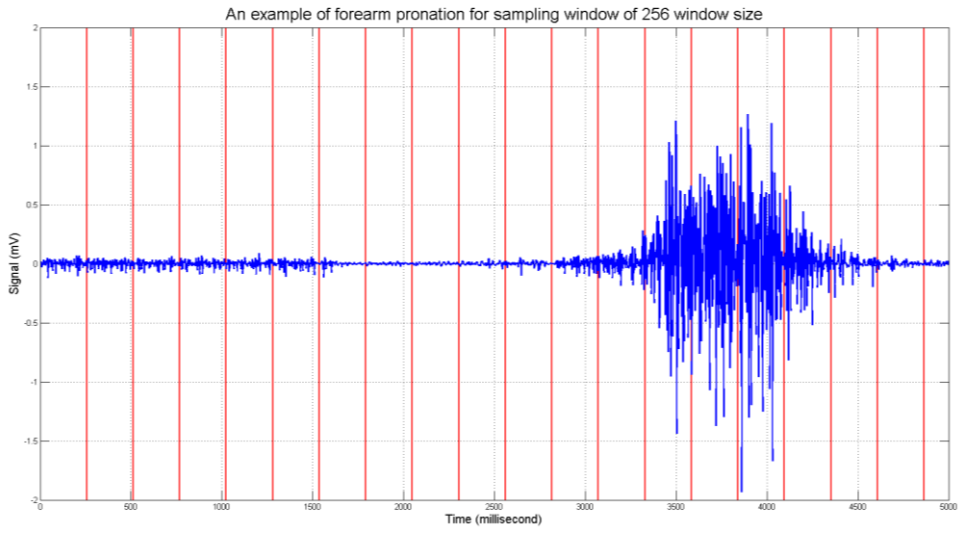

Fig. 3.11 An example of forearm pronation for a sampling window of 256 samples

Furthermore, the contractive sEMG signal less than 100 milliseconds in one window is stipulated as no movement because the spasms lead to the abnormal sEMG signal from muscle of persistent contraction. The amyostasia that is muscle sickness generates muscle contraction from 4 times to 6 times in every second. It means that the contractive sEMG signal is between 250 milliseconds and 166 milliseconds. Since, the contractive sEMG signal length less than 100 millisecond means muscle spasms without any intent movement. The 100 milliseconds are optimal time to build a suitable sensitivity classification system and it improves the stability for classification system. In conclusion, the contractive sEMG signal less than 100 samples in one window is stipulated no movement in this thesis shown in Fig. 3.12.

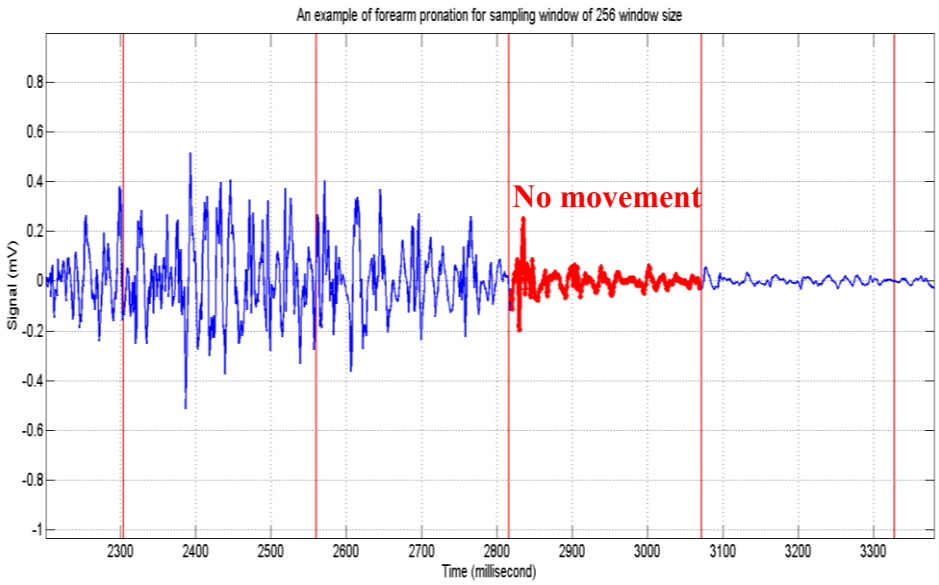

Fig. 3.12 Example of stipulated no movement window

3.3.4 Pre-processing

The filtered sEMG signals are sent to PC in Matlab from Biopac through a USB port. Matlab (Matlab 2014a, 8.3.0.532, 64-bit) is used to process the filtered sEMG signals. Because the filtered sEMG signal is the voltage of millivolt, it is easy to be interfered by noises. However, the filtering procedures are very difficult to remove the interference of random noises [47]. For example, the white Gaussian noise. Hence, the filtered sEMG signal requires a denoised algorithm to remove these random noises.

Nowadays, there are many algorithms for noise reduction. The wavelet denoising algorithm provides the high effect to remove random noises [48]. On one hand, the magnitude thresholding removes noise from signals with two or more components. In order to reduce the noise in the signal, selected wavelet coefficients are reduced or removed. Two most popular denoised algorithms are hard thresholding algorithm and soft thresholding algorithm.

The hard thresholding algorithm judges simply to keep or remove the coefficients shown in Fig. 3.13 (a). The soft thresholding algorithm recognizes the coefficients containing both signal and noise to isolate the signal by removing the noisy part from all coefficients shown in Fig. 3.13 (b). Hence, soft thresholding is carried out to remove noise from filtered sEMG signal.

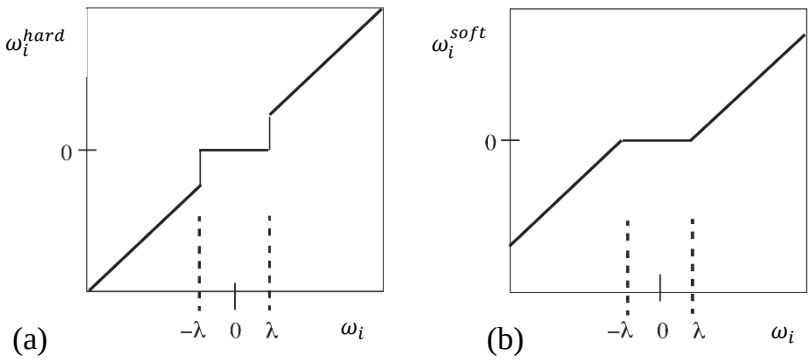

Fig. 3.13 The hard thresholding algorithm (a) and the soft thresholding algorithm (b)

Moreover, the equation of soft thresholding algorithm is shown in Eq. (3.3),

$$\omega_i^{Soft} = \begin{cases} 0 & |\omega_i| < \lambda \\ sign(\omega_i)(|\omega_i| - \lambda) & |\omega_i| \geq \lambda \end{cases}, \tag{3.3}$$

where ω_i is sequentially indexed coefficients, the λ is the value of threshold and the detail is shown after the section for sequentially indexed coefficients ω_i. Moreover, the absolute value of the sequentially indexed coefficients ω_i are smaller than the threshold λ, which equal to zero. It means that the sequentially indexed coefficients ω_i of zero do not change the value of sEMG signal. The absolute value of the sequentially indexed coefficients ω_i are bigger than the threshold λ, which are calculated by the equation of $sign(\omega_i)(|\omega_i| - \lambda)$.

The denoised system is shown in Fig. 3.14. It has four components to process the filtered sEMG signals.

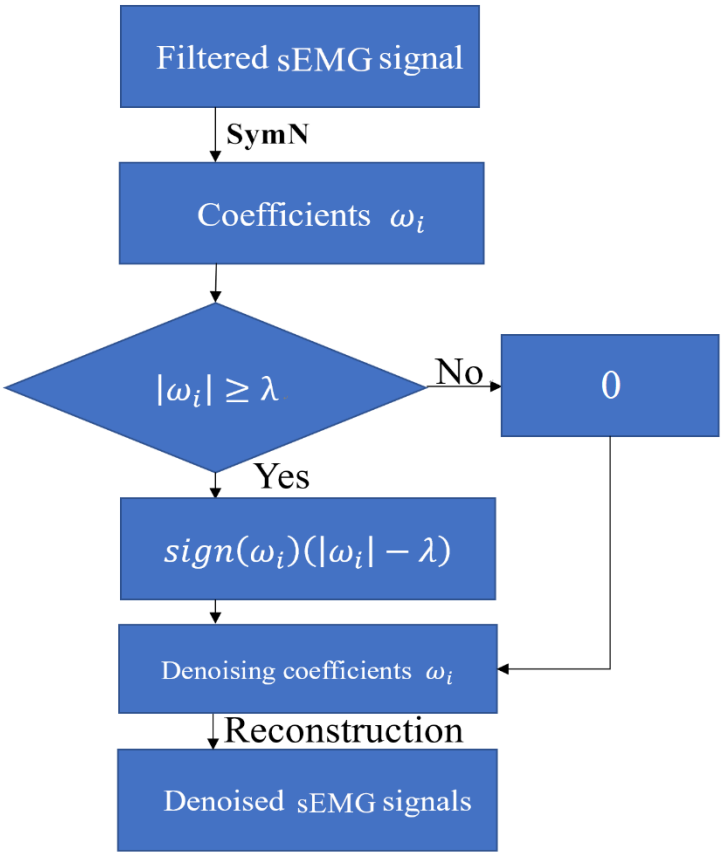

Fig. 3.14 Denoising system

In the first component of denoised system, the formula shown in Eq. (3.4) is used to compare SymN for calculation of levels of decomposition,

$$SNR = 10 \times log_{10}\left(\frac{\left|\sqrt{\sum {x_{signal}}^2}\right|}{\left|\sqrt{\sum {x_{signal}}^2}\right| - \left|\sqrt{\sum {x_{dsignal}}^2}\right|}\right), \quad (3.4)$$

where x_{signal} is the filtered sEMG signal data, $x_{dsignal}$ is the denoised signal data and SNR is value of signal-to-noise ratio (SNR). In addition, the SNR is calculated based on per window size of 256 samples basis.

In this thesis, the Symlet wavelets are used. It is a more symmetrical model based on Daubechies wavelets. The general characteristics of Symlet wavelets are shown in Table 3.6.

Table 3.6: The general characteristics of Symlets wavelets

Family	Symlets
Short name	Sym
Order N	N= 2,3,…
Orthogonal	Yes
Compact support	Yes
DWT	Possible
CWT	Possible
Support width	2N-1
Filters length	2N
Regularity	About 0.2 N for large N
Symmetry	Nearly symmetric
Number of vanishing moments for ψ	N

In the Table 3.6, the SymN has high regularity which is sparse basis with low smooth error. It renders the smooth process to signals decomposition. In addition, the smoothness of vanishing moments increases with the increase of N in SymN. The higher smoothness of vanishing moments makes not only higher localization ability in frequency domain, but also higher ability to partition the frequency band for signals. But the higher N in SymN increases the calculated amount, which reduces the compact support in time domain. The symmetry of SymN is higher than dbN, which reduces the phase distortion to the signal analysis and reconstruction.

Moreover, a discrete input signal of length N can be broken down into exactly N components without any loss of information using discrete orthonormal wavelets as Symlet wavelets [49]. Hence, Symlet wavelets is applied to calculate signal of decomposition levels i. Result is shown in Fig. 3.15, the SNR does not change significantly when the signal uses Sym5 to Sym15. Therefore, the Sym5 in my denoised system is applied to calculate decomposition levels i shown in Table 3.7. In addition, the length of decomposition low-pass filter for Sym5 is 10, it means that the length of data in full level of decomposition M is approximate 20.

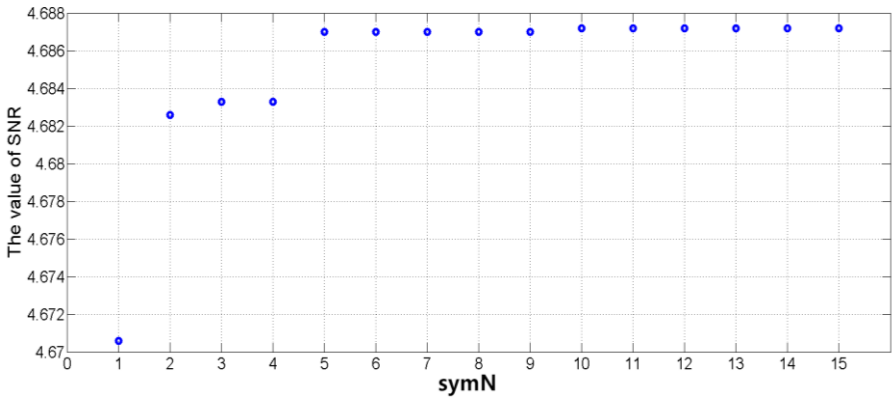

Fig. 3.15 The SNR of SymN for calculation of levels for decomposition

Table 3.7: Decomposition levels i by Sym5

Window size	decomposition levels i by Sym5
1024 samples	6
512 samples	5
256 samples	4
128 samples	3

In the second component, the SymN wavelet is also used in multiresolution algorithm. In the Fig. 3.16, it compares Sym1 to Sym8 by SNR. The SNR is similar when the signal uses Sym4 to Sym8. So, the Sym4 is used to calculate sequentially indexed coefficients ω_i based on multiresolution algorithm shown in the Fig. 3.17.

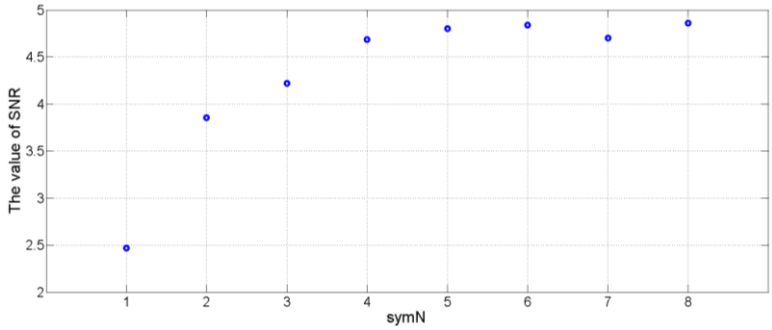

Fig. 3.16 The SNR of SymN for denoising signal

Moreover, the sequentially indexed coefficients ω_i shown in Fig. 3.18 has two components. They are approximation $S_{m,n}$ and detail coefficient $T_{m,n}$. The formulas are shown in Eq. (3.5) and Eq. (3.6)

$$S_{m+1,n} = \frac{1}{\sqrt{2}} \sum_k c_k S_{m,2n+k}, \tag{3.5}$$

$$T_{m+1,n} = \frac{1}{\sqrt{2}} \sum_k b_k S_{m,2n+k}, \tag{3.6}$$

where m is level of decomposition, n is number of sequence, scaling coefficient $\frac{1}{\sqrt{2}}c_k$ and wavelet function coefficient $\frac{1}{\sqrt{2}}b_k$ represents the low-pass filter and high-pass filter in wavelet transform, respectively. The two coefficients are calculated by Eq. (3.7) and Eq. (3.10) by SymN.

$$\emptyset(t) = \sum_k c_k \emptyset(2t-k) \tag{3.7}$$

$$\psi(t) = \sum_k (-1)^k c_{N_k-1-k} \phi(2t-k) \tag{3.8}$$

where $\emptyset(t)$ is a scaling function, $\psi(t)$ is a wavelet function. In addition, the Symlet wavelets are defined by scaling function $\emptyset(t)$ and wavelet function $\psi(t)$. This ordering of scaling coefficients used in the wavelet equation allows for wavelets and corresponding scaling equations to have support over the same interval $[0, N_{k-1}]$. Eq. (3.10) is calculated by Eq. (3.8) and Eq. (3.9). The Eq. (3.10) is used in my denoised system for wavelet function coefficient $\frac{1}{\sqrt{2}}b_k$.

$$\sum_k b_k = \sum_k (-1)^k C_{N_k-1-k} = 0 \tag{3.9}$$

$$\psi(t) = \sum_{k=0}^{N_{k-1}} b_k \phi(2t-k) \tag{3.10}$$

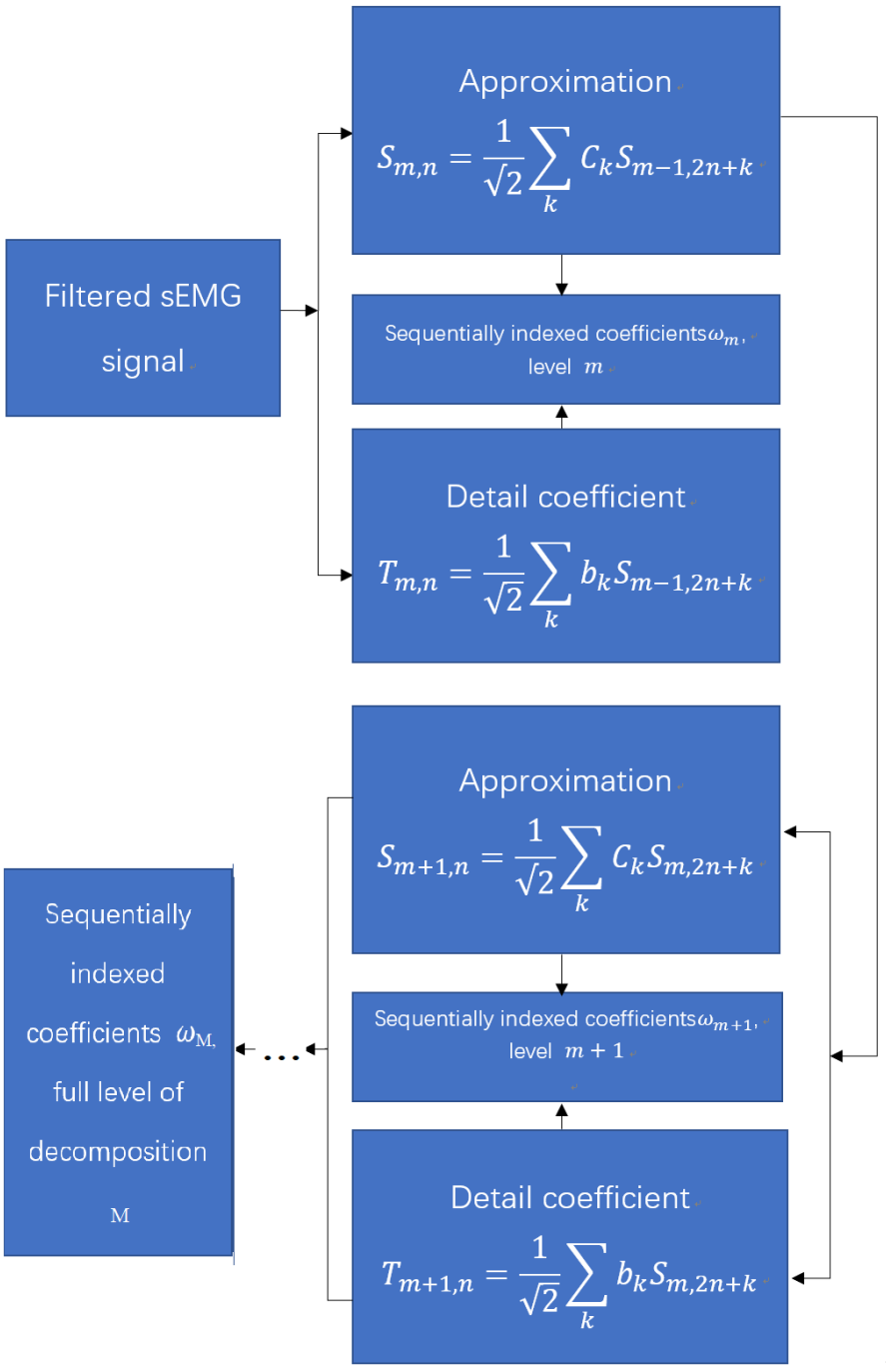

Fig. 3.17 Multiresolution algorithm

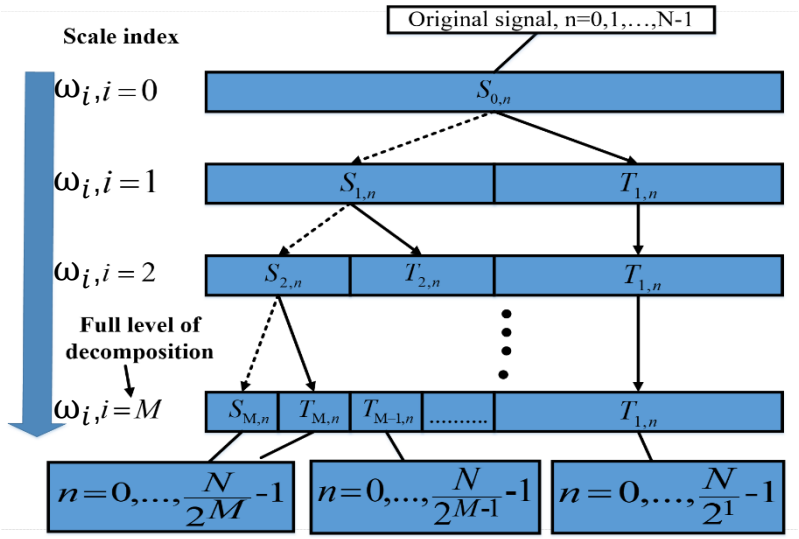

Fig. 3.18 The sequentially indexed coefficients ω_i

In the third component, the processing of threshold λ is shown in the Fig. 3.19. The full level of sequentially indexed coefficients ω_i is decomposed into 2 sections of decomposition which are the first section of approximation $S_{m,n}$ and the second section of detail coefficient $T_{m,n}$. So 2 sections $N_{section}$ are calculated by the sequentially indexed coefficients ω_i in the full level of decomposition.

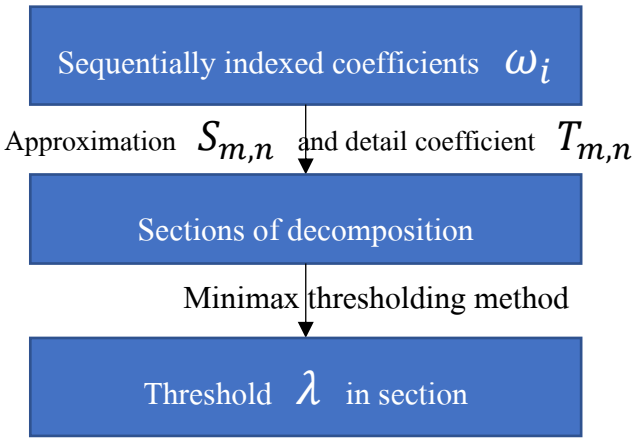

Fig. 3.19 The processing of threshold λ

Then, defined the minimax quantities $\Lambda^*_{N_{section}}$ is calculated by Eq. (3.11) based on minimax thresholding method in every section. The threshold $\lambda \equiv$ the largest λ attaining $\Lambda^*_{N_{section}}$ above [50].

$$\Lambda^*_{N_{section}} \equiv \inf_{\lambda} \sup_{\omega_i} \left\{ \frac{R_\lambda(\omega_i)}{{N_{section}}^{-1} + min(\omega_i^2, 1)} \right\} \tag{3.11}$$

where $N_{section}$ is length of section, the risk of the component $R_\lambda(\omega_i)$ is shown in Eq. (3.12).

$$R_\lambda(\omega_i) = E(\widehat{\omega_i} - \omega_i)^2 \tag{3.12}$$

where $\widehat{\omega_i}$ is the estimate $\widehat{\omega_i}$ of ω_i.

Finally, the denoised sequentially indexed coefficients ω_i is calculated by Eq. (3.3) in every level of decomposition. At the end, the fourth component is that the denoised sEMG signal is reconstructed based on denoised sequentially indexed coefficients ω_i of full level of decomposition. The process of reconstruction for denoised sEMG signal is shown in Fig. 3.20 and an example for denoised system is shown in Fig. 3.21.

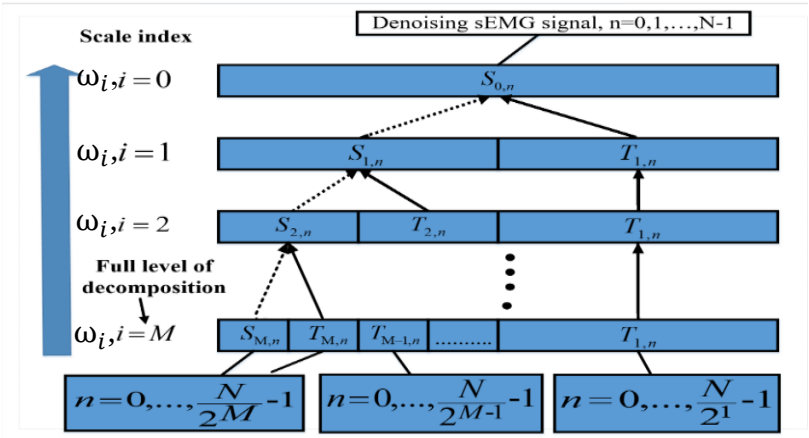

Fig. 3.20 The reconstruction of sequentially indexed coefficients ω_i

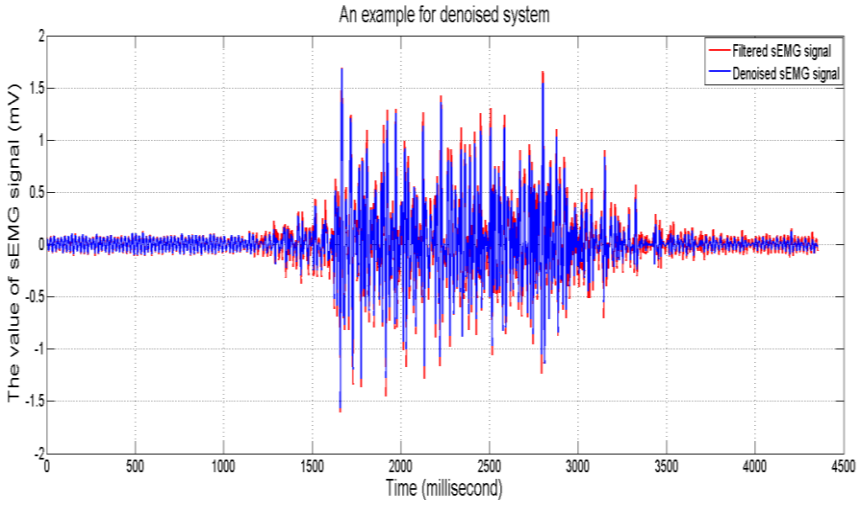

Fig. 3.21 An example for denoised system

In the Fig. 3.21, the noise is removed from the filtered sEMG signal. In order to analyze the benefit of the denoised system in frequency domain, the filtered sEMG signal is shown in Fig. 3.22 (a), the denoised sEMG signal is shown in Fig. 3.22 (b) and the removed sEMG signal is shown in Fig. 3.22 (c). Moreover, the filtered sEMG signal is the voltage of millivolt, it mostly distributes in the low frequency band and it is easy to be interfered by noises. The filtering procedures are very difficult to

remove the interference of random noises [47]. However, the denoised system based on wavelet denoising algorithm can remove these noises [48].

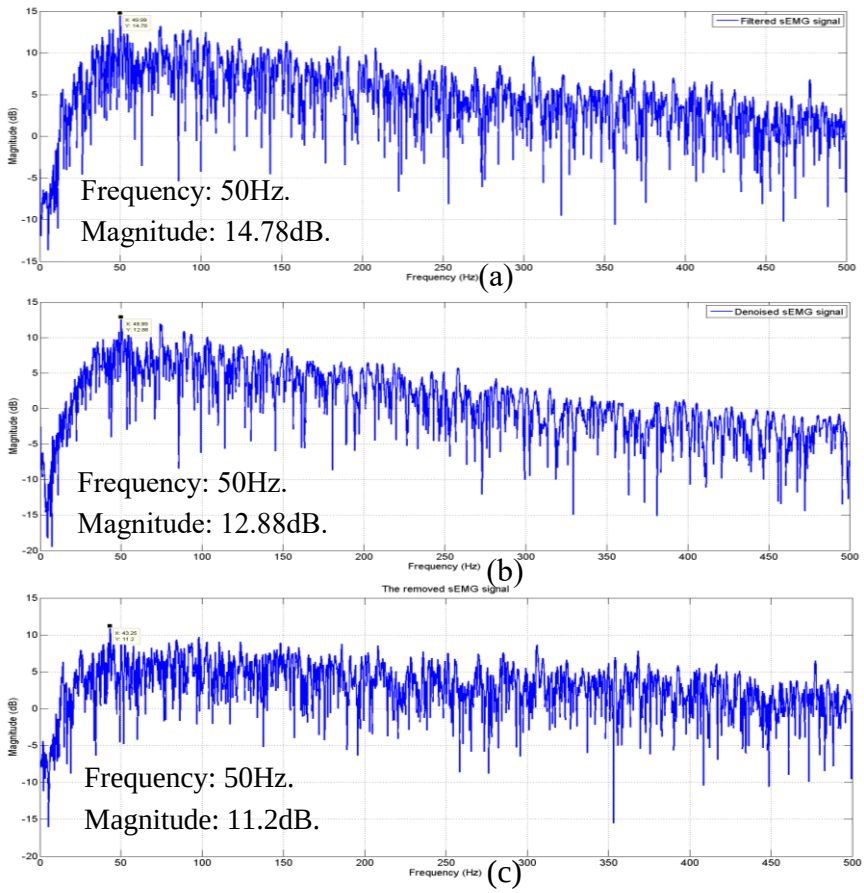

Fig. 3.22 In frequency domain, the filtered sEMG signal (a), the denoised sEMG signal (b) and the removed sEMG signal (c)

Through comparing electrical noise in the filtered sEMG signal and the denoised sEMG signal the denoised system reduces the electrical noise of the filtered sEMG signals at 50 Hz.

In addition, the removed sEMG signal in frequency domain is shown in Fig. 3.22 (c). It is calculated by the filtered sEMG signal minus the denoised sEMG signal. The removed sEMG signal mostly distributes in the low frequency band. It means that the denoised system reduces the interference of noises in low frequency band to sEMG signal, especially for electrical noise.

According to the characteristic of the removed sEMG signal, the power spectrum density of removed sEMG signal is shown in Fig. 3.23 (a). Its distribution matches uniform distribution in the frequency band of 30 Hz to 500Hz, because the band-pass filter also reduces the noises outside the pass-band.

The histogram for the amplitude of the removed sEMG signal is shown in Fig. 3.23 (b). The amplitude distribution matches the Gaussian distribution. Hence, the removed sEMG signal is white Gaussian noise, which is hard to be reduced by band-pass filter.

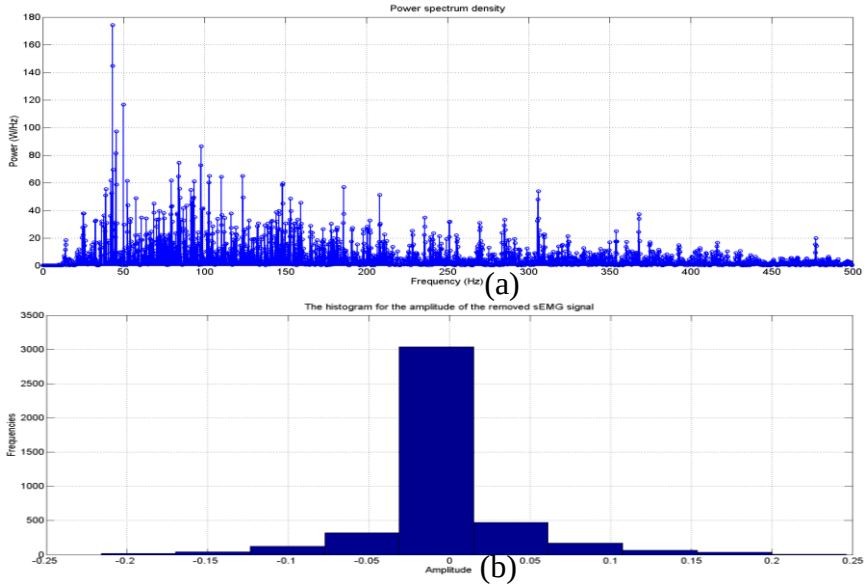

Fig. 3.23 In the power spectrum density of removed sEMG signal (a) and the histogram for the amplitude of the removed sEMG signal (b)

In conclusion, the denoised system not only reduces the electrical noise but also the white Gaussian noise which is removed difficultly by the band-pass filter.

The four examples of denoised sEMG signal of motion case are shown in Fig. 3.24 to Fig. 3.27. The denoised sEMG signals of elbow joint of flexion motion are shown in Fig. 3.24. The Fig. 3.25 shows the denoised sEMG signals of elbow joint of extension motion. It shows the denoised sEMG signals of forearm pronation motion in Fig. 3.26. The denoised sEMG signals of forearm supination motion are shown in Fig. 3.27.

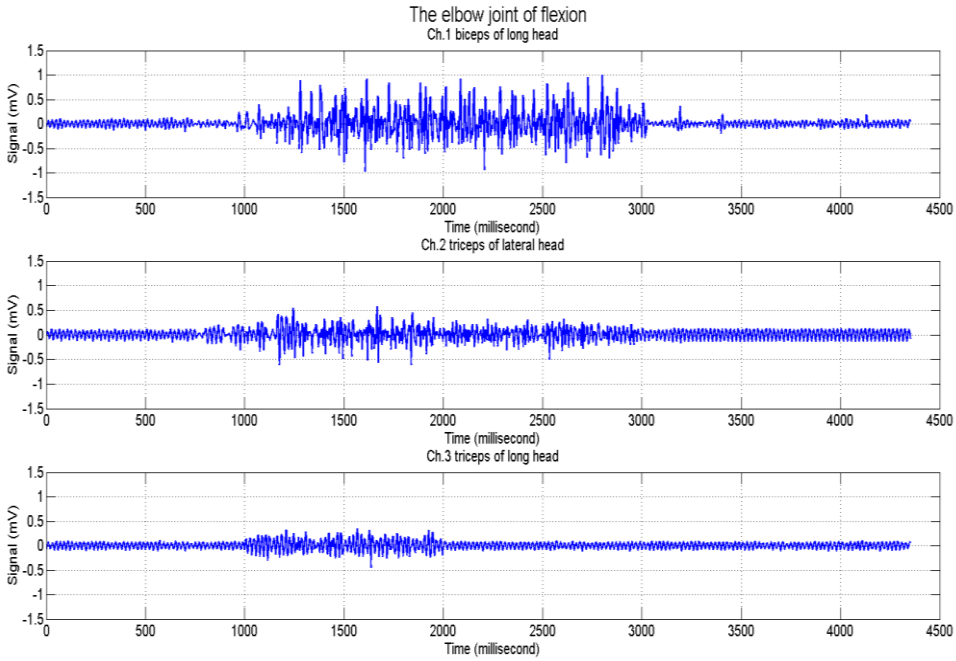

Fig. 3.24 The denoised sEMG signals of elbow joint of flexion motion

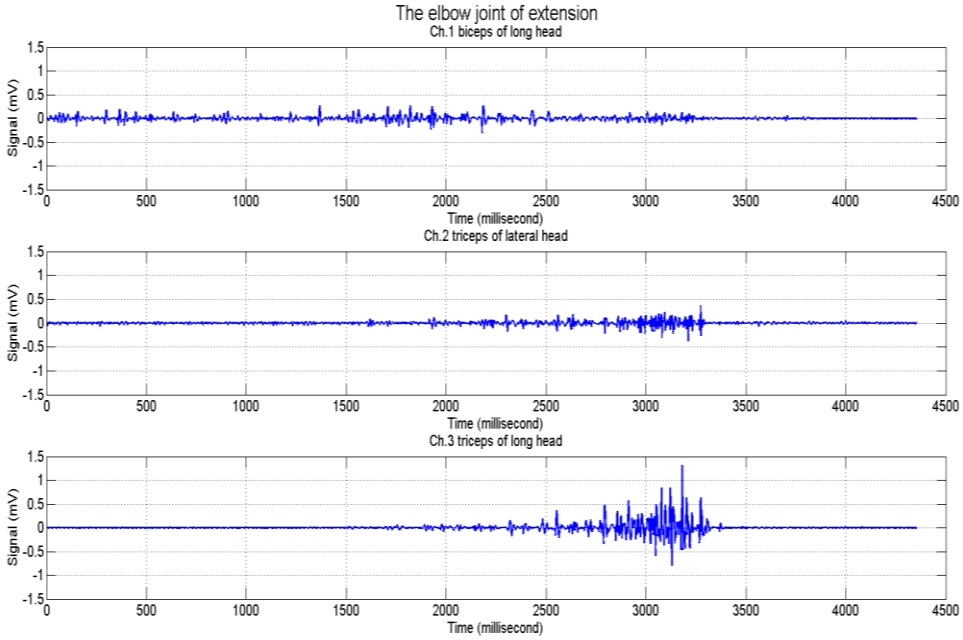

Fig. 3.25 The denoised sEMG signals of elbow joint of extension motion

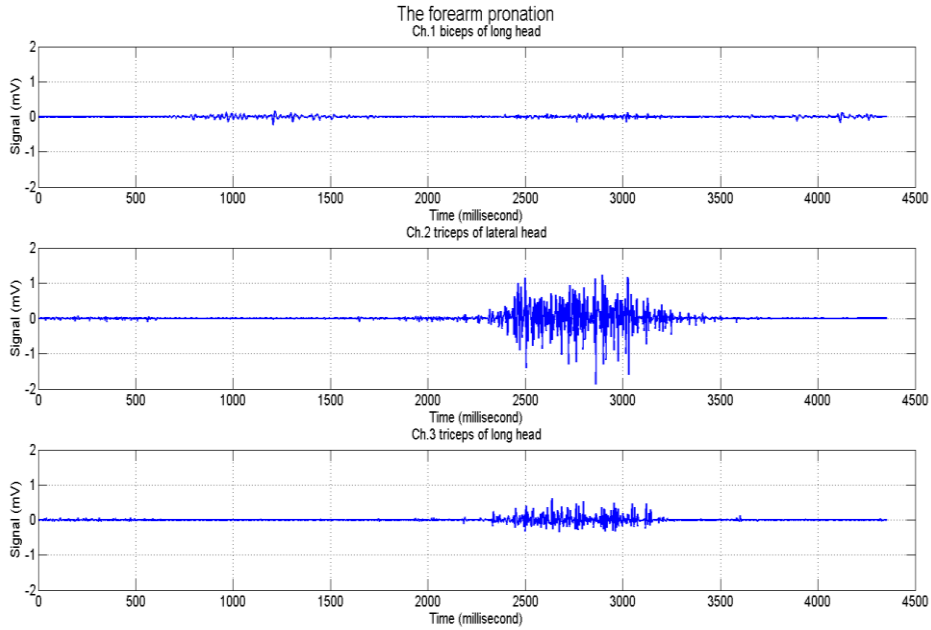

Fig. 3.26 The denoised sEMG signals of forearm pronation motion

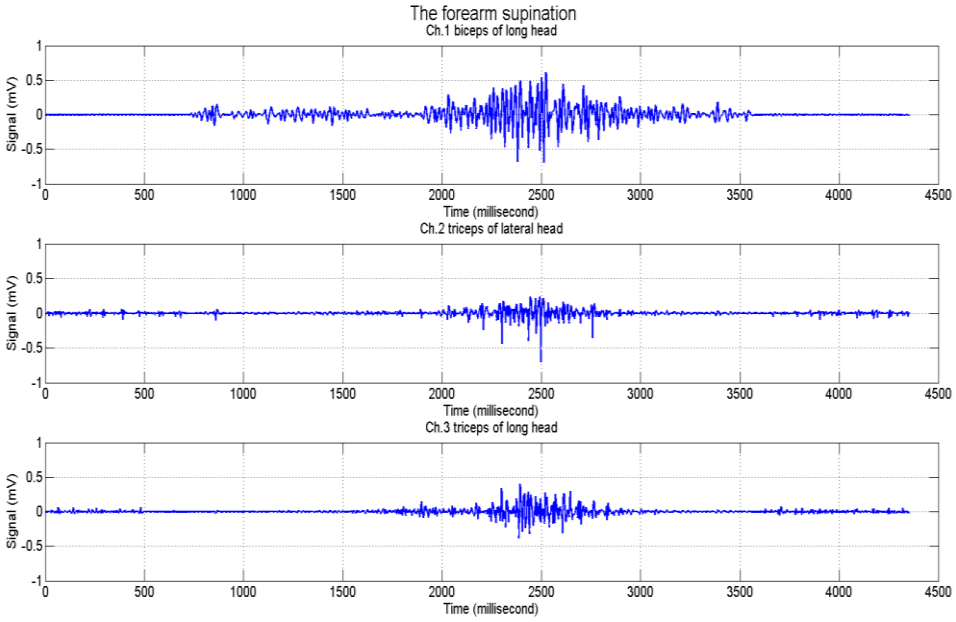

Fig. 3.27 The denoised sEMG signals of forearm supination motion

In addition, there is another algorithm to denoise the input sEMG signal that is a moving average algorithm. Because the elbow motions are activated at low

frequency [51], but the algorithm does not provide a beneficial result. The comparison is shown below for moving average algorithm.

The moving average algorithm can analyze the data of time series by averaging a sliding window and the function of moving average algorithm is a low-pass filter with filter coefficients equalling to the reciprocal of the length of sliding window. The moving average algorithm can reduce the effect of periodicity interference for signals, it not only has high smoothness but also low sensitivity. However, it does not limit the occasional pulse interference efficiently. Therefore, it is applied to the high frequency oscillation system without the situation of high pulse interference. It is favourable to avoid the shifting induced by using only 'past' data for a lot of applications. When using data equally spaced on any side of the point in the series where the mean is calculated, a central moving average can be computed. Hence, that using an odd number of datum points is required in the sample window.

At first, the length of window n_w for calculation is calculated by Eq. (3.13).

$$\mathrm{n}_w = \mathrm{N}_s - 1 + (\mathrm{N}_s \; mod \; 2) \tag{3.13}$$

where N_s is length of window for setup.

The process of moving average algorithm is shown in Fig. 3.28. It has three steps for the calculation. At the first, the length of window follows the consecutive

odd numbers to increase length of window until the $y(m_w)$ shown in Eq. (3.14) that length of window equal n_w.

$$m_w = \frac{n_w + 1}{2} \tag{3.14}$$

Then, the constant number is used for length of window. The window slides to extract average from each sliding time. At the end, the $y(m_i + 1)$ shown in Eq. (3.15) of smoothed sEMG signal is calculated by the reverse first step. Finally, the smoothed sEMG signal is shown in Fig. 3.29.

$$m_i = M_s - m_w \tag{3.15}$$

where M_s is the length of denoised sEMG signal.

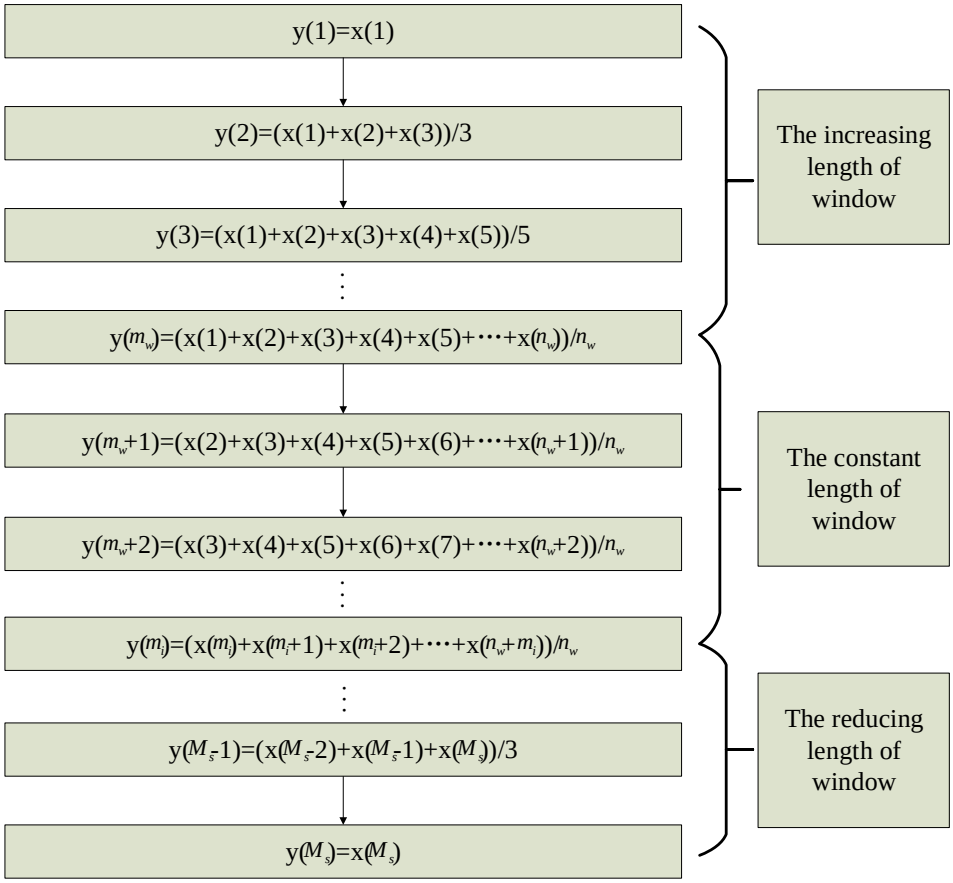

Fig. 3.28 The moving average algorithm

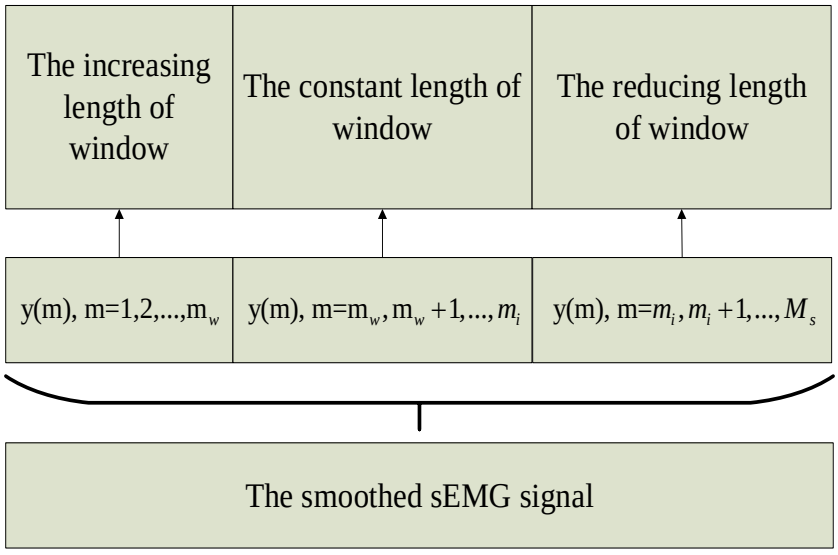

Fig. 3.29 The smoothed sEMG signal

Since, the function of moving average algorithm is a low-pass filter. The amplitude frequency responses are shown in Fig. 3.30 for the setup length 10 to 100 of window N_s, which are calculated by Eq. (3.16),

$$H(j\omega) = \frac{|Y(j\omega)|}{|X(j\omega)|}, \tag{3.16}$$

where $|Y(j\omega)|$ is the modulus of FFT of smoothed sEMG signal and $|X(j\omega)|$ is the modulus of FFT of denoised sEMG signal.

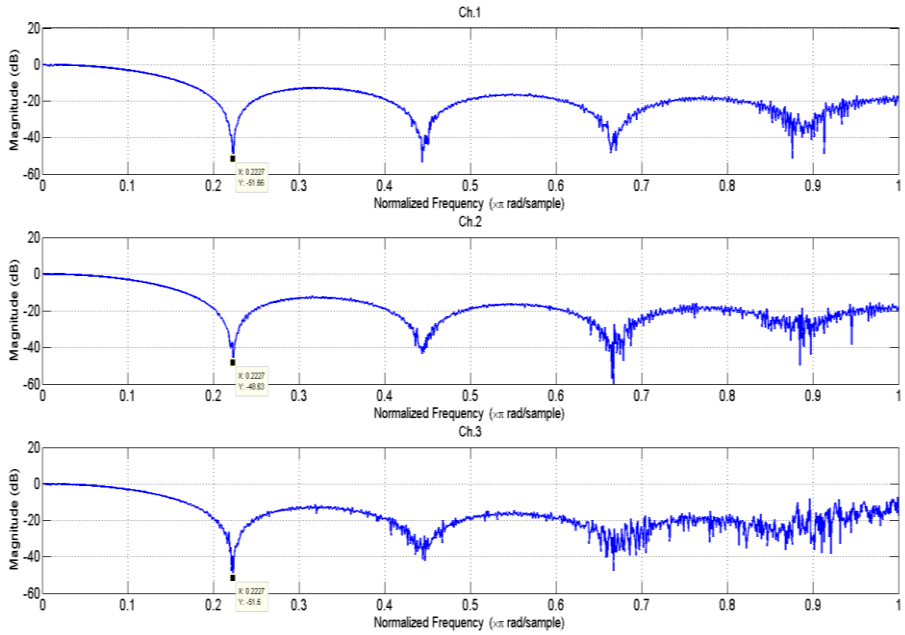

Fig. 3.30 The amplitude frequency response for the setup length 10 of window

In the Fig. 3.30, the stopband edge ω_s is 0.223π, it means that the stopband edge ω_s in the setup length 10 of window is 111.5 Hz by product of 0.223 and 500Hz which is the stopband edge of the band pass filter.

Table 3.8: The cut-off band for each setup N_s length of window

The setup length N_s of window	Passband edge ω_p	Stopband edge ω_s
10	0 Hz	111.5 Hz (0.223π)
20	0 Hz	53 Hz (0.106π)
30	0 Hz	34.5 Hz (0.069π)
40	0 Hz	25.5 Hz (0.051π)
50	0 Hz	20.5 Hz (0.041π)
60	0 Hz	17 Hz (0.034π)
70	0 Hz	14 Hz (0.028π)
80	0 Hz	12.5 Hz (0.025π)
90	0 Hz	11 Hz (0.022π)
100	0 Hz	10.5Hz (0.021π)

According to the analysis of the amplitude frequency responses, the passband edge ω_p and stopband edge ω_s for each setup length N_s of window are calculated and it is shown in Table 3.8. The stopband edge ω_s with the setup length 40 to 100 of window is lower than 30 Hz. In addition, the signal measurement system sets up a band-pass filter of 30Hz to 500Hz, it means that only noises are passed by the moving average algorithm. Because the pass-band of moving average algorithm overlaps with the band pass filter used to filter the raw EMG signals, the moving average algorithm does not achieve a high benefit for the noise reduction.

3.3.5 Features extraction

In order to detect each motion of sEMG signals clearly in the time domain, the 5 features of sEMG signals shown in Table 3.9 are analyzed as follows:

Table 3.9: The 5 features of sEMG signals

Number	Feature of sEMG signals	Abbreviation
1	Mean absolute value	MAV
2	Frequency of signal slope change	SC
3	Root mean square	RMS
4	Signal length	SL
5	Zero crossing	ZC

MAV of detected sEMG is used to reflect the status of a stimulated muscle. The value of MAV is high when the muscle contracts and it is low when muscle relaxes. The formula calculates the average of amplitude of denoised sEMG siganls shown in Eq. (3.17),

$$\mathrm{MAV} = \frac{1}{N}\sum_{n=1}^{N}|x_n|, \tag{3.17}$$

where N is the length of sEMG signal, and x_n is denoised sEMG signal.

SC is refleted by slope changes. The value of SC is high when the muscle contracts and it is low when muscle relaxes. In addition, the SC reflects the high frequency content of sEMG signal. The SC is shown in Eq. (3.18),

$$SC = \frac{1}{N-2}\sum_{n=1}^{N-2} f_{n_{sc}}, \tag{3.18}$$

$$f_{n_{sc}} = \begin{cases} 1, & (x_n - x_{n-1})(x_n - x_{n+1}) > \lambda_{sc} \\ 0, & else \end{cases}, \tag{3.19}$$

where λ_{sc} is threshold. It is calculated with sEMG signal in no movement, the maximum value from $(x_n - x_{n-1})(x_n - x_{n+1})$ is used to be the threshold λ_{sc}. The $f_{n_{sc}}$ are calculated by each value of $(x_n - x_{n-1})(x_n - x_{n+1})$. When the value of $(x_n - x_{n-1})(x_n - x_{n+1})$ is higher than threshold λ_{sc}, the $f_{n_{sc}}$ equals to 1, the $f_{n_{sc}}$ equals to 0 for other conditions.

RMS shown in Eq. (3.20) reflects the energy of sEMG signals. The value of RMS is high when the muscle contracts and it is low when muscle relaxes,

$$RMS = \sqrt{\frac{1}{N}\sum_{n=1}^{N} x_n^2}. \tag{3.20}$$

SL shown in Eq. (3.21) is the signal length of N samples. This feature interprets amplitude of sEMG signal and frequency. Moreover, the value of SL is high when the muscle contracts and it is low when muscle relaxes,

$$SL = \frac{1}{N-1}\sum_{n=1}^{N-1} |x_{n+1} - x_n|. \tag{3.21}$$

ZC shown in Eq. (3.22) reflects the frequency of sEMG data through the zero. In addition, the value of ZC is high when the muscle contracts and it is low when muscle relaxes,

$$ZC = \frac{1}{N-2}\sum_{n=1}^{N-2} f_{n_{zc}}, \tag{3.22}$$

$$f_{n_{zc}} = \begin{cases} 1, & x_n x_{n+1} < 0, |x_n - x_{n+1}| > \lambda_{zc} \\ 0, & else \end{cases}, \tag{3.23}$$

where λ_{zc} is threshold. It is calculated with sEMG signal with no movement. The maximum value from $|x_n - x_{n+1}|$ is used to be the threshold λ_{zc} for ZC. The $f_{n_{zc}}$ are calculated by each value of $x_n x_{n+1}$ and $|x_n - x_{n+1}|$. The $f_{n_{zc}}$ equals to 1 when the value of $x_n x_{n+1}$ is negative and $|x_n - x_{n+1}|$ is higher than threshold λ_{zc}, the $f_{n_{zc}}$ equals to 0 for other conditions.

In addition, the feature distributions from subject 8 are shown in Fig. 3.31 to Fig. 3.35.

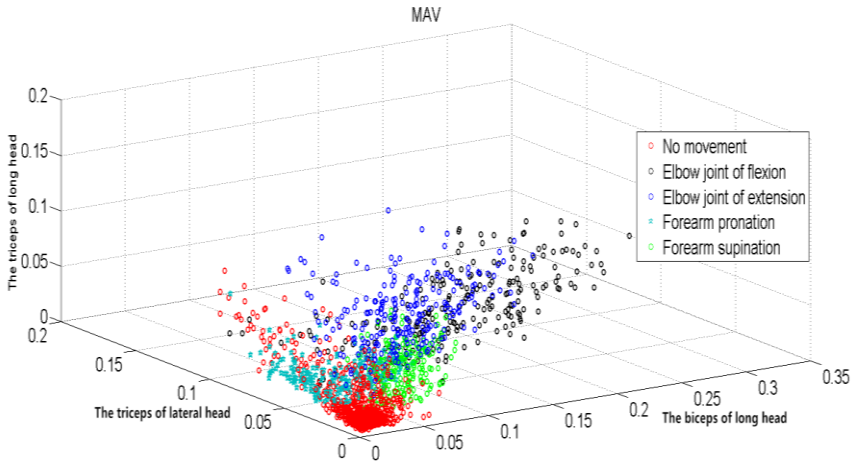

Fig. 3.31 An example of MAV distribution for subject 8

In the Fig. 3.31, the MAV is based on the data of subject 8: (1) the MAV values of no movement approximate to 0 on all axes, (2) the MAV value of elbow joint of flexion is high on the biceps of long head axis, (3) the MAV value of elbow joint of extension is high on the triceps of long head axis, (4) the MAV value of forearm pronation on the triceps of lateral head axis is high, (5) the value on the biceps of long head axis is high for the MAV of forearm supination, but it is lower than the value of elbow joint of flexion. The MAV values follow the kinesiology in section 3.1.

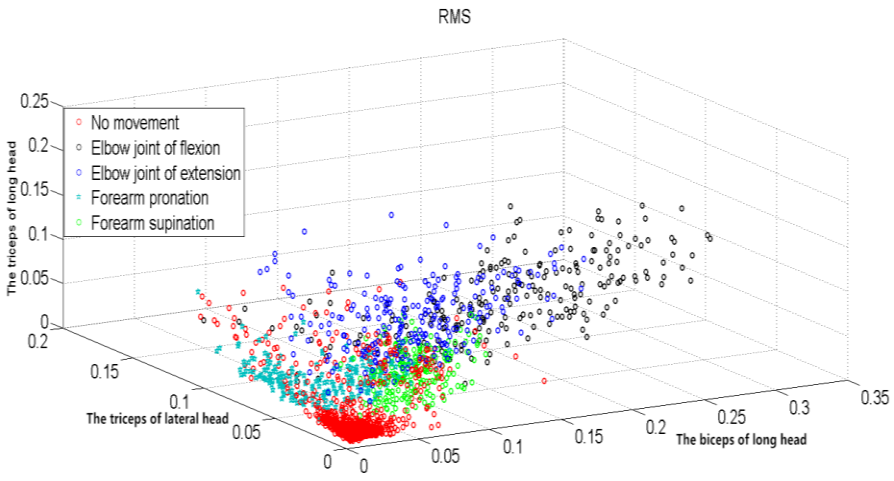

Fig. 3.32 An example of RMS distribution for subject 8

In the Fig. 3.32, the RMS is extracted from the sEMG signals of subject 8: (1) the RMS values of no movement close to 0 on all axes, (2) the RMS value of elbow joint of flexion is high on the biceps of long head axis, (3) the RMS value of elbow joint of extension is high on the triceps of long head axis, (4) the RMS value of forearm pronation on the triceps of lateral head axis is high, (5) the value on the biceps of long head axis is high for the RMS of forearm supination and the value is lower than the value of elbow joint of flexion. The RMS values obey the kinesiology in section 3.1.

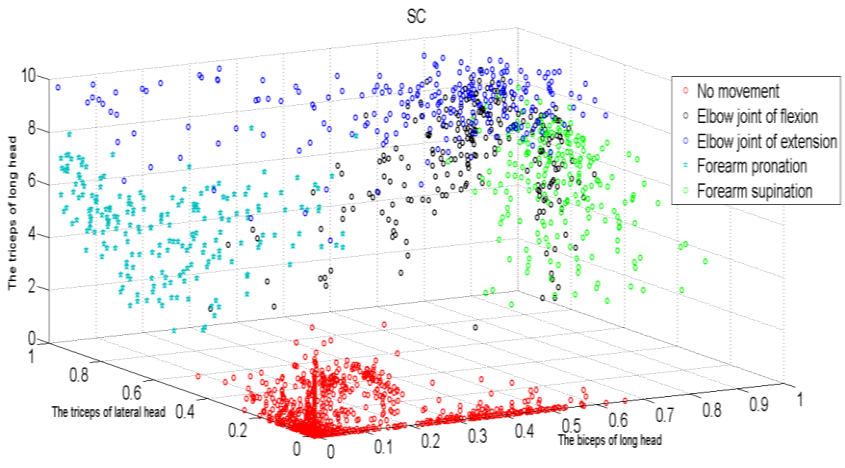

Fig. 3.33 An example of SC distribution for subject 8

In the Fig. 3.33, the SC is calculated by the data of subject 8: (1) the SC values of no movement distribute around 0 on all axes, (2) the SC value of elbow joint of flexion on the triceps of lateral head axis is high, (3) the SC value of elbow joint of extension is high on the triceps of long head axis, (4) the SC value of forearm pronation is high on the triceps of lateral head axis, (5) the value on the biceps of long head axis is lower than the value of elbow joint of flexion for the SC of forearm supination. The SC values comply with the kinesiology in section 3.1.

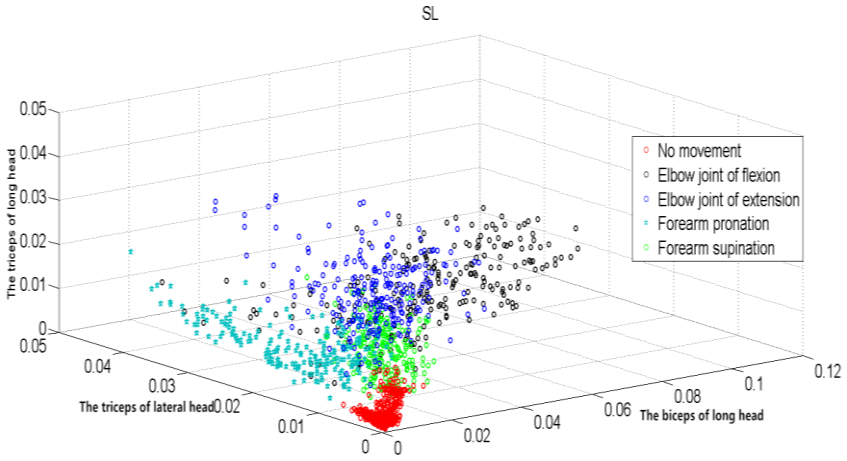

Fig. 3.34 An example of SL distribution for subject 8

In the Fig. 3.34, the SL is based on the data of subject 8: (1) the SL values of no movement approximate to 0 on all axes, (2) the value on the biceps of long head axis is high for the SL of elbow joint of flexion, (3) the SL value of elbow joint of extension on the triceps of long head axis is high, (4) the SL value of forearm pronation is high on the triceps of lateral head axis, (5) the value on the biceps of long head axis is high for the SL of forearm supination, but it is lower than the value of elbow joint of flexion. The SL values follow the kinesiology in section 3.1.

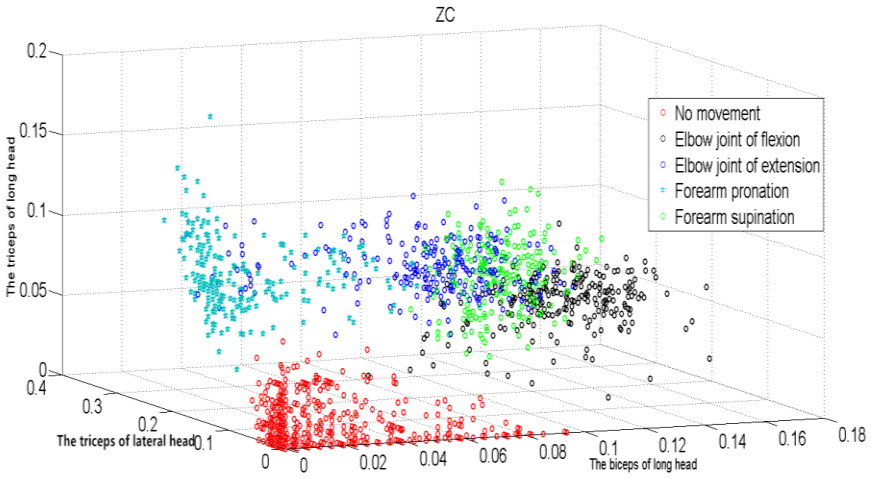

Fig. 3.35 An example of ZC distribution for subject 8

In the Fig. 3.35, the ZC is extracted from the data of subject 8: (1) the ZC values of no movement distribute around 0 on all axes, (2) the ZC value of the elbow joint of flexion is high on the biceps of long head axis, (3) the ZC value of elbow joint of extension on the triceps of long head axis is high, (4) the ZC value of forearm pronation is high on the triceps of lateral head axis, (5) the value on the biceps of long head axis is lower than the value of elbow joint of flexion for the ZC of forearm supination. The ZC values obey the kinesiology in section 3.1.

On the other hand, the features in frequency domain are also used for classification. The [52] and [53] concludes that the features in frequency domain are used for muscle force estimation and muscle condition, normally. The degree of muscle force is different for everyone, which is even different for every muscle. Therefore, it is very difficult to apply the features of frequency domain in a standard criterion. They are power spectrum density (PSD), mean frequency (MNF) and median frequency

(MDF). These three features are used to compare the valuation for the five motions detection. Moreover, two conditions are designed to select the features in frequency domain: (1) the feature values of contracted muscle should be higher than the feature values of other muscles, (2) the feature values of elbow joint of flexion, extension, forearm pronation and supination should be better than the feature values of no movement. If the feature follows the two conditions, the feature can be used to detect motions for classification system.

At the first, the PSD shown in Eq. (3.24) reflects the power of sEMG signal in frequency domain,

$$PSD = \frac{\left|X_{fft}(k)\right|^2}{N}, \tag{3.24}$$

where $X_{fft}(k)$ is the FFT of signal, N is the length of $X_{fft}(k)$.

The PSD is a group of data that is used to analyze the condition of muscle [54]. But it will increase so many dimensions of feature and generates a long processing time. Hence, the PSD is not suitable to use in this thesis.

Next, the MNF shown in Eq. (3.25) detects the average frequency by the sum of product of power spectrum and the frequency to divide the total spectrum intensity. It summarizes the average frequency of the denoised sEMG signals,

$$\text{MNF} = \sum_{n=1}^{N} f_n P_n \Big/ \sum_{n=1}^{\text{N}} P_n, \tag{3.25}$$

where the f_n is the frequency of sEMG power spectrum, the P_n is the sEMG power spectrum and the N is the length of frequency.

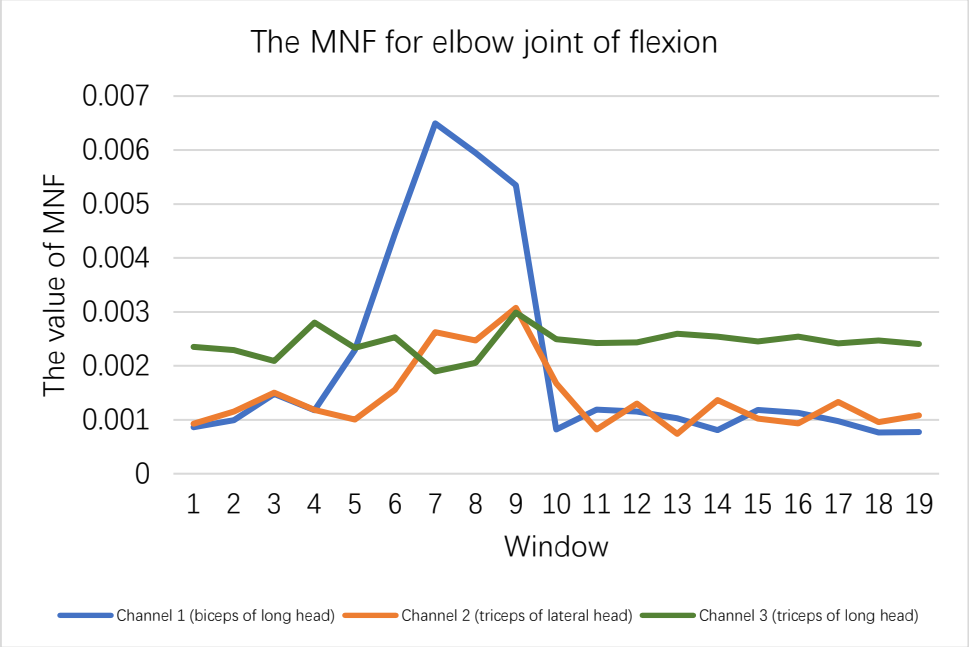

Fig3.36 The MNF for elbow joint of flexion

The MNF values of each motion that sampling window size of 256 samples in one subject are shown in Fig. 3.36 to Fig. 3.39. The MNF values for elbow joint of flexion are shown in Fig. 3.36. The MNF of elbow joint of flexion is from window 5 to window 10. As following the two conditions, the window 5 to window 10 of channel 1 (biceps of long head) should be higher than window 5 to window 10 of other 2 channels and the window 5 to window 10 should be higher than other windows in channel 1. Hence, the window 5 and window 10 do not match the two conditions. Other windows match the two conditions.

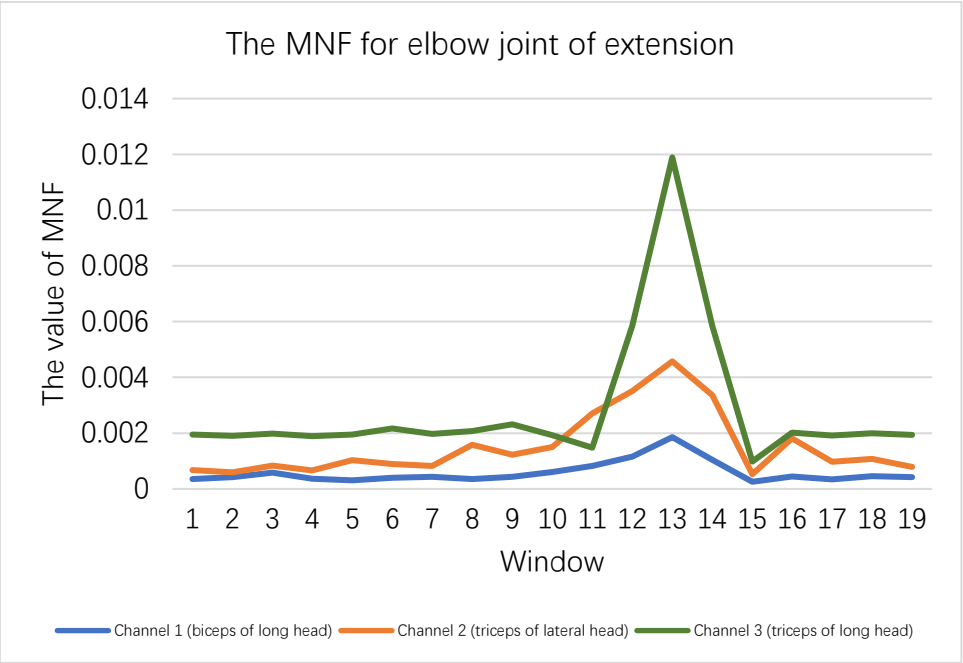

Fig. 3.37 The MNF for elbow joint of extension

In the Fig. 3.37, the MNF values for elbow joint of extension are shown. From the window 11 to window 14 is the MNF values of elbow joint of extension. In the two conditions design, the window 11 to window 14 of channel 3 (triceps of long head) should be higher than window 11 to window 14 of other 2 channels and the window 11 to window 14 should be higher than other windows in channel 3. Hence, only window 11 do not follow the two conditions. Other windows follow the two conditions.

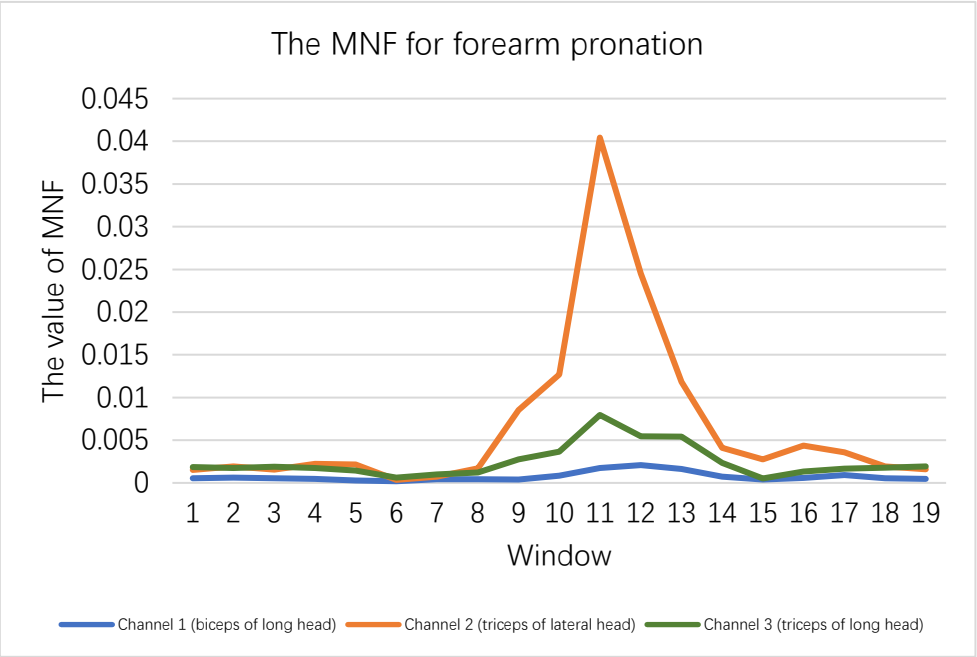

Fig. 3.38 The MNF for forearm pronation

The MNF values for forearm pronation are shown in Fig. 3.38. From the window 9 to window 17 is the MNF of forearm pronation. The window 9 to window 17 of channel 2 (triceps of lateral head) should be higher than window 9 to window 17 of other 2 channels and the window 9 to window 17 should be higher than other windows in channel 2. In addition, all of windows match the two conditions.

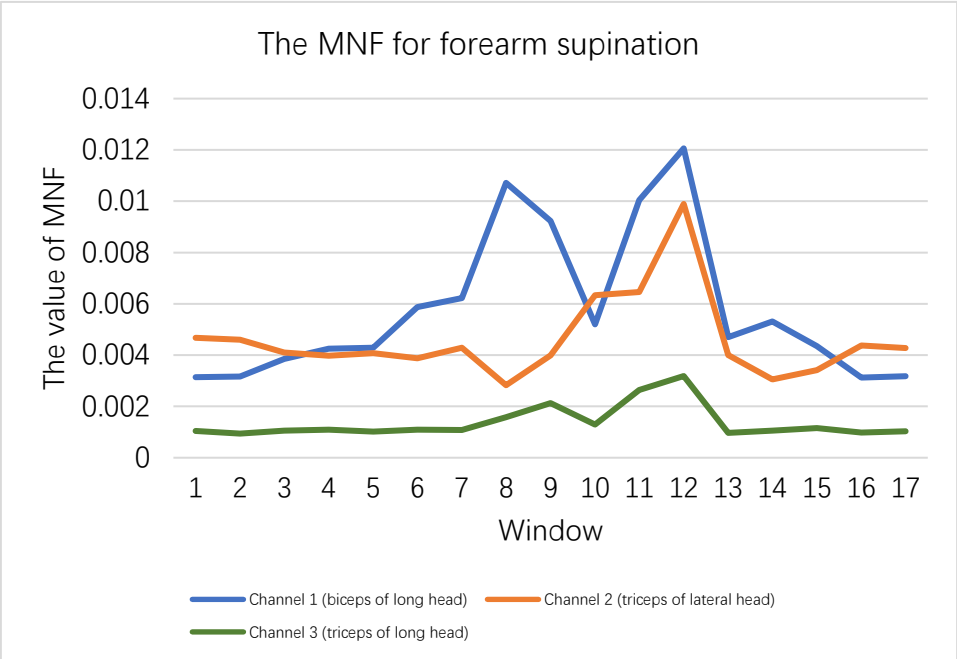

Fig. 3.39 The MNF for forearm supination

The MNF values for forearm supination are shown in Fig. 3.39. From the window 7 to window 13 is the MNF of forearm supination. The window 7 to window 13 of channel 1 (biceps of long head) should be higher than window 7 to window 13 of other 2 channels and the window 9 to window 17 should be higher than other windows in channel 1. So the window 10 and window 13 do not match the two conditions. Other windows match the two conditions.

In conclusion, the MNF features are compared by each motion. The elbow joint of extension and forearm pronation have a high matching condition. But the elbow joint of flexion and forearm supination have a low matching condition. It means that the MNF feature is not suitable to detect the motion for classification system.

At the third, the MDF is calculated by Eq. (3.26), it searches the frequency at which the power spectrum of denoised sEMG signals is divided into two equally section,

$$MDF = \sum_{n=MDF}^{N} P_n, \tag{3.26}$$

$$\sum_{n=MDF}^{N} P_n = \frac{1}{2}\sum_{n=1}^{N} P_n. \tag{3.27}$$

In addition, the conditions of MDF and MNF are similar because the features are two kinds of averages in statistics. Hence, the results of MDF for each motions are not shown in this thesis. The conclusion of MDF features is not suitable to detect the motion for classification system.

In conclusion, the PSD, MDF and MNF give the low benefit to classification system. Therefore, the five features in time domain, MAV, SC, RMS, SL and ZC, are used in the input layer of classifier shown in Fig. 3.40. Moreover, the five features are used in other researches of sEMG for classification.

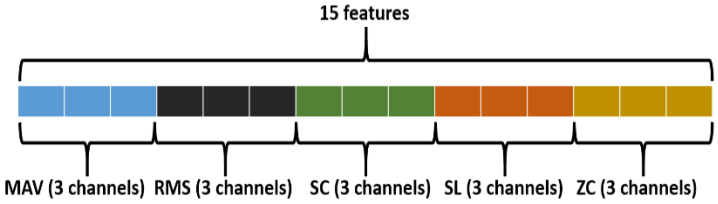

Fig. 3.40 The input structure of 15 features

3.3.6 Classification system

In this thesis, the classifier of 3 channels recognizes five motions: (1) no movement, (2) elbow joint of flexion, (3) elbow joint of extension, (4) forearm pronation and (5) forearm supination. Moreover, the classifier of 2 channels shown in Fig. 3.41 and the classifier of 3 channels shown in Fig. 3.42 are compared.

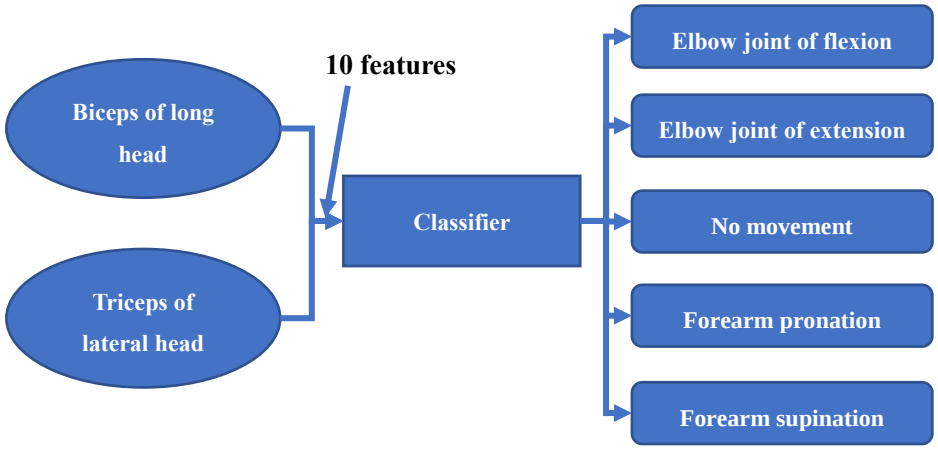

Fig. 3.41 The structure of the classifier of 2 channels

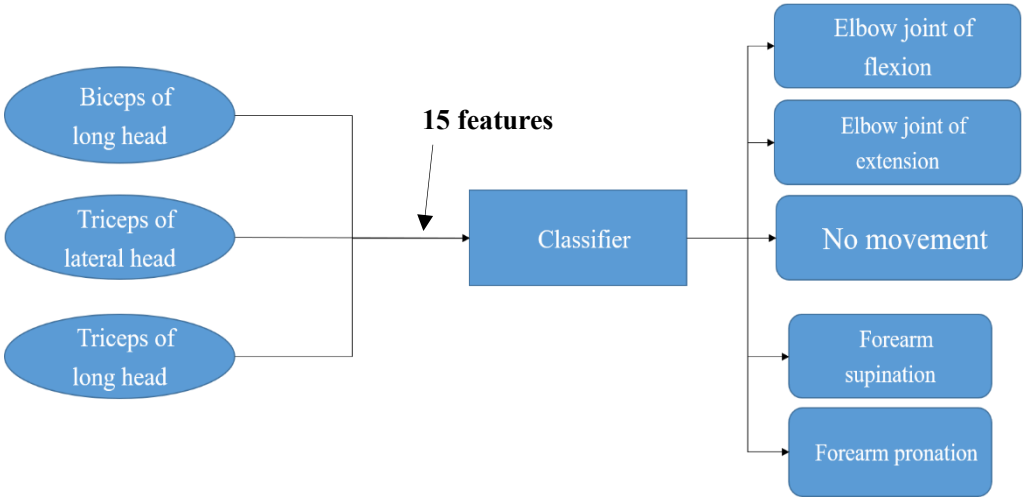

Fig. 3.42 The structure of classifier of 3 channels

In addition, the classification system uses back propagation network (BP network). The BP network is a kind of artificial neural network (ANN). It is a method with hidden layer of multilayer feedforward network. The error data backward propagate to modify the weight and threshold. The BP network is able to solve the problem of linear inseparable and it is very effective in the pattern recognition, regression, approach and compression.

Moreover, steepest descent method is a very classical method in BP network. It has a factor of momentum to improve the processing time. Steepest descent method is also called a gradient descent method. It is a first-order iterative optimization algorithm. Steepest descent method is used to find a local minimum of a function. It takes steps proportional to the negative of the gradient (or approximate gradient) of the function at the current point. Error signal propagates backward in classifier.

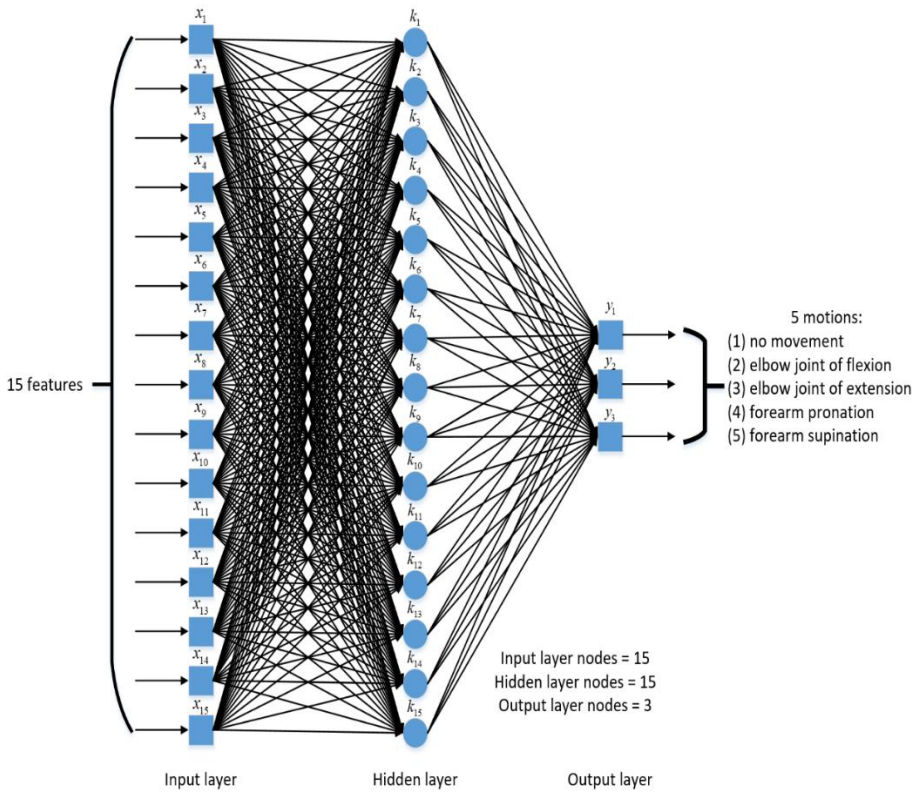

Fig. 3.43 The structure of BP network for the classifier

In BP network design, the input layer nodes are M, the output layer nodes are J, the hidden layer nodes are I, the i of hidden layer node is k_i,the j of output layer node is y_j, the ω_{ij} is a link weight from k_i to y_j, the u is input and the v is output for every layer.

In addition, the structure of classifier of 3 channels is shown in the Fig. 3.43. Hence, the input layer nodes M are 15. The hidden layer nodes I are 15. The output layer nodes J are 3. The j of output layer node is $v_j^j(n)$ in Eq. (3.28),

$$v_j^i(n) = g\left(u_j^i(n)\right), \tag{3.28}$$

where the j of input layer node is $u_j^j(n)$.

The e(n) is $e_j(n)$ of second derivative and the differential is first partial derivative shown in Eq. (3.29),

$$\frac{\partial e(n)}{\partial e_j(n)} = e_j(n)\,. \tag{3.29}$$

Eq. (3.30) is calculation for partial derivative,

$$\frac{\partial e_j(n)}{\partial v_j^i(n)} = -1\,. \tag{3.30}$$

Eq. (3.31) and Eq. (3.32) are output layer of derivative,

$$\frac{\partial v_J^j(n)}{\partial u_J^j(n)} = g' u_J^j(n)\,; \tag{3.31}$$

$$\frac{\partial u_J^j(n)}{\partial \omega_{ij}(n)} = v_I^i(n)\,. \tag{3.32}$$

The local gradient describes the value of modified weight shown in Eq. (3.33),

$$\delta_J^j = -\frac{\partial e(n)}{\partial u_J^j(n)} = -\frac{\partial e(n)}{\partial e_j(n)} \cdot \frac{\partial e_j(n)}{\partial v_J^j(n)} \cdot \frac{\partial v_J^j(n)}{\partial u_J^j(n)} = e_j(n) g'\left(u_J^j(n)\right). \tag{3.33}$$

The local gradient equals to the product between the error and derivative of transform function. The threshold and weight are modified together and the threshold modify from local gradient between input layer and hidden layer.

Moreover, the error of classifier is calculated by the mean squared errors (MSE) shown in Eq. (3.35),

$$e_n = \mathrm{Y}_{output_n} - y_{output_n}\,, \tag{3.34}$$

where Y_{output_n} are the user motions, y_{output_n} are the predicted motions by BP network.

$$MSE = \frac{1}{N}\sum_{n=1}^{N}(\hat{e}_n - e_n)^2\,, \tag{3.35}$$

where N is the training times, $\hat{e}_n$ is the mean of e_n.

The errors of classifier are judged by error margin. When the MSE is greater than error margin, the algorithm is defined MSE without convergence. The weight is modified from MSE and gradient $\frac{\partial e(n)}{\partial \omega_{ij}(n)}$, until the MSE is converged. In this modified step, the errors are propagated backward. The value of gradient $\frac{\partial e(n)}{\partial \omega_{ij}(n)}$ is shown in Eq. (3.36),

$$\frac{\partial e(n)}{\partial \omega_{ij}(n)} = \frac{\partial e(n)}{\partial e_j(n)} \cdot \frac{\partial e_j(n)}{\partial v_j^j(n)} \cdot \frac{\partial v_j^j(n)}{\partial u_j^j(n)} \cdot \frac{\partial u_j^j(n)}{\partial \omega_{ij}(n)} = -e_j(n)g'\left(u_J^j(n)\right)v_I^i(n). \tag{3.36}$$

The weight is shown in Eq. (3.37). The weight ω_{ij} modifies between hidden layer and output layer,

$$\Delta\omega_{ij}(n) = -\eta e_j(n)g'\left(u_J^j(n)\right)v_I^i(n) = \eta\delta_J^j v_I^i(n), \tag{3.37}$$

where i and j are the hidden layer node in J and the output layer node in I, respectively.

Steepest descent method has factor of momentum shown in Eq. (3.38),

$$\Delta\omega(n) = -\eta(1-\alpha)\nabla e(n) + \alpha\Delta\omega(n-1), \quad (3.38)$$

where $\nabla e(n)$ is gradient and the learning rate is η. Normally, it is known that value of factor of momentum is 0.1 to 0.8 and 0.8 is used for the factor of momentum in this thesis.

After first training, there is a factor of momentum $\alpha(0 < \alpha < 1)$ in the modified weight processing. The direction and amplitude of modified weight are not only from $\Delta\omega(n)$, but also from $\Delta\omega(n-1)$. Thus it makes the modified convergence faster. If $\Delta\omega(n)$ and $\Delta\omega(n-1)$ of gradient direction are the same, it means that the value of $|-\eta(1-\alpha)\nabla e(n)|$ plus the $\alpha\Delta\omega(n-1)$ and the weight of result is larger. As a result, the convergence speeds up. On the other hand, when the $\Delta\omega(n)$ and $\Delta\omega(n-1)$ of gradient direction are opposite, the $|-\eta(1-\alpha)\nabla e(n)|$ minus $\alpha\Delta\omega(n-1)$, the weight of result is smaller, which is easier to find the minimum point. The value of modified weights was saved in the modified weight processing.

Moreover, the classifier has 6 steps that follow the BP network design in the classification system shown in the Fig. 3.44. It is worth mentioning that all of

setups are shown based on the 8 healthy subjects with sampling window size of 256 samples, because it provides the best accuracy.

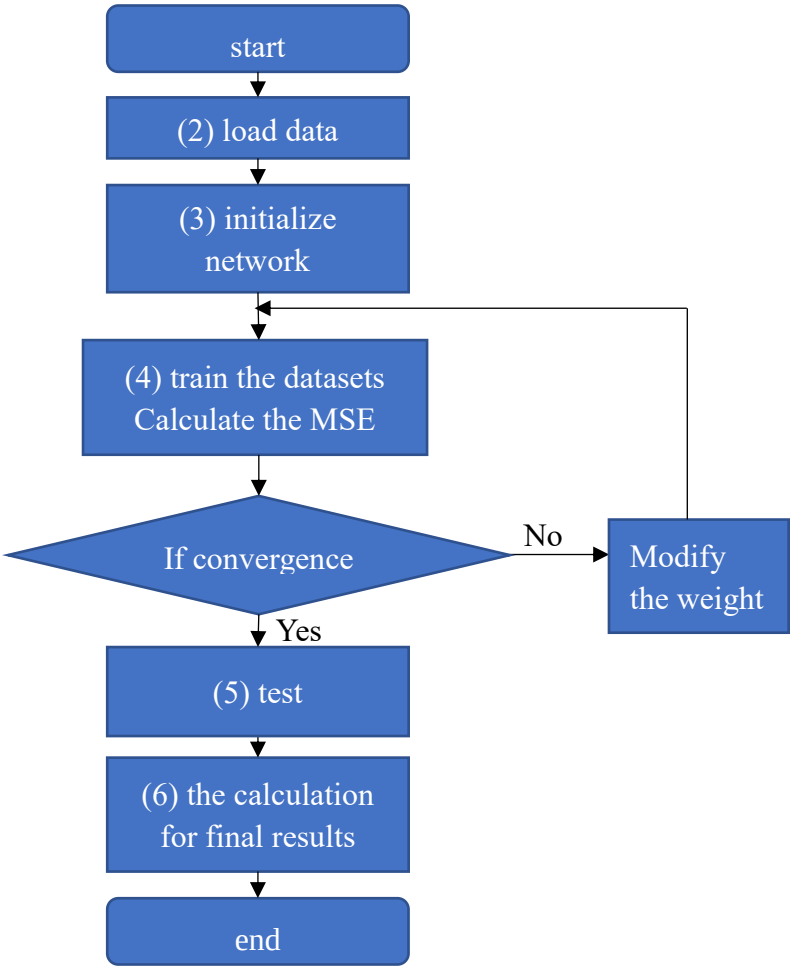

Fig. 3.44 The classification system

In the Fig. 3.44, the first and second step are used to initialize the 15 features from 8 healthy subjects. The numbers of window for training data are shown in Table 3.10 for the classification system. The 15 features are normalized by Minmax algorithm shown in Eq. (3.39),

$$X_n = \frac{x_f - x_{min}}{x_{max} - x_{min}}, \tag{3.39}$$

where the x_f is the value for each feature, the x_{min} is the minimum of x_f, the x_{max} is the maximum of x_f.

Table 3.10: The numbers of window for training data based on the sampling window size of 256 samples

Subject	No movement	Elbow joint of flexion	Elbow joint of extension	Forearm pronation	Forearm supination
1	1612	144	144	136	196
2	1405	144	99	118	134
3	1516	86	75	95	68
4	2121	140	125	150	247
5	1666	279	290	254	271
6	1697	266	283	205	309
7	2170	144	173	141	132
8	1550	316	306	291	297
Total	13737	1519	1495	1390	1654

In the Table 3.10, the total training data for no movement are 13737 windows based on the window size of 256 samples. The total training data for elbow joint of flexion are 1519 windows based on the window size of 256 samples. The total training data for elbow joint of extension are 1495 windows based on the window size of 256 samples. The total training data for forearm pronation are 1390 windows based on the window size of 256 samples. The total training data for forearm supination are 1654 windows based on the window size of 256 samples.

The third step initializes the BP network. The training method is steepest descent method having factor of momentum in batch mode. In addition, the transfer function in hidden layer is Tan-Sigmoid function shown in Eq. (3.40) and Fig. 3.45,

$$tansig(n) = \frac{2}{1 + e^{-2n}} - 1, \tag{3.40}$$

where range of n is minus infinity to infinite and range of $tansig(n)$ is -1 to 1. The tan-sigmoid function works as transform function in the hidden layer or the output layer. The tan-sigmoid with smoothing function and differentiable characteristic is better than the linear function in accuracy and fault tolerance, because tan-sigmoid with nonlinear amplifying function maps to the range of -1 to 1 from the range of minus infinity to infinity. The tan-sigmoid function is used in hidden layer and it achieves the results of hidden layer in a limited range.

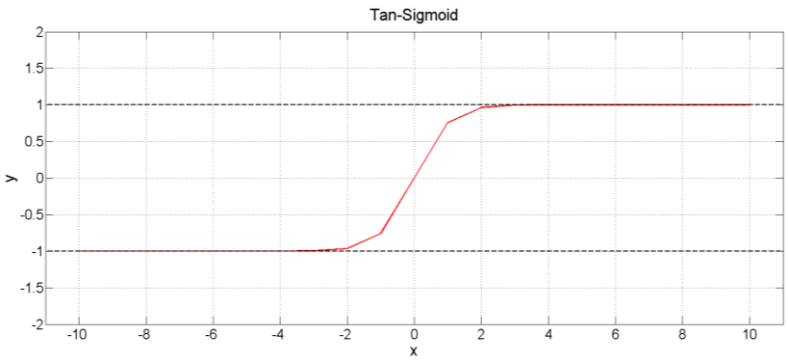

Fig. 3.45 Tan-Sigmoid function

In the third step, the threshold and weight are modified together. It means that there is constant value of one in the input layer. Therefore, a weight of matrix is not only between input layer and hidden layer in size of $3 \times \mathrm{N}$ but also between

hidden layer and output layer in size of $(\mathrm{N}+1)\times 1$, where N is the number of hidden layer node.

Initially, a low random value is assigned for the weight. The number of hidden layer nodes are calculated by Eq. (3.41),

$$I=\sqrt{M+J}+a, \tag{3.41}$$

where M and J are the number of input layer nodes and the number of output layer nodes respectively, a is a constant from 0 to 10.

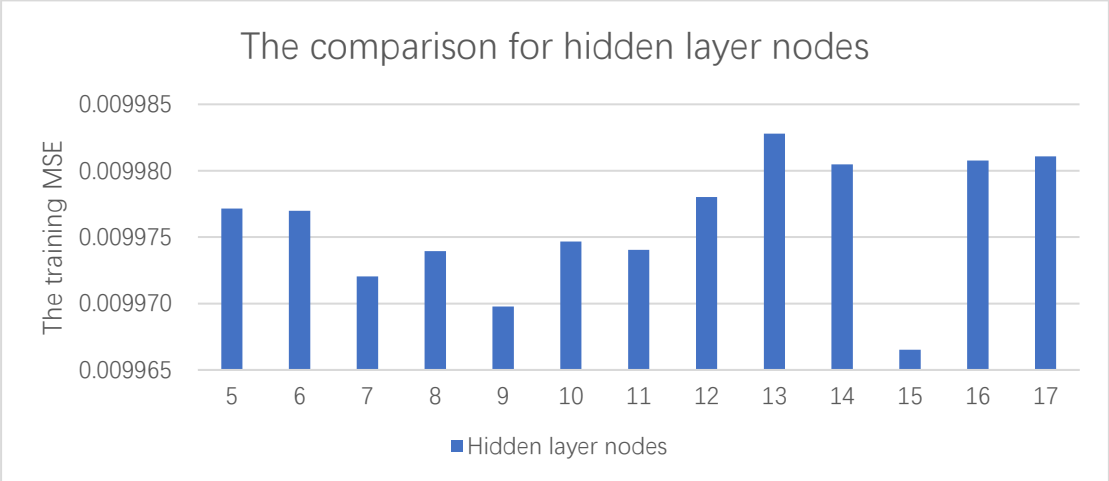

Fig. 3.46 The comparisons based on sampling window size of 256 samples

Furthermore, the BP network with 1 hidden layer nodes to 17 hidden layer nodes are compared based on sampling window size of 256 samples shown in Fig. 3.46. The 1 to 4 hidden layer nodes do not show in the Fig. 3.46, because it does not match the performance goal 0.01. Moreover, the 15 hidden layer nodes of BP network

achieve the best training MSE of 0.009967. The other parameters of BP network are shown in Table 3.11.

Table 3.11: The parameters of BP network

Parameter	Value
The maximum training times	3000
The training MSE goal	0.01
The learning ratio	0.6
The factor of momentum	0.8
The hidden layer nodes	15
The training output for no movement	(0, 0, 1)
The training output for elbow joint of flexion	(0, 1, 0)
The training output for elbow joint of extension	(1, 0, 0)
The training output for forearm pronation	(1, 1, 0)
The training output for forearm supination	(1, 1, 1)

Moreover, the 2 numbers output is not suitable and accurate. Hence, the training output uses 3 numbers to classify five motions. On one hand, the training output for no movement is (0, 0, 1). The training output for the elbow joint of flexion is (0, 1, 0). The training output for the elbow joint of extension is (1, 0, 0). The training output for the forearm pronation is (1, 1, 0). The training output for the forearm pronation is (1, 1, 1). Because the five motions are detected, the training output need at least 3 numbers to separate it.

On the other hand, the testing output for each motion is the same as the training output. Except the 5 testing outputs for each motion, the other results are recognized as no movement. For example, the (0, 0, 0) is recognized as no movement.

In addition, the transfer function in output layers is linear transfer function shown in Fig. 3.47. The equation of linear transfer function $\mathrm{lin}(n)$ is shown in Eq. (3.42), the transfer function achieves the results of output layers from hidden layers. Because the inputs of hidden layers are the data with a limited range, the linear transfer function is used in the output layers, it means that the values of the linear transfer function equal to the values of tan-sigmoid in the BP network.

$$y_{\mathrm{lin}(n)} = \mathrm{x}_{\mathrm{lin}(n)}. \tag{3.42}$$

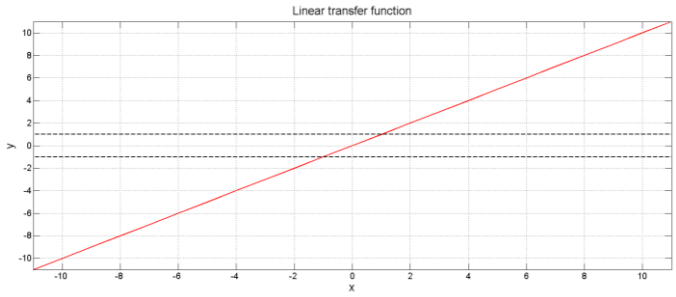

Fig. 3.47 Linear transfer function

The fourth step calculates the MSE, the weight is modified from error and gradient $\frac{\partial e(n)}{\partial \omega_{ij}(n)}$, until the MSE converges. It means that the training times stop at which the MSE is smaller than training MSE goal (error margin). The MSE of training data is shown in Fig. 3.48 to Fig. 3.55 for each healthy subject with sampling window size of 256 samples.

The fifth step tests the classification system. The testing data is also normalized by min-max algorithm. The MSE of testing data is shown in Table 3.12 to Table 3.19.

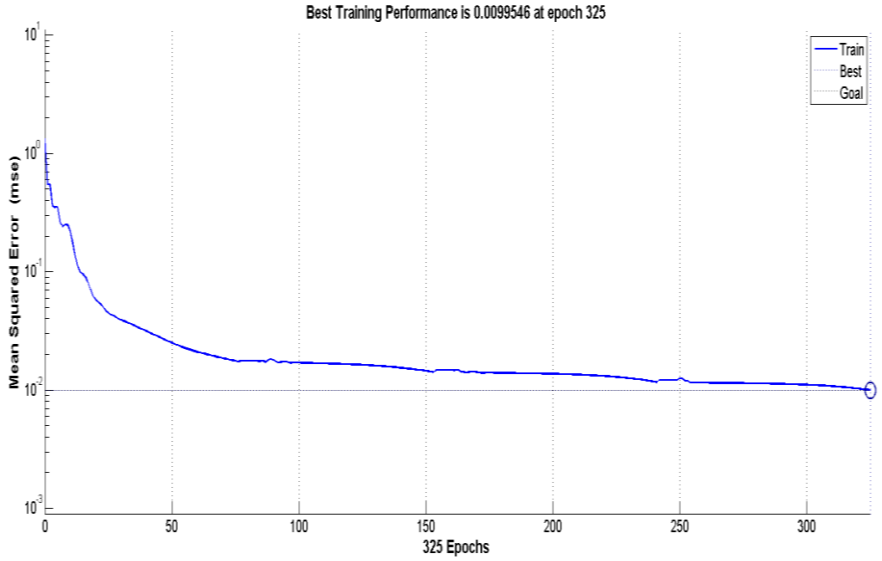

Fig. 3.48 The MSE for Subject 1

The MSE of training data of subject 1 is shown in Fig. 3.48. The best training MSE is 0.0099546 when the classifier is trained 325 times. After the classifier of subject 1 is trained, it is tested by the testing data. The testing result is shown in Table 3.12. The average of testing MSE is 0.0102997. The maximum of testing MSE is 0.0135177. The minimum of testing MSE is 0.0071363.

Table 3.12: The MSE of testing data for subject 1

Subject 1	The testing MSE
Average	0.0102997
Maximum	0.0135177
Minimum	0.0071363

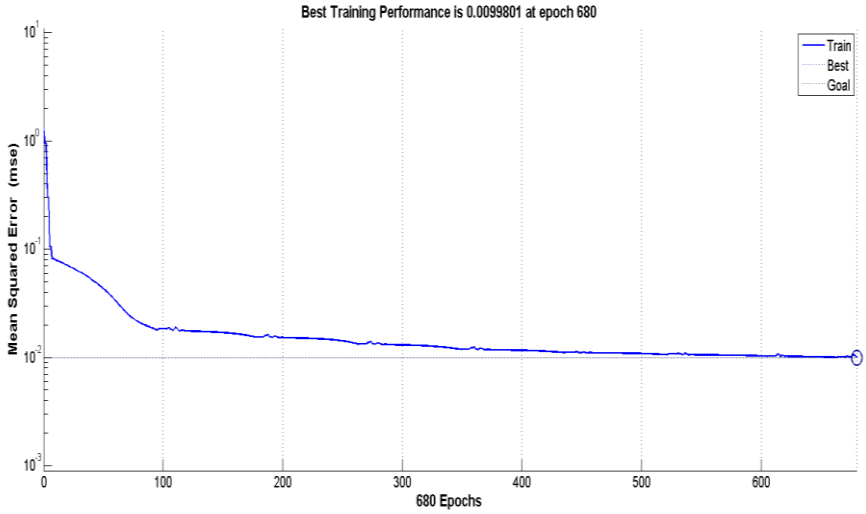

Fig. 3.49 The MSE for subject 2

The MSE of training data of subject 2 is shown in Fig. 3.49. The best training MSE is 0.0099801 when the classifier is trained 680 times. After the classifier of subject 2 is trained, it is tested by the testing data. The testing result is shown in Table 3.13. The average of testing MSE is 0.0117686. The maximum of testing MSE is 0.0176062. The minimum of testing MSE is 0.0048701.

Table 3.13: The MSE of testing data for subject 2

Subject 2	The testing MSE
Average	0.0117686
Maximum	0.0176062
Minimum	0.0048701

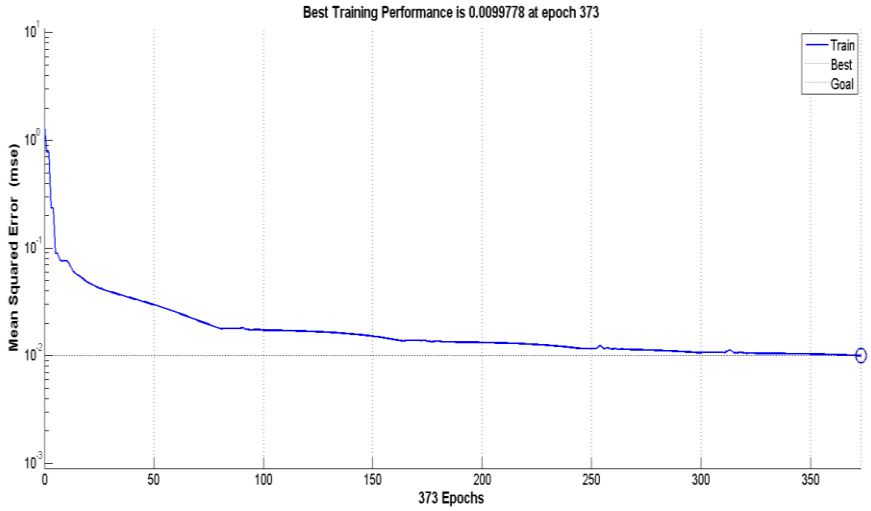

Fig. 3.50 The MSE for subject 3

The MSE of training data of subject 3 is shown in Fig. 3.50. The best training MSE is 0.0099778 when the classifier is trained 373 times. After the classifier of subject 3 is trained, it is tested by the testing data. The testing result is shown in Table 3.14. The average of testing MSE is 0.0104910. The maximum of testing MSE is 0.0138346. The minimum of testing MSE is 0.0069430.

Table 3.14: The MSE of testing data for subject 3

Subject 3	The testing MSE
Average	0.0104910
Maximum	0.0138346
Minimum	0.0069430

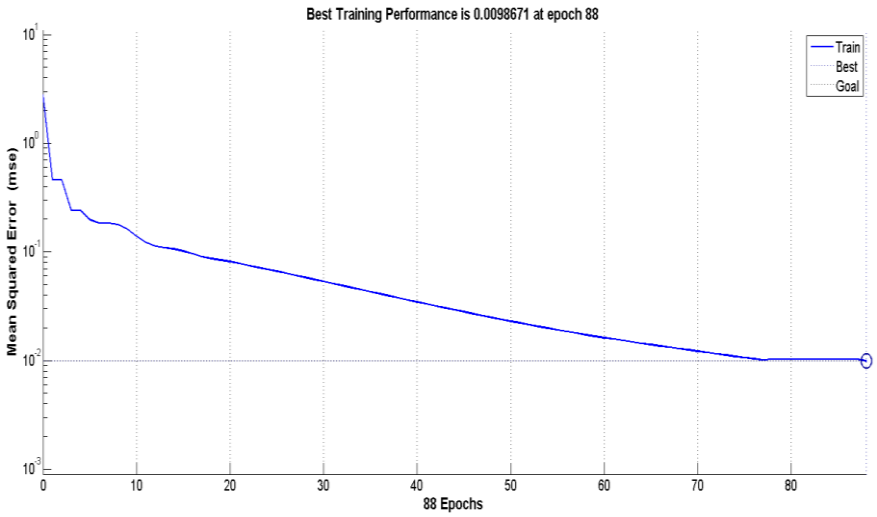

Fig. 3.51 The MSE for subject 4

The MSE of training data of subject 4 is shown in Fig. 3.51. The best training MSE is 0.0098671 when the classifier is trained 88 times. After the classifier of subject 4 is trained, it is tested by the testing data. The testing result is shown in Table 3.15. The average of testing MSE is 0.0108173. The maximum of testing MSE is 0.0125557. The minimum of testing MSE is 0.0085762.

Table 3.15: The MSE of testing data for subject 4

Subject 4	The testing MSE
Average	0.0108173
Maximum	0.0125557
Minimum	0.0085762

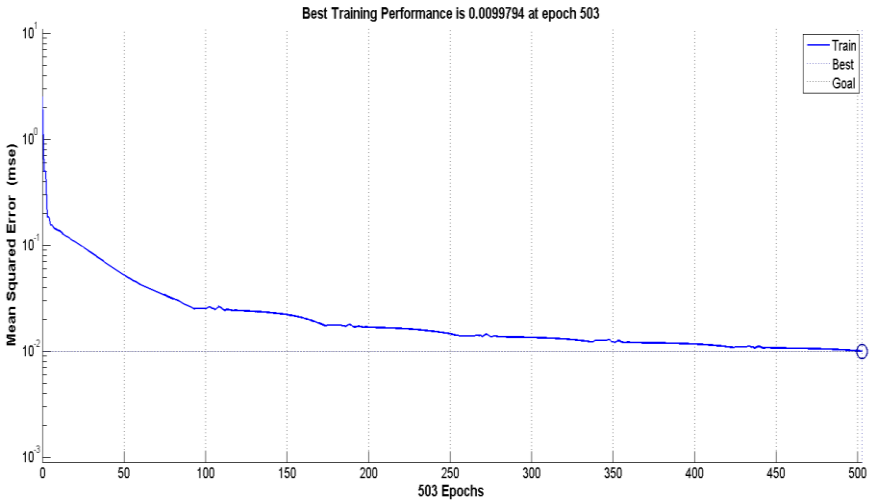

Fig. 3.52 The MSE for subject 5

The MSE of training data of subject 5 is shown in Fig. 3.52. The best training MSE is 0.0099794 when the classifier is trained 503 times. After the classifier of subject 5 is trained, it is tested by the testing data. The testing result is shown in Table 3.16. The average of testing MSE is 0.0103682. The maximum of testing MSE is 0.0110569. The minimum of testing MSE is 0.0091951.

Table 3.16: The MSE of testing data for subject 5

Subject 5	The testing MSE
Average	0.0103682
Maximum	0.0110569
Minimum	0.0091951

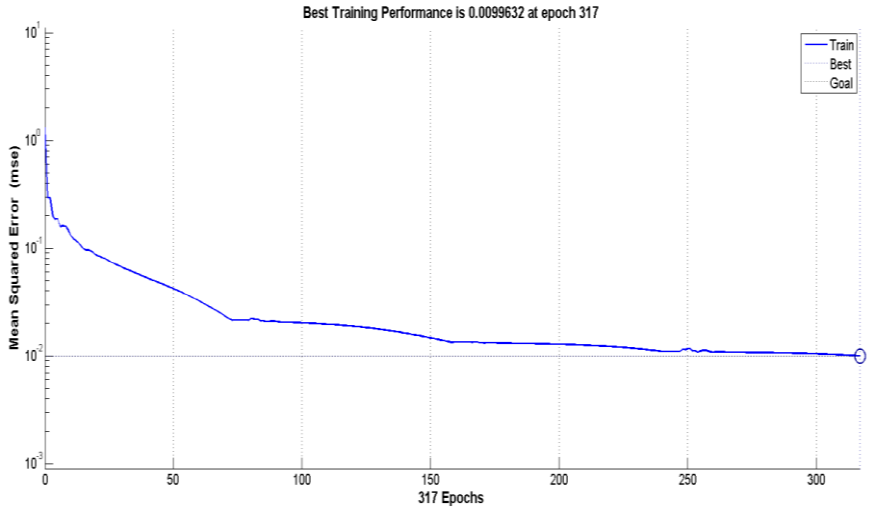

Fig. 3.53 The MSE for subject 6

The MSE of training data of subject 6 is shown in Fig. 3.53. The best training MSE is 0.0099632 when the classifier is trained 317 times. After the classifier of subject 6 is trained, it is tested by the testing data. The testing result is shown in Table 3.17. The average of testing MSE is 0.0113420. The maximum of testing MSE is 0.0149940. The minimum of testing MSE is 0.0096542.

Table 3.17: The MSE of testing data for subject 6

Subject 6	The testing MSE
Average	0.0113420
Maximum	0.0149940
Minimum	0.0096542

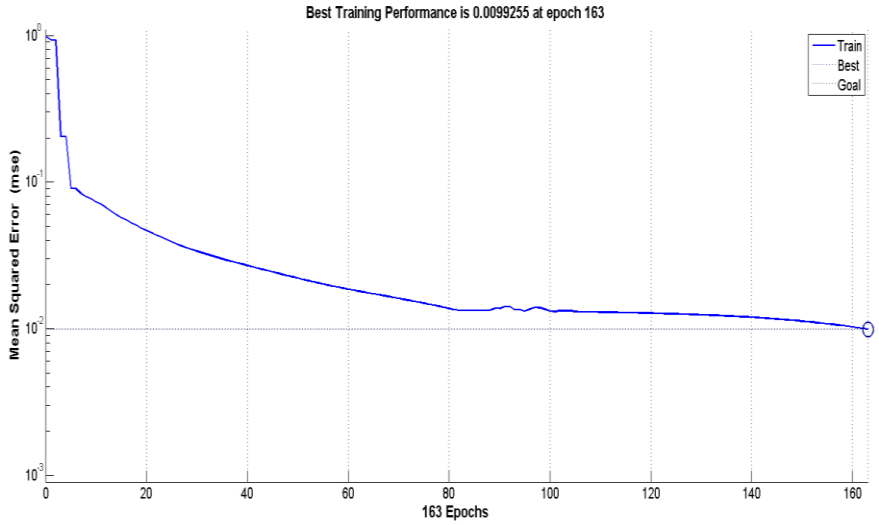

Fig. 3.54 The MSE for subject 7

The MSE of training data of subject 7 is shown in Fig. 3.54. The best training MSE is 0.0099255 when the classifier is trained 163 times. After the classifier of subject 7 is trained, it is tested by the testing data. The testing result is shown in Table 3.18. The average of testing MSE is 0.0108846. The maximum of testing MSE is 0.0126408. The minimum of testing MSE is 0.0090235.

Table 3.18: The MSE of testing data for subject 7

Subject 7	The testing MSE
Average	0.0108846
Maximum	0.0126408
Minimum	0.0090235

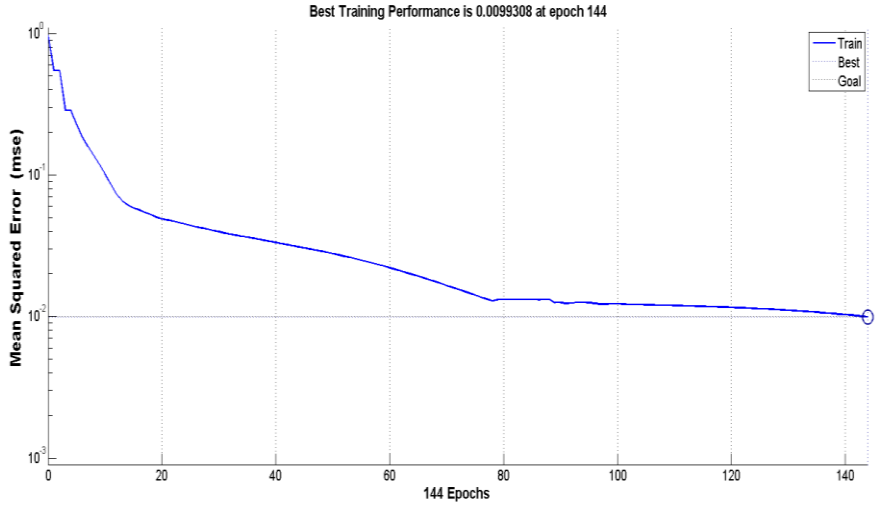

Fig. 3.55 The MSE for subject 8

The MSE of training data of subject 8 is shown in Fig. 3.55. The best training MSE is 0.0099308 when the classifier is trained 144 times. After the classifier of subject 8 is trained, it is tested by the testing data. The testing result is shown in Table 3.19. The average of testing MSE is 0.0102909. The maximum of testing MSE is 0.0116894. The minimum of testing MSE is 0.0087863.

Table 3.19: The MSE of testing data for subject 8

Subject 8	The testing MSE
Average	0.0102909
Maximum	0.0116894
Minimum	0.0087863

In addition, the numbers of windows for test data based on the sampling window size of 256 samples are shown in Table 3.20.

Table 3.20: The numbers of windows for test data

based on the sampling window size of 256 samples

Subject	No movement	Elbow joint of flexion	Elbow joint of extension	Forearm pronation	Forearm supination
1	480	36	24	36	56
2	554	68	42	46	50
3	606	34	28	40	52
4	725	53	42	46	77
5	551	101	105	73	90
6	569	85	93	71	102
7	717	43	65	51	44
8	520	111	101	90	98
Total	4722	531	500	453	569

In the Table 3.20, the total test data for no movement are 4722 windows based on the window size of 256 samples. The total test data for elbow joint of flexion are 531 windows. The total test data for elbow joint of extension are 500 windows. The total test data for forearm pronation are 453 windows. The total test data for forearm supination are 569 windows.

After the test, an example of the output from BP network based on subject 8 is shown in Fig. 3.56. The output results are approximated values based on the training output of motions. Hence, the final step of the K-means clustering method is needed to calculate the final output. The K-means clustering is a method of vector quantization in signal processing area, which is very effective to the cluster analysis of data mining. This method is used to divide the output results into each cluster by which distance between data and mean of cluster is smallest. The distance is calculated by the Euclidean distance shown in Eq. (3.43),

$$D_i = \sqrt{\left(\widehat{y_{i_1}} - y_{i_1}\right)^2 + \left(\widehat{y_{i_2}} - y_{i_2}\right)^2 + \left(\widehat{y_{i_3}} - y_{i_3}\right)^2}, \tag{3.43}$$

where $\widehat{y_{i_1}}$ is the average of first number for output y_{i_1}, $\widehat{y_{i_2}}$ is the average of second number for output y_{i_2}, $\widehat{y_{i_3}}$ is the average of third number for output y_{i_3}. The means of cluster for each motion are shown in Table 3.21 to Table 3.25.

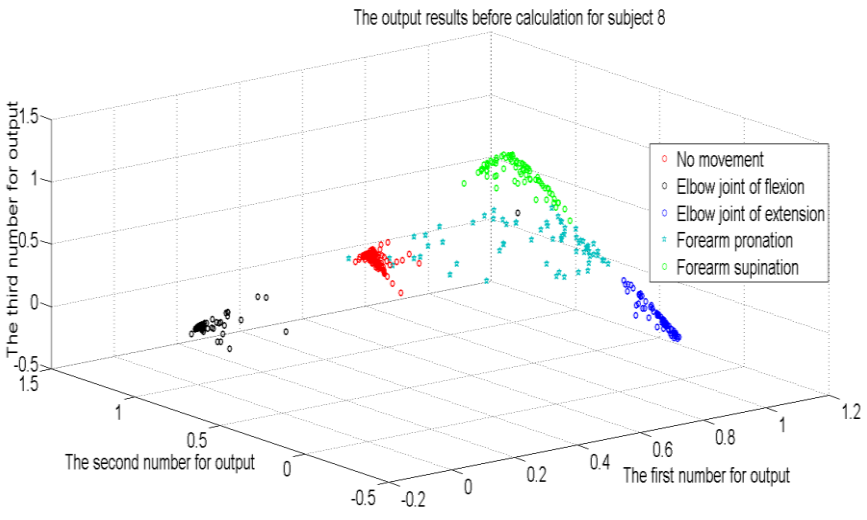

Fig. 3.56 The output from BP network based on subject 8

Table 3.21: The mean of cluster for no movement

Subject	Training output		
	0	0	1
1	-0.00098	0.00049	1.00666
2	-0.04910	0.05306	0.94482
3	-0.00733	-0.00125	0.98059
4	-0.00012	0.03661	0.98126
5	0.00388	0.00494	1.00177
6	0.00761	-0.00091	1.01563
7	0.00830	-0.00291	1.00218
8	-0.00081	-0.00976	0.99647

Table 3.22: The mean of cluster for elbow joint of flexion

Subject	Training output		
	1	1	0
1	0.04119	0.95791	0.01481
2	0.26284	0.14247	0.66625
3	0.03260	0.93757	-0.04039
4	0.08327	1.04136	0.00943
5	0.45318	0.49310	-0.04871
6	0.56800	0.72131	-0.03152
7	0.02152	1.04585	0.20318
8	0.03557	1.00361	-0.03595

Table 3.23: The mean of cluster for elbow joint of extension

Subject	Training output		
	1	0	0
1	0.85230	0.56969	0.09600
2	0.85515	0.33881	0.09539
3	0.94509	0.57344,	0.17949
4	1.15177	0.48781	0.70858
5	0.56312	0.58277	0.04031
6	0.74277	0.73967	0.26387
7	0.91698	0.49453	0.32727
8	0.99866	0.12818	-0.06937

Table 3.24: The mean of cluster for forearm pronation

Subject	Training output		
	1	1	0
1	1.03203	0.52022	0.00546
2	0.94331	0.90580	-0.00950
3	1.01039	0.60328	0.05722
4	0.88267	0.92578	0.26311
5	0.99846	0.93381	0.20171
6	0.51591	0.64055	0.09619
7	1.11634	0.60952	0.17699
8	0.87820	0.70585	0.29507

Table 3.25: The mean of cluster for forearm supination

Subject	Training output		
	1	1	1
1	0.98422	0.95842	0.94397
2	0.89227	0.89491	0.89709
3	0.91794	0.66331	0.81684
4	0.98445	0.65835	0.52696
5	1.06016	0.96558	0.89047
6	1.01550	0.74000	0.81543
7	0.78180	0.70887	0.21994
8	1.02063	1.00579	0.66821

The final outputs are calculated by the K-means clustering method. Specially, the other results except the 5 training outputs for each motion are recognized as no movement. For example, the (0, 0, 0) is recognized as no movement. After that, the final outputs can be used to control an artificial prosthesis. In this thesis, the servo motors are used to simulate the artificial prosthesis.

3.3.7 Control system

In this thesis, the final results are recognized by classification system in Matlab. It means that the user motion intents are realized. Thus, the next component is motor drive to control prosthesis. In this thesis, the robot arm is used to demonstrate the motion recognition of classifier.

In addition, the final results need a controller to connect the 6 degrees of freedom (DOF) robot arm clamp kit shown in Fig. 3.57 for generating the robot arm motions. The Arduino MEGA 2560 shown in Fig. 3.58 is a low cost open-source hardware available designed with a simple microcontroller that is used to control the prosthesis [55]. Its physical computing platform is easy to read and write. This controller has 54 digital input and output pins, 16 analog inputs, 4 hardware serial ports, a 16 MHz crystal oscillator, a power jack, an ICSP header, a USB connection and a reset button. The USB cable simply connects this controller to a computer.

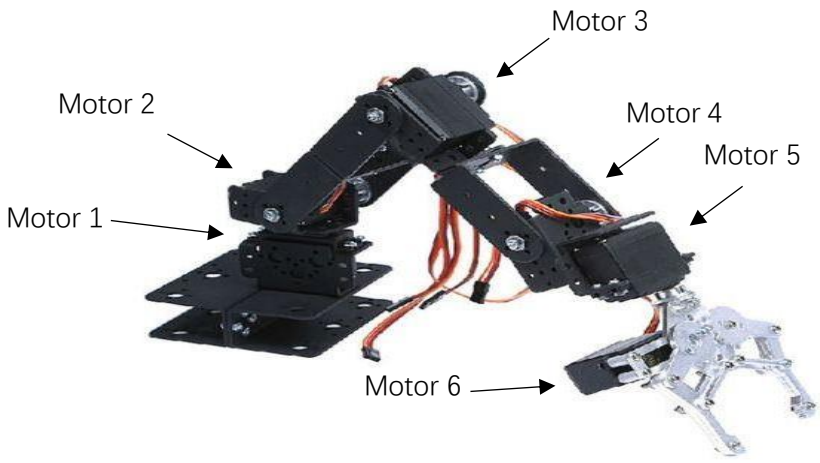

Fig. 3.57 The 6 degrees of freedom (DOF) robot arm clamp kit

Fig. 3.58 The Arduino MEGA 2560

Moreover, the 6 DOF robot arm clamp has 6 the Towardpro MG 996R servo motors shown in Table 3.26. The servo motor provides the precise control of angular or linear position, velocity and acceleration. It shown in Fig. 3.59 consists of 3 lines: (1) power line, (2) ground, (3) control line. The motor functions of prosthesis are: (1) the servo motor 1 is used for upper limb medial rotation or lateral rotation on shoulder, (2) the servo motor 2 is used for arm of abduction or adduction, (3) the servo motor 3 is used for elbow joint of flexion or extension, (4) the servo motor 4 is used for wrist of flexion or extension, (5) the servo motor 5 is used for forearm of pronation or supination, (6) the servo motor 6 is used for holding the hand.

Table 3.26: The information of Towardpro MG 996R servo motor

Modulation	Digital
Torque (4.8 V)	130.54 oz-in (9.40 kg-cm)
Torque (6.0 V)	152.76 oz-in (11.00 kg-cm)
Speed (4.8 V)	0.19 sec/60°
Speed (6.0 V)	0.15 sec/60°
Weight	1.94 oz (55.0 g)
Length	1.60 in (40.7 mm)
Width	0.78 in (19.7 mm)
Height	1.69 in (42.9 mm)
Pulse width	1 ms
Connector type	JR

According to the 4 detected motions in this thesis, the servo motor 3 and 5 are used to control the prosthesis. On the one hand, the servo motor 3 is controlled by final results of elbow joint of flexion and extension. On the other hand, the servo motor 5 is controlled by final results of forearm pronation and supination. The ranges of servo motor 3 and 5 are shown in Table 3.27.

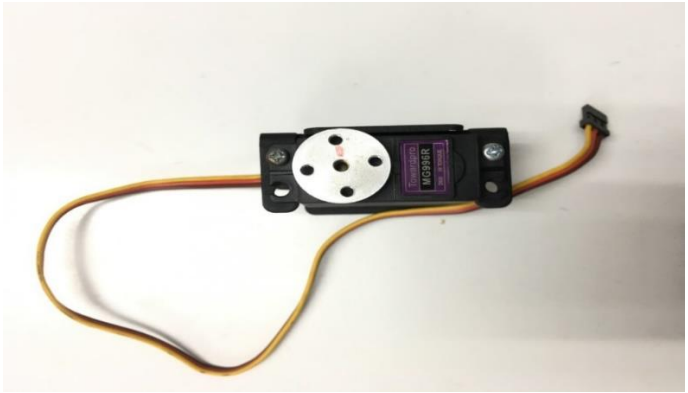

Fig. 3.59 Towardpro MG 996R servo motor

Table 3.27: The range of servo motors

Motor 3	Initial position	Termination of the position
Elbow joint of flexion	0°	150°
Elbow joint of extension	150°	0°
Motor 5	Initial position	Termination of the position
Forearm pronation	0°	225°
Forearm supination	180°	0°

Therefore, two devices are used in control system. The control scheme shown in Fig. 3.60 has 2 steps. At the first step, the final results of numbers of windows for each motion shown in Table 3.28 are sent to Arduino device by the Matlab support package for Arduino hardware. Currently the Matlab enables the computer to communicate the external devices such as sensors, motors, Arduino and so on. In addition, the Matlab Support Package for Arduino Hardware communicates with Arduino devices via Matlab command line interface. This support package provides the ability to set the device communication information and drive the devices function attached to Arduino hardware.

Table 3.28: The final results of numbers of windows for each motion

Test data	Number of windows
No movement	10
Elbow joint of flexion	10
Elbow joint of extension	10
Forearm pronation	10
Forearm supination	10

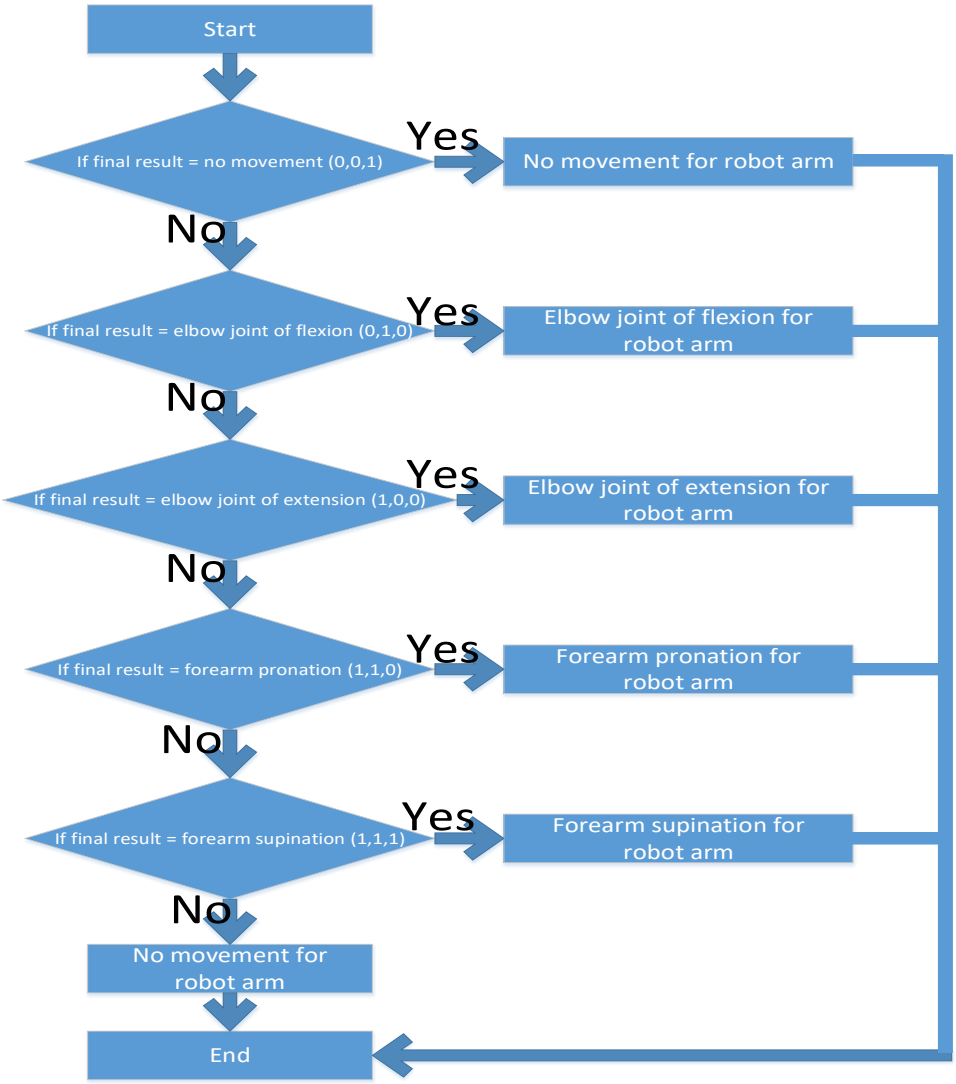

Fig. 3.60 The control scheme

At the second step, the controller will move the robot arm accordingly. It means that if the final result is no movement (0,0,1), the controller generates the no movement to robot arm. If the final result is not no movement (0,0,1), the final result is sent to the next judgment layer. The second judgment layer controls the robot arm to do elbow joint of flexion if the final result is elbow joint of flexion (0,1,0) and so on, the robot arm of elbow joint of extension is activated by the final result which is elbow

joint of extension (1,0,0) in third judgment layer, the final result which is forearm pronation (1,1,0) controls the robot arm to activate forearm pronation in fourth judgment layer, the robot arm of forearm supination is generated with final result which is forearm supination (1,1,1) in the fifth judgment layer. After that, the other results except the 5 final results for each motion are recognized as no movement. For example, the (0, 0, 0) is recognized as no movement. Moreover, the robot arm follows the range of each motion in Table 3.25: (1) the robot arm of elbow joint of flexion is activated from 0° to 150°, (2) the robot arm of elbow joint of extension is activated from 150° to 0°, (3) the robot arm of forearm pronation is activated from 225° to 0°, (4) the robot arm of forearm supination is activated from 180° to 0°.

In addition, the control panel shown in Fig. 3.61 is generated by Matlab with guide graphical user interface. It is a self-contained function in Matlab applications with GUI front ends that automate a task or calculation and it typically contains many controls, including buttons, toolbars, menus and sliders. This function builds many Matlab products with custom user interfaces.

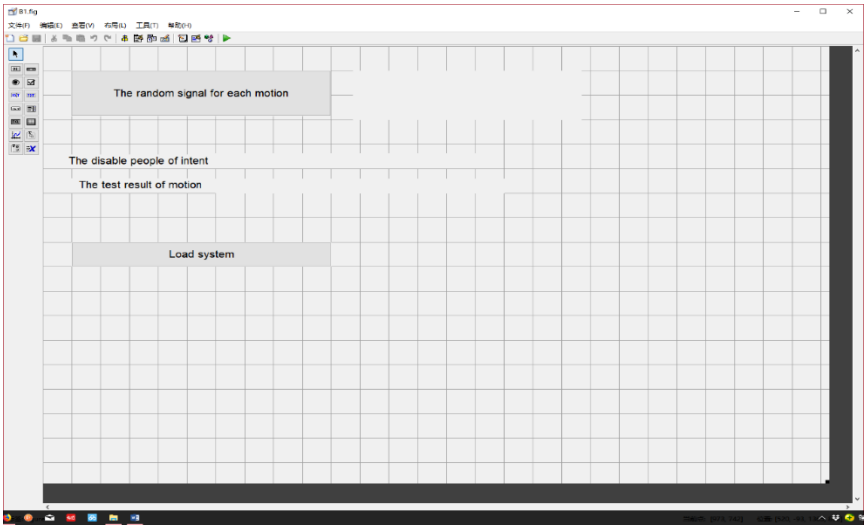

Fig. 3.61 The control panel

The function of the button named ‘Load system’ in Fig. 3.61 is initialization of the classification system and control system. It means that the NNT is trained and the control system is loaded. Next, the button named ‘The random signal for each motion’ in Fig. 3.61 is used to process the random case of sEMG signals with the whole system. Initially, the random case of sEMG signals of 3 channels are passed through the band-pass filter and processed by the denoised system. Then, all five features are extracted. After that, the five features are used to train and test BP network and the final result is calculated by k-means clustering algorithm. Hence, the final result is shown in the monitor 2. The user intent motion is shown in the monitor 3 at the same time. If the results between final result and user intent motion are equal, the monitor 1 displays ‘Correct recognition’ shown in Fig. 3.61. The monitor 1 displays ‘Wrong recognition’ when the results are not equal. In addition, an example of the control panel is shown in Fig. 3.62.

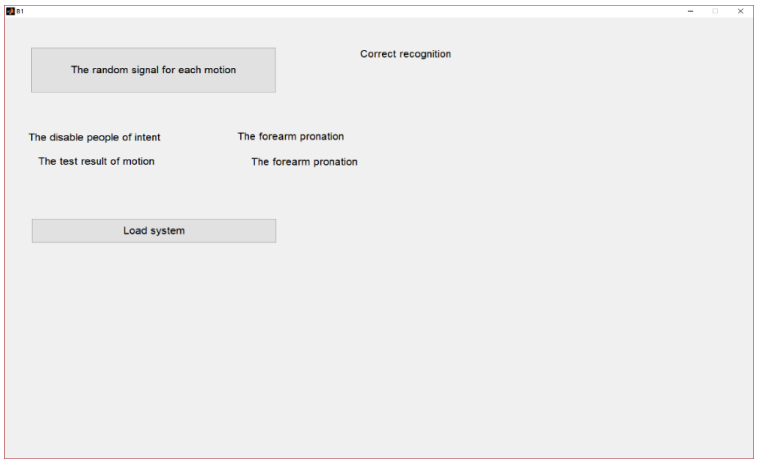

Fig. 3.62 An example of the control panel

In the Fig. 3.62, the user intent motion is the forearm pronation. The test result outputs the forearm pronation by the system. Hence, the middle top area of the control panel shows the ‘Correct recognition’.

CHAPTER 4

Result

4.1 The result for the electrical noise reduction in the signal measurement and the pre-processing system

As the methodology describes, the electrical noise is reduced by the band-pass filter in signal measurement system and the denoised system in the pre-processing system. The benefits of the band-pass filter shown in Table 4.1 are calculated by Eq. (4.1) based on 8 subjects in channel 1.

$$\mathrm{N}_{filtered} = \frac{\overline{n_{raw}} - \overline{n_{filtered}}}{\overline{n_{raw}}} \times 100\%, \tag{4.1}$$

where the $\overline{n_{raw}}$ is the average electrical noise in the raw sEMG signal of channel 1 for each motion, $\overline{n_{filtered}}$ is the average electrical noise in the filtered sEMG signal of channel 1 for each motion.

Moreover, the benefits of the denoised system shown in Table 4.1 are calculated by Eq. (4.2) based on 8 subjects in channel 1.

$$\mathrm{N}_{denoised} = \frac{\overline{n_{filtered}} - \overline{n_{denoised}}}{\overline{n_{filtered}}} \times 100\%, \tag{4.2}$$

where the $\overline{n_{filtered}}$ is the average electrical noise in the filtered sEMG signal of channel 1 for each motion, $\overline{n_{denoised}}$ is the average electrical noise in the denoised sEMG signal of channel 1 for each motion.

Table 4.1: The benefits of the band-pass filter and the denoised system

based on 8 subjects in channel 1

Motion	The electrical noise at 50 Hz in raw sEMG signal (dB)	The electrical noise at 50 Hz in filtered sEMG signal (dB)	The electrical noise at 50 Hz in denoised sEMG signal (dB)
No movement	29.75	14.28	12.91
Elbow joint of flexion	31.91	15.63	13.57
Elbow joint of extension	29.88	14.63	13.22
Forearm pronation	29.85	14.61	13.15
Forearm supination	31.73	15.34	13.45

In the Table 4.1, the benefits of band-pass filter and denoised system are calculated based on 8 subjects in channel 1. The electrical noise of no movement in the raw sEMG signal of channel 1 is reduced 52% by the band-pass filter. The electrical noise of elbow joint of flexion is reduced 51.02% by the band-pass filter. The electrical noise of elbow joint of extension is reduced 51.04% by the band-pass filter. The electrical noise of forearm pronation is reduced 51.06% by the band-pass filter. The electrical noise of forearm supination is reduced 51.65% by the band-pass filter.

Moreover, the electrical noise of no movement in the filtered sEMG signal of channel 1 is reduced 9.59% by the denoised system. The electrical noise of elbow joint of flexion is reduced 13.18% by the denoised system. The electrical noise of elbow joint of extension is reduced 9.64% by the denoised system. The electrical

noise of forearm pronation is reduced 9.99% by the denoised system. The electrical noise of forearm supination is reduced 12.32% by the denoised system.

In conclusion, the electrical noise of no movement in the raw sEMG signal of channel 1 is reduced 56.61% by the band-pass filter and the denoised system. The electrical noise of elbow joint of flexion is reduced 57.47%. The electrical noise of elbow joint of extension is reduced 55.76%. The electrical noise of forearm pronation is removed 55.95%. The electrical noise of forearm supination is removed 57.61%. Therefore, the band-pass filter and the denoised system cause 56.68% reduction of electrical noise in channel 1. It also achieves the electrical noise reduction in other 2 channels.

4.2 The result for the classifier of 2 channels

According to the methodology, this thesis has four systems: (1) the signal measurement system, (2) the pre-processing system, (3) the classification system, (4) the control system. Moreover, the structure of the classifier of 2 channels is shown in Fig. 4.1. The difference between the classifier of 2 channels and 3 channels is only the input layer nodes shown in Fig. 4.2. The classifier of 2 channels removes the channel of triceps of long head.

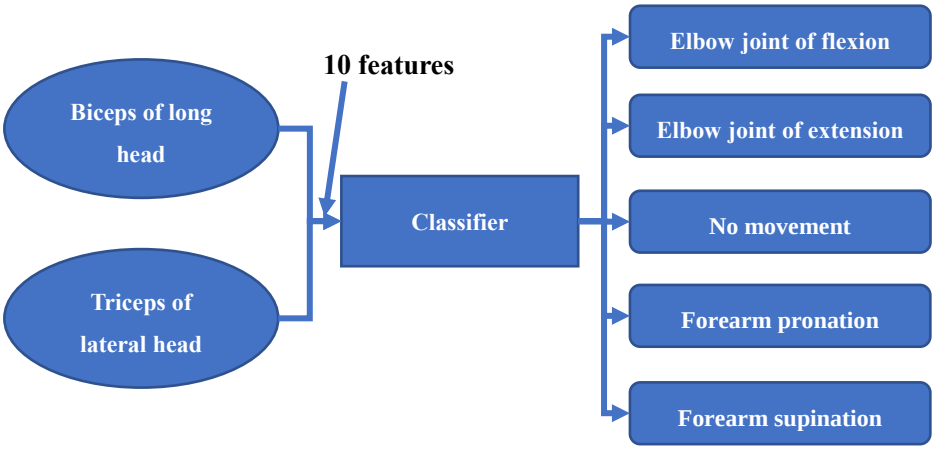

Fig. 4.1 The structure of the classifier of 2 channels

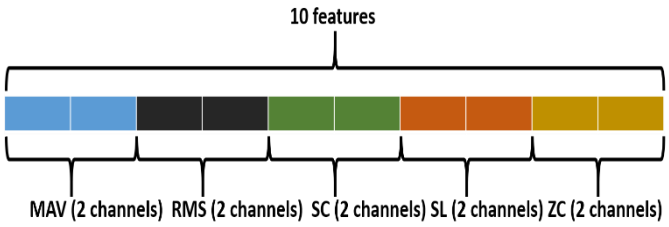

Fig. 4.2 The structure of input layer for the classifier of 2 channels

After the classifier of 2 channels is tested, the result for sampling window size comparison is shown in Fig. 4.3. The sampling window size of 1024

samples, 512 samples, 256 samples and 128 samples are compared. The numbers of window for training data and test datasets measured in the experiment are based on each sampling window size shown in Table 4.2. Moreover, the test datasets of each motion are different, because the classifier is user-dependent. It means that the test results have reference value to the daily use.

Table 4.2: The numbers of window for training data and test data based on each sampling window size of 8 subjects

The numbers of window for training data				
The sampling window size	1024 samples	512 samples	256 samples	128 samples
No movement	3431	6865	13737	27473
Elbow joint of flexion	379	758	1519	3037
Elbow joint of extension	372	746	1495	2990
Forearm pronation	346	695	1390	2779
Forearm supination	413	826	1654	3308
The numbers of window for test data				
The sampling window size	1024 samples	512 samples	256 samples	128 samples
No movement	1180	2361	4722	9444
Elbow joint of flexion	132	265	531	1063
Elbow joint of extension	125	250	500	1001
Forearm pronation	113	226	453	906
Forearm supination	142	284	569	1138

In the Table 4.2, the numbers of window for training data and test data based on the window size of 1024 samples, 512 samples, 256 samples and 128 samples are shown. In the test data based on window size of 1024 samples, the test data for no

movement are 1180 windows based on the window size of 1024 samples. The test data for elbow joint of flexion are 132 windows based on the window size of 1024 samples. The test data for elbow joint of extension are 125 windows based on the window size of 1024 samples. The test data for forearm pronation are 113 windows based on the window size of 1024 samples. The test data for forearm supination are 142 windows based on the window size of 1024 samples. The details for the window sizes of 512 samples, 256 samples and 128 samples are shown in Table 4.2.

Moreover, the sEMG signal is processed based on the sampling window basis. The total delay time and the average accuracy of 8 healthy subjects in each window size are shown in Fig. 4.3. All of results are calculated by the average of the 10 identical experiments and the classification is done on each window independently.

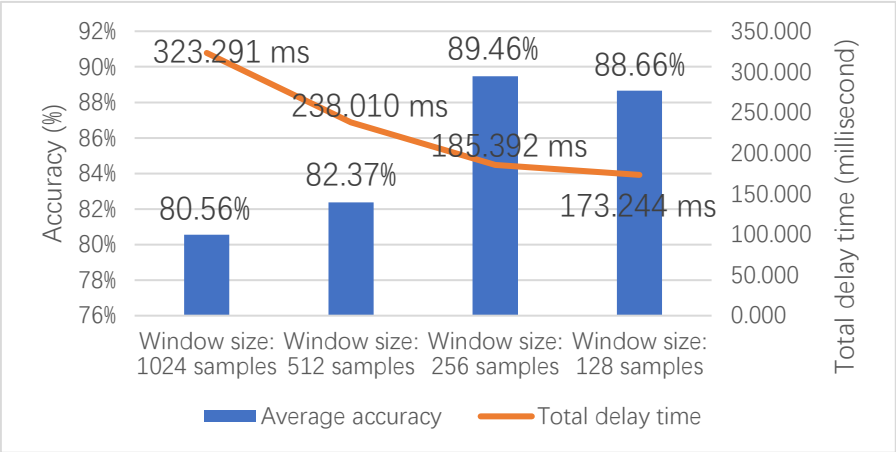

Fig. 4.3 The result for sampling window size comparison based on the classifier of 2 channels

In the Fig. 4.3, the sampling window size of 1024 samples outputs the accuracy of 80.56% for the classifier of 2 channels. The sampling window size of 512 samples gives the accuracy of 82.37%. The sampling window size of 256 samples achieves the best accuracy that is 89.46. The sampling window size of 128 samples provides the accuracy of 88.66%. As a result, the sampling window size of 256 samples is the best for the accuracy of the motion detection in the classifier of 2 channels.

Furthermore, the sampling window size of 1024 samples has the total delay time of 323.291 milliseconds. The sampling window size of 512 samples gives the total delay time of 238.010 milliseconds. The sampling window size of 256 samples provides the total delay time of 185.392 milliseconds. The sampling window size of 128 samples outputs the shortest total delay time of 173.544 milliseconds. In addition, the user can accept the total delay time up to 300 milliseconds to 400 milliseconds, so that the sampling window size of 256 samples achieves not only the acceptable delay

time, but also the best accuracy. The sampling window size of 256 samples in classifier of 2 channels is better than other sampling window sizes for disable people to use.

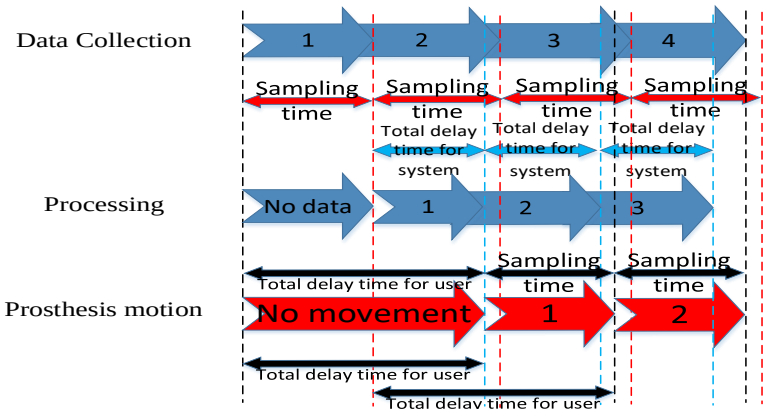

Fig. 4.4 The system timeline for classifier of 2 channels

The system timeline for the classifier of 2 channels is shown in Fig. 4.4. The complete system requires raw sEMG signal to enter into the signal measurement system first, then the pre-processing system, classification system and control system are used to drive the prosthesis. It means that the users have to wait 441.392 milliseconds to drive the artificial robot arm. The delay time in each component of system is shown in Table 4.3 to Table 4.6. All of results are calculated by the average of the 10 identical experiments.

Table 4.3: The delay time based on window size of 1024 samples

Component	Delay time (ms)	Std. (ms)
Pre-processing (denoised system)	149.199	3.580
Pre-processing (features extraction)	119.656	14.437
Classification	54.437	1.297
Total	323.291	15.725

In the Table 4.3, the delay time based on window size of 1024 samples in each component of system is shown. The delay time in the denoised system is 149.199 milliseconds and the standard deviation is 3.580 milliseconds. The delay time in the features extraction system is 119.656 milliseconds and the standard deviation is 14.437 milliseconds. The delay time in the classification system is 54.437 milliseconds and the standard deviation is 1.297 milliseconds. Hence, the total delay time in the pre-processing system and the classification system is 323.291 milliseconds and the standard deviation is 15.725 milliseconds. It is not suitable to use, because the users have to wait 1347.291 milliseconds to drive the artificial robot arm.

Table 4.4: The delay time based on window size of 512 samples

Component	Delay time (ms)	Std.
Pre-processing (denoised system)	131.304	57.324
Pre-processing (features extraction)	53.579	2.142
Classification	53.126	0.794
Total	238.010	58.052

In the Table 4.4, the delay time based on window size of 512 samples in each component of system is shown. The delay time in the denoised system is 131.304 milliseconds and the standard deviation is 57.324 milliseconds. The delay time in the features extraction system is 53.579 milliseconds and the standard deviation is 2.142 milliseconds. The delay time in the classification system is 53.126 milliseconds and the standard deviation is 0.794 milliseconds. Hence, the total delay time in the pre-processing system and the classification system is 238.010 milliseconds and the standard deviation is 58.052 milliseconds. It is not suitable to use, because the users have to wait 750.010 milliseconds to drive the artificial robot arm.

Table 4.5: The delay time based on window size of 256 samples

Component	Delay time (ms)	Std.
Pre-processing (denoised system)	108.695	52.008
Pre-processing (features extraction)	23.564	1.574
Classification	53.134	2.585
Total	185.392	53.284

In the Table 4.5, the delay time based on window size of 256 samples in each component of system is shown. The delay time in the denoised system is 108.695 milliseconds and the standard deviation is 52.008 milliseconds. The delay time in the features extraction system is 23.564 milliseconds and the standard deviation is 1.574 milliseconds. The delay time in the classification system is 53.134 milliseconds and the standard deviation is 2.585 milliseconds. Hence, the total delay time in the pre-processing system and the classification system is 185.392 milliseconds and the standard deviation is 53.284 milliseconds. It is suitable to use, because the users have to wait 441.392 milliseconds to drive the artificial robot arm and the sampling window size of 256 samples provides the best accuracy in the classifier of 2 channels.

Table 4.6: The delay time based on window size of 128 samples

Component	Delay time (ms)	Std.
Pre-processing (denoised system)	106.782	35.531
Pre-processing (features extraction)	13.313	0.718
Classification	53.148	1.799
Total	173.244	35.063

In the Table 4.6, the delay time based on window size of 128 samples in each component of system is shown. The delay time in the denoised system is 106.782 milliseconds and the standard deviation is 35.531 milliseconds. The delay time in the features extraction system is 13.313 milliseconds and the standard deviation is 0.718 milliseconds. The delay time in the classification system is 53.148 milliseconds and the standard deviation is 1.799 milliseconds. Hence, the total delay time in the pre-processing system and the classification system is 173.244 milliseconds and the standard deviation is 35.063 milliseconds. Therefore, the users have to wait 301.244 milliseconds to drive the artificial robot arm. It is not suitable to use, because and the sampling window size of 128 samples provides the lower accuracy than the sampling window size of 256 samples in the classifier of 2 channels.

In conclusion, the sampling window size of 256 samples achieves the best accuracy 89.46% and the acceptable delay time 441.392 milliseconds in the classifier of 2 channels based on 8 healthy subjects.

4.3 The comparison for the classifier of 2 channels

In order to detect the best accuracy in classifier of 2 channels, the channel 1 of biceps of long head and the channel 3 of triceps of long head are compared. Because the proposed method utilizes the channel 2 of triceps of lateral head to activate the forearm pronation in section 3.1. In this comparison, the classifier of the channel 1 of biceps of long head and the channel 2 of triceps of lateral head shown in Fig. 4.5 is defined as A. The classifier of the channel 2 of triceps of lateral head and the channel 3 of triceps of long head shown in Fig. 4.6 is defined as B. The comparison of classifier A and the classifier B is shown in Fig. 4.7. All of results are calculated by the average of the 10 identical experiments.

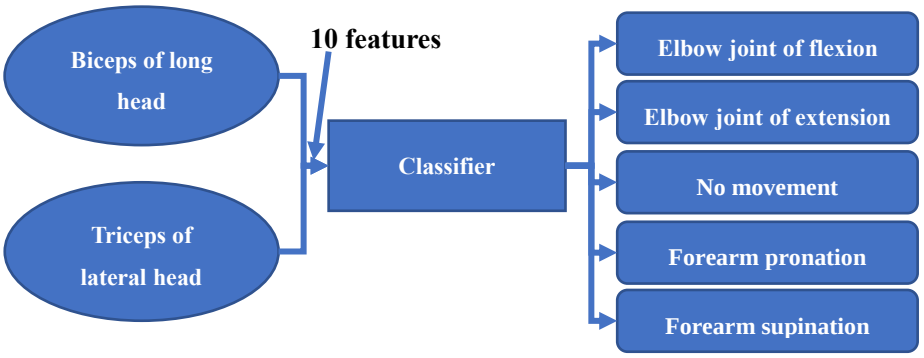

Fig. 4.5 The structure of the classifier A

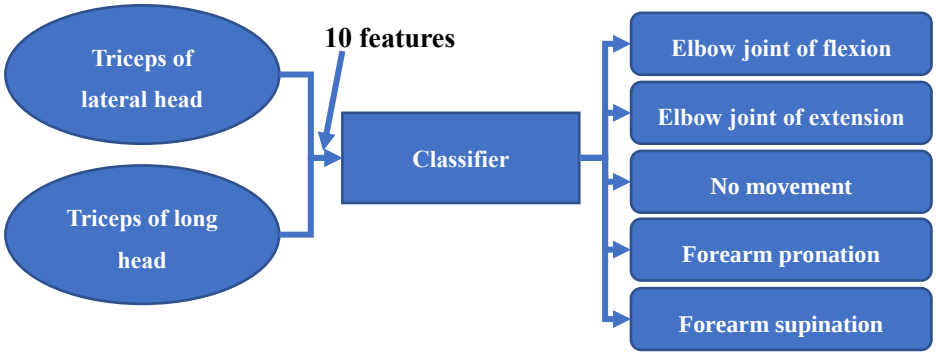

Fig. 4.6 The structure of the classifier B

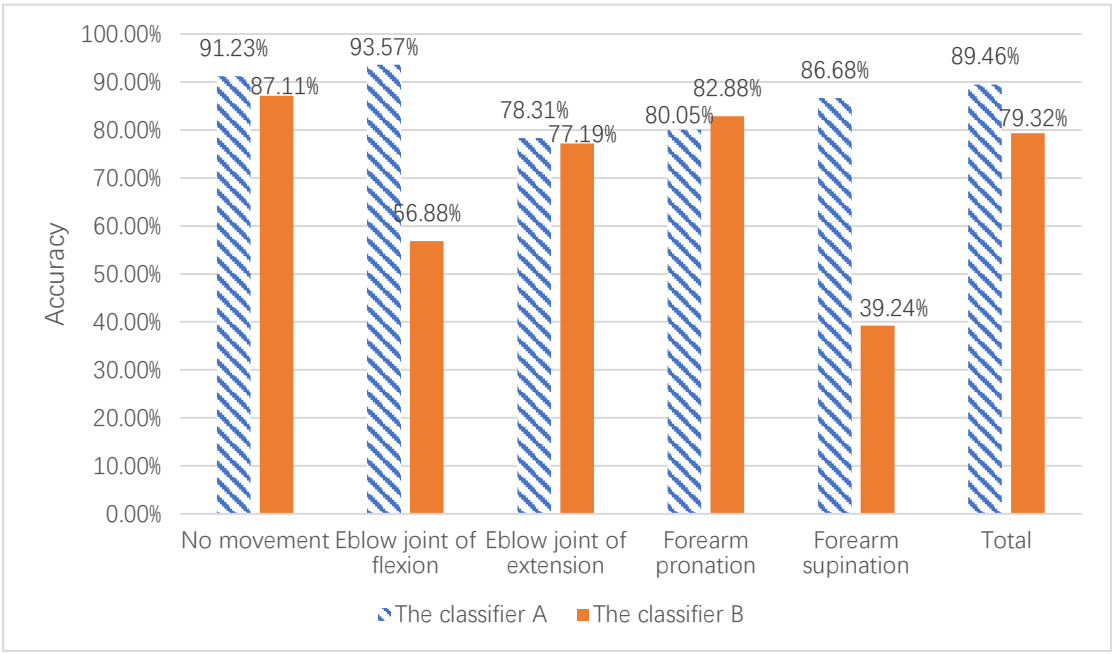

Fig. 4.7 The comparison of classifier A and the classifier B

In the Fig. 4.7, the accuracy of the classifier A is 4.12% higher than the classifier B in the no movement. The accuracy of the classifier A is 36.69% higher than the classifier B in the elbow joint of flexion. The accuracy of the classifier A is 36.69% higher than the classifier B in the elbow joint of flexion. The accuracy of the classifier A is 1.12% higher than the classifier B in the elbow joint of extension. The accuracy of the classifier A is 2.83% lower than the classifier B in the forearm pronation. The

accuracy of the classifier A is 47.44% higher than the classifier B in the forearm supination. The total accuracy of the classifier A is 10.14% higher than the classifier B in five motions.

In conclusion, the classifier A is more accurate than the classifier B. Hence, the biceps of long head and the triceps of lateral head are used in the classifier, which achieves the higher accuracy.

4.4 The result for the classifier of 3 channels

In addition, the classifier of 3 channels shown in methodology is an extend model based on the classifier of 2 channels. The datasets are same as the classifier of 2 channels in Table 4.2.

4.4.1 The comparison for 1 hidden layer node to 17 hidden layer nodes in the classifier of 3 channels

Moreover, the numbers of hidden layer nodes affect the performance of classifier. If the numbers are too small, the correlation of data that the BP network needed is not enough to estimate the motions accurately. If the numbers are too large, it leads to the classifier in overfitting and the training time is increased. In order to achieve the best accuracy, the 1 hidden layer node to 17 hidden layer nodes are compared shown in Fig. 4.8. In fact, the 15 hidden layer nodes are used into the classifier of 2 channels and 3 channels. All of results are calculated by the average of the 10 identical experiments.

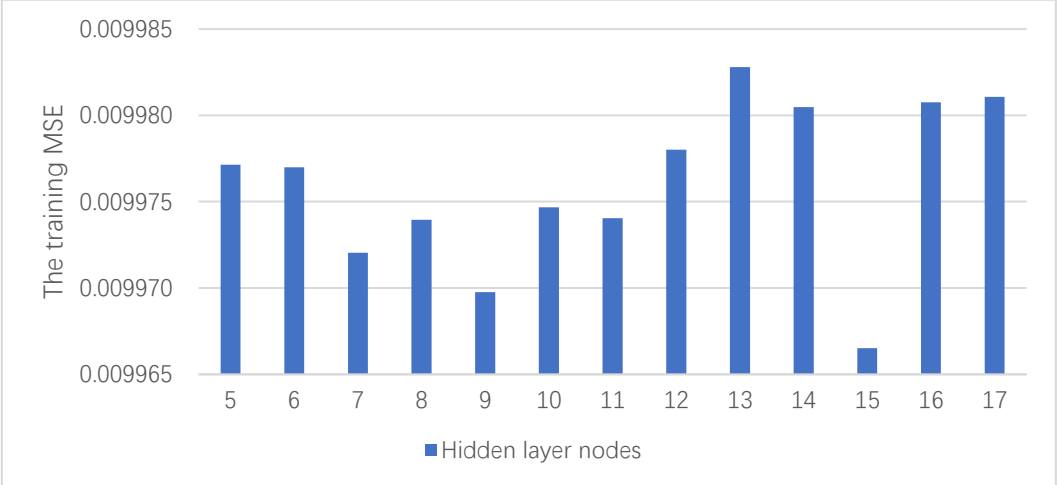

Fig. 4.8 The comparison for hidden layer nodes

In the Fig. 4.8, the 15 hidden layer nodes provide the best training MSE which is 0.009967. However, the training MSE of the 1 hidden layer node to the 4 hidden layer nodes outputs the correlation of data for classifier that is not enough, so it does not match the performance goal 0.01 and it does not show in the Fig. 4.8.

In conclusion, the 15 hidden layer nodes provide the best training MSE and it is applied into the classifier of 3 channels.

4.4.2 The comparison for training output of each motion

The section 4.4.1 compares the 1 hidden layer node to 17 hidden layers nodes in the classifier of 3 channels. The 2 numbers to 4 numbers for training output shown in Table 4.8 are compared in this section. In addition, the 0, 1 and -1 are used for the training output, experientially. The tan-sigmoid is used into the classifier of 3 channels and the range of training output is -1 to 1 which is used for 2 numbers of the training output, because the classifier recognizes five motions. The range of 0 to 1 is used for 3 numbers and 4 numbers of training output, which is enough to detect five motions.

Table 4.7: The 2 numbers to 4 numbers for training output

Motion	2 numbers for training output	3 numbers for training output	4 numbers for training output
No movement	(0,1)	(0,0,1)	(0,0,0,0)
Elbow joint of flexion	(1,0)	(0,1,0)	(1,0,0,0)
Elbow joint of extension	(1,1)	(1,0,0)	(0,1,0,0)
Forearm pronation	(-1,1)	(1,1,0)	(0,0,1,0)
Forearm supination	(-1,-1)	(1,1,1)	(0,0,0,1)

The accuracies of the 2 numbers to 4 numbers training output in the classifier of 3 channels are compared based on the subject 8 and it is shown in Table 4.9. All of results are calculated by the average of the 10 identical experiments.

Table 4.8: The result for the 2 numbers to 4 numbers training output based on subject 8

Motion	2 numbers for training output	3 numbers for training output	4 numbers for training output
No movement	94.78%	99.91%	91.90%
Elbow joint of flexion	91.35%	99.18%	95.00%
Elbow joint of extension	78.33%	98.65%	79.25%
Forearm pronation	86.82%	97.62%	82.16%
Forearm supination	93.45%	98.70%	95.80%
Average accuracy	92.47%	99.54%	91.45%

In the Table 4.9, the training output of 3 numbers provides the best accuracy. The training output of 4 numbers gives the worst accuracy. The elbow joint of extension and forearm pronation are not detected well by the training output of 2 numbers and 4 numbers.

In conclusion, the best accuracy is achieved by the classifier of 3 channels. The input data is based on the sampling window size of 256 samples. The classifier has 1 input layer, 1 hidden layer and 1 output layer. 15 input layer nodes, 3 hidden layer nodes and 3 output layer nodes are utilized into the classifier of 3 channels.

An example of the classifier of 3 channels for subject 8 is shown in Fig. 4.10 and the structure for the classifier of 3 channels is shown in Fig. 4.11.

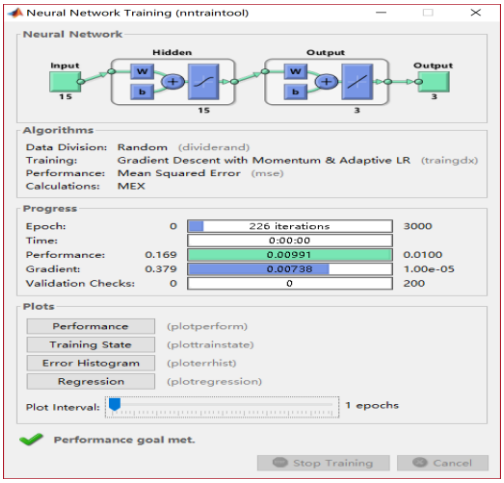

Fig. 4.9 The classifier of 3 channels for subject 8

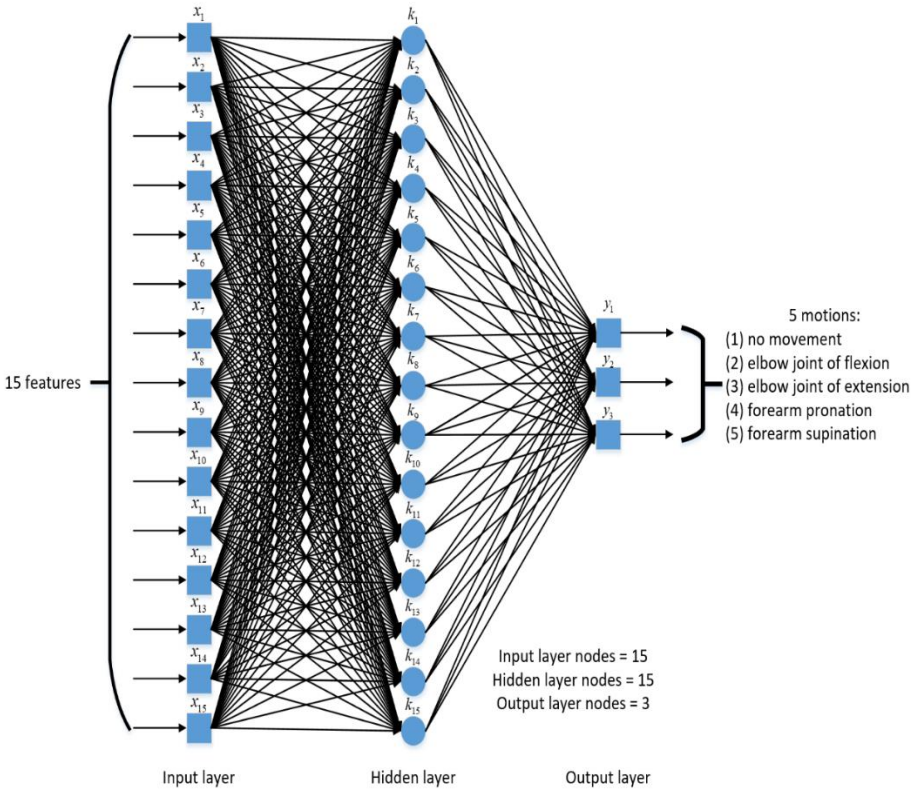

Fig. 4.10 The structure of BP network for the classifier of 3 channels

4.4.3 The delay time for the classifier of 3 channels

The total delay time shown in Fig. 4.11 and Table 4.9 only increases 18.904 milliseconds that is 460.296 milliseconds.

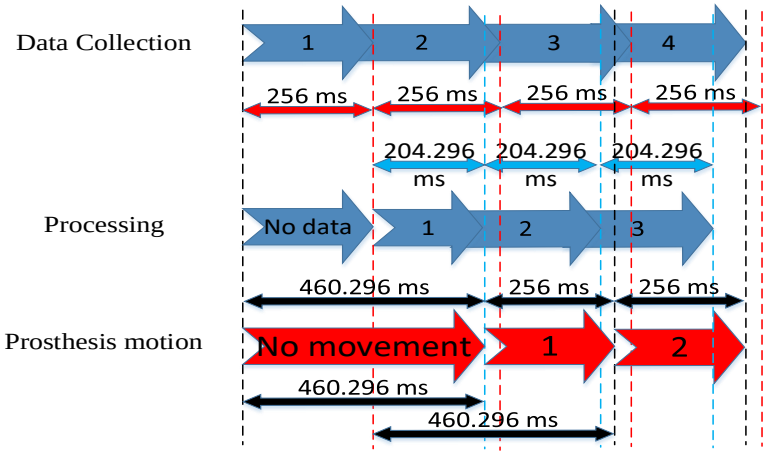

Fig. 4.11 The system timeline for classifier of 3 channels based on the sampling window size of 256 samples

Table 4.9: The delay time based on classifier of 3 channels

Component	Delay time (ms)	Std.
Pre-processing (denoised system)	114.481	46.150
Pre-processing (features extraction)	37.182	2.021
Classification	52.634	1.378
Total	204.296	45.573

In the Table 4.9, the delay time based on window size of 256 samples in each component of system is shown. The delay time in the denoised system is 114.481 milliseconds and the standard deviation is 46.150 milliseconds. The delay time in the features extraction system is 37.182 milliseconds and the standard deviation is 2.021

milliseconds. The delay time in the classification system is 52.634 milliseconds and the standard deviation is 1.378 milliseconds. Hence, the total delay time in the pre-processing system and the classification system is 204.296 milliseconds and the standard deviation is 45.573 milliseconds. It is suitable to use. Because the users have to wait 460.296 milliseconds to drive the artificial robot arm.

4.5 The comparisons for the classifier of 2 channels and 3 channels

In the section 4.2, the sampling window size of 256 samples achieves the best accuracy for the classifier of 2 channels. Therefore, the comparison between classifier of 2 channels and 3 channels is based on the sampling window size of 256 samples. Furthermore, the accuracy of classifier is tested on a subject-by-subject basis. The test result of each subject for the classifier of 3 channels is shown in Fig. 4.12 to Fig. 4.19.

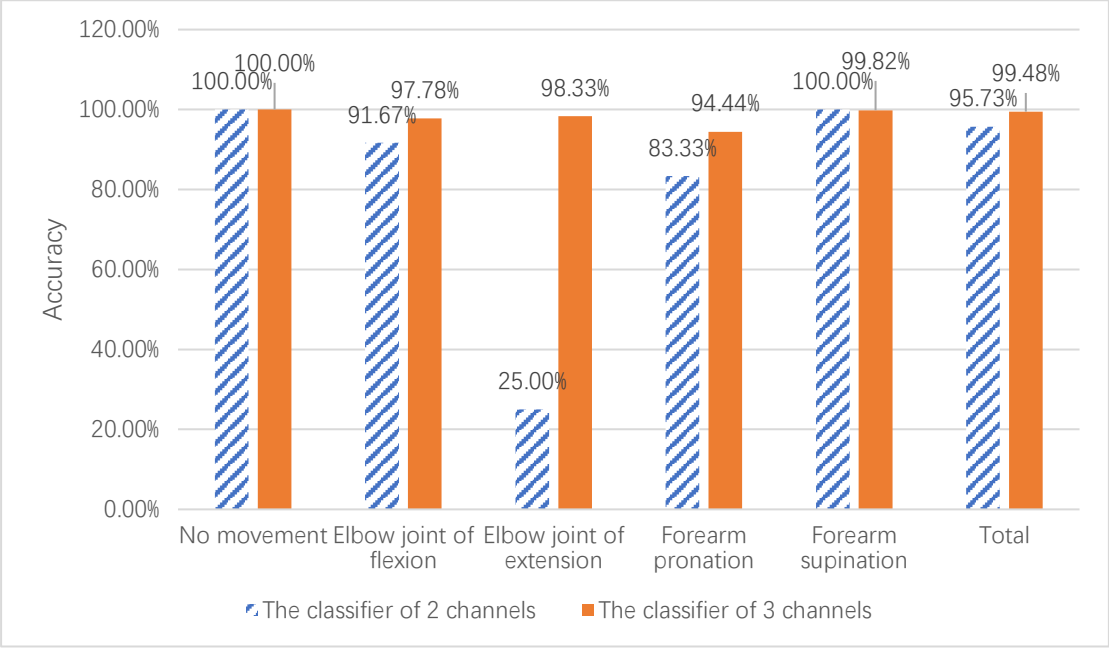

Fig. 4.12 The comparison for the classifier of 2 channels and 3 channels based the sampling window size of 256 samples from subject 1

In the Fig. 4.12, the accuracy is tested based on subject 1. The accuracy of the classifier of 3 channels is equal the classifier of 2 channels in the no movement. The accuracy of the classifier of 3 channels is 6.11% higher than the classifier of 2

channels in the elbow joint of flexion. The accuracy of the classifier of 3 channels is 73.33% higher than the classifier of 2 channels in the elbow joint of extension. The classifier of 2 channels does not detect the elbow joint of extension accurately. The accuracy of the classifier of 3 channels is 11.11% higher than the classifier of 2 channels in the forearm pronation. The classifier of 2 channels does not detect the forearm pronation accurately. The accuracy of the classifier of 3 channels is 0.18% lower than the classifier of 2 channels in the forearm supination. The total accuracy of the classifier of 3 channels is 3.75% higher than the classifier of 2 channels in 5 motions. Therefore, the classifier of 3 channels is more accurate than the classifier of 2 channels in the 5 motions of subject 1.

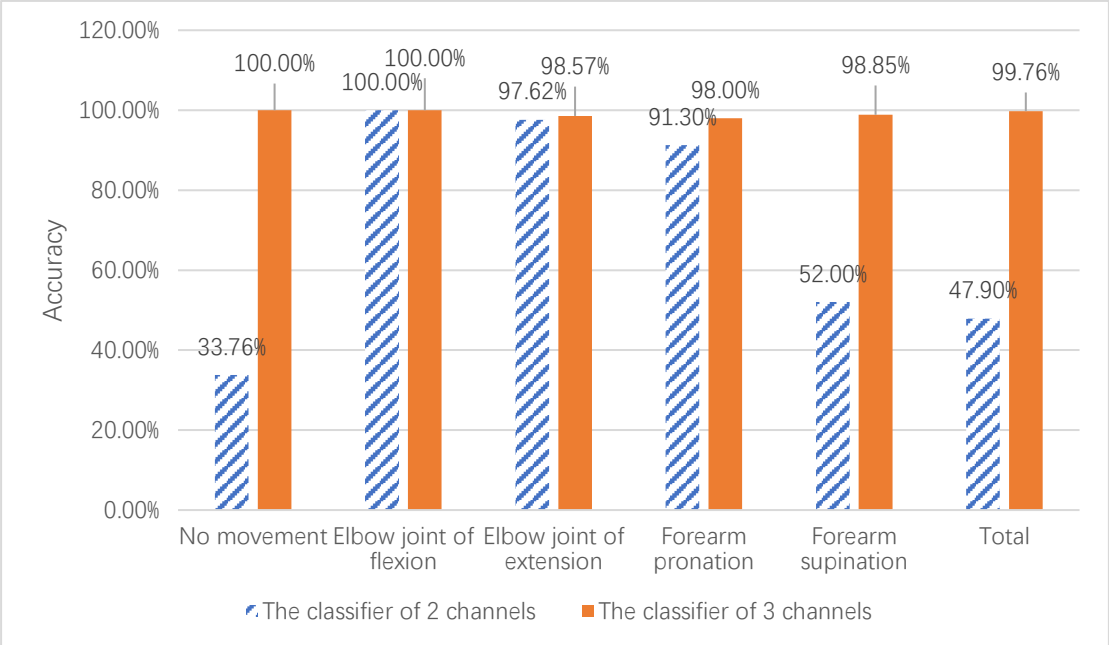

Fig. 4.13 The comparison for the classifier of 2 channels and 3 channels based the sampling window size of 256 samples from subject 2

In the Fig. 4.13, the accuracy is tested based on subject 2. The accuracy of the classifier of 3 channels is 66.24% higher than the classifier of 2 channels in the no movement. The classifier of 2 channels does not detect the no movement accurately. The accuracy of the classifier of 3 channels is equal the classifier of 2 channels in the elbow joint of flexion. The accuracy of the classifier of 3 channels is 0.95% higher than the classifier of 2 channels in the elbow joint of extension. The accuracy of the classifier of 3 channels is 6.7% higher than the classifier of 2 channels in the forearm pronation. The accuracy of the classifier of 3 channels is 46.85% lower than the classifier of 2 channels in the forearm supination. The classifier of 2 channels does not detect the forearm supination accurately. The total accuracy of the classifier of 3 channels is 51.86% higher than the classifier of 2 channels in 5 motions. Therefore, the classifier

of 3 channels is more accurate than the classifier of 2 channels in the 5 motions of subject 2.

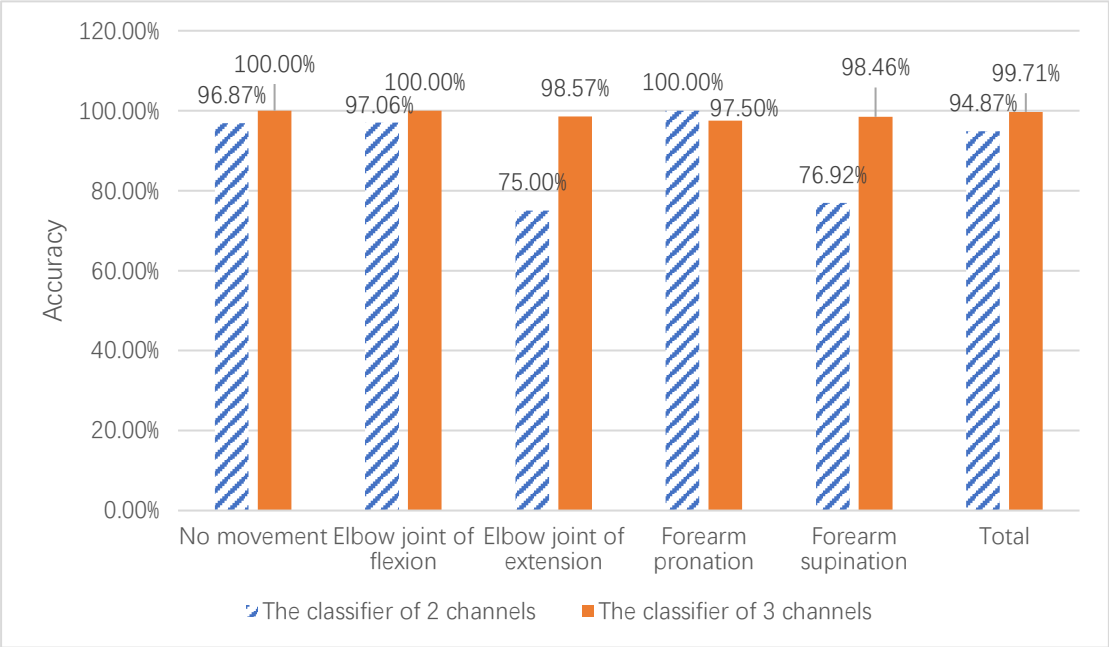

Fig. 4.14 The comparison for the classifier of 2 channels and 3 channels based the sampling window size of 256 samples from subject 3

In the Fig. 4.14, the accuracy is tested based on subject 3. The accuracy of the classifier of 3 channels is 3.13% higher than the classifier of 2 channels in the no movement. The accuracy of the classifier of 3 channels is 2.94% higher than the classifier of 2 channels in the elbow joint of flexion. The accuracy of the classifier of 3 channels is 23.57% higher than the classifier of 2 channels in the elbow joint of extension. The classifier of 2 channels does not detect the elbow joint of extension accurately. The accuracy of the classifier of 3 channels is 2.5% lower than the classifier of 2 channels in the forearm pronation. The accuracy of the classifier of 3 channels is

21.54% higher than the classifier of 2 channels in the forearm supination. The classifier of 2 channels does not detect the forearm supination accurately. The total accuracy of the classifier of 3 channels is 4.84% higher than the classifier of 2 channels in 5 motions. Therefore, the classifier of 3 channels is more accurate than the classifier of 2 channels in the 5 motions of subject 3.

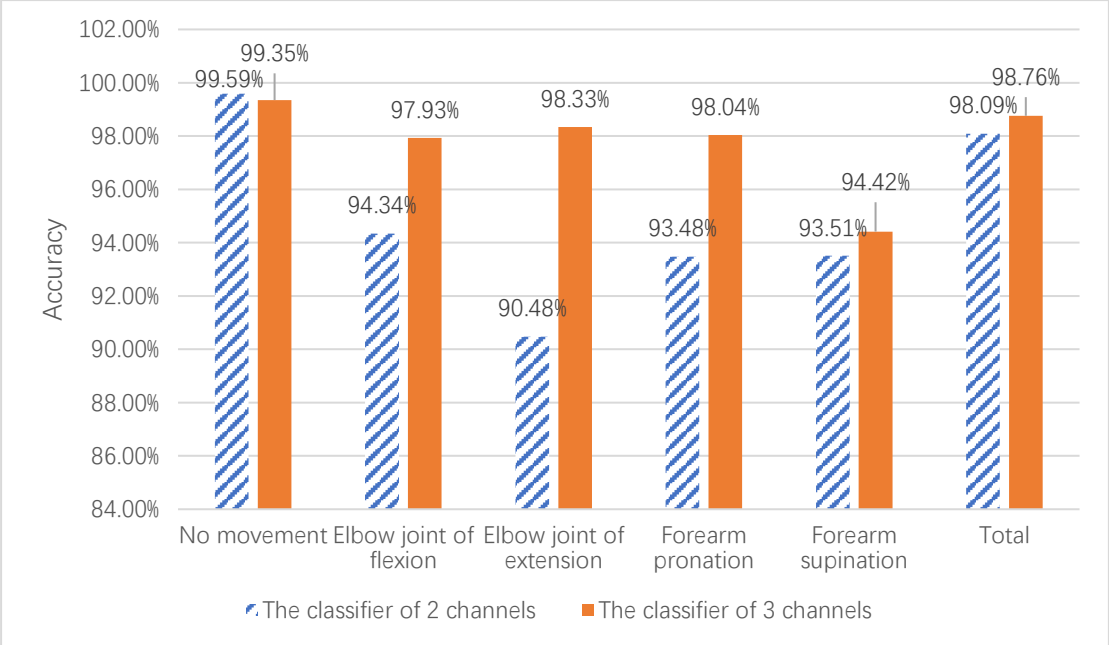

Fig. 4.15 The comparison for the classifier of 2 channels and 3 channels based the sampling window size of 256 samples from subject 4

In the Fig. 4.15, the accuracy is tested based on subject 4. The accuracy of the classifier of 3 channels is 0.24% lower than the classifier of 2 channels in the no movement. The accuracy of the classifier of 3 channels is 3.59% higher than the classifier of 2 channels in the elbow joint of flexion. The accuracy of the classifier of 3 channels is 7.85% higher than the classifier of 2 channels in the elbow joint of

extension. The accuracy of the classifier of 3 channels is 4.56% higher than the classifier of 2 channels in the forearm pronation. The accuracy of the classifier of 3 channels is 0.91% higher than the classifier of 2 channels in the forearm supination. The total accuracy of the classifier of 3 channels is 0.67% higher than the classifier of 2 channels in 5 motions. Therefore, the classifier of 3 channels is more accurate than the classifier of 2 channels in the 5 motions of subject 4.

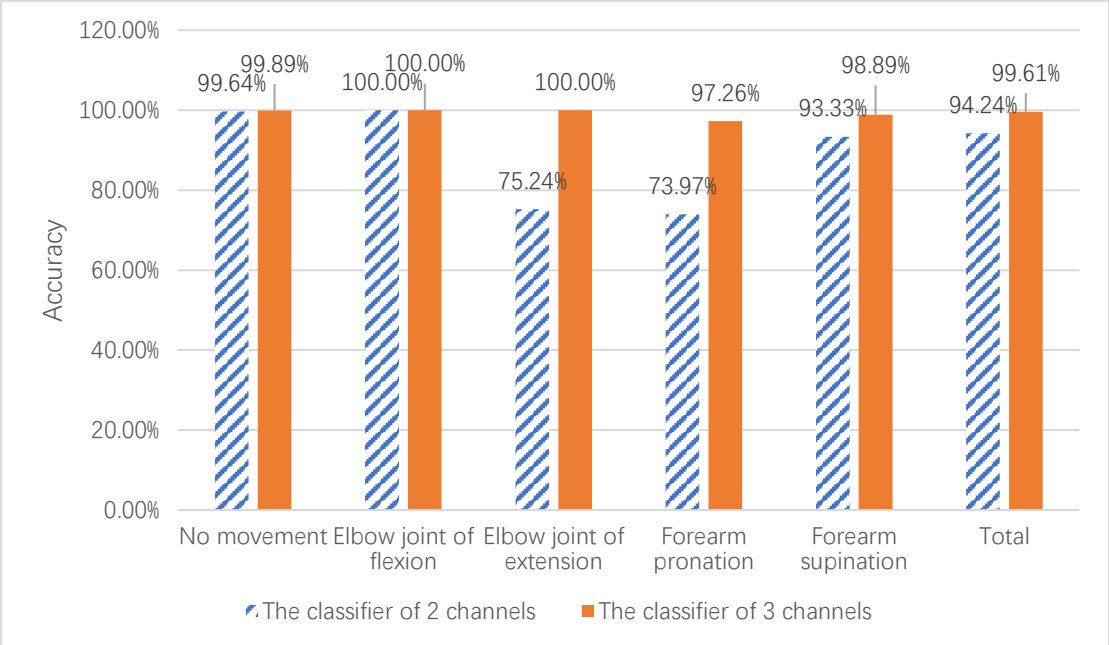

Fig. 4.16 The comparison for the classifier of 2 channels and 3 channels based the sampling window size of 256 samples from subject 5

In the Fig. 4.16, the accuracy is tested based on subject 5. The accuracy of the classifier of 3 channels is 0.25% higher than the classifier of 2 channels in the no movement. The accuracy of the classifier of 3 channels is equal the classifier of 2 channels in the elbow joint of flexion. The accuracy of the classifier of 3 channels is 24.76% higher than the classifier of 2 channels in the elbow joint of extension. The classifier of 2 channels does not detect the elbow joint of extension accurately. The accuracy of the classifier of 3 channels is 23.29% higher than the classifier of 2 channels in the forearm pronation. The classifier of 2 channels does not detect the forearm pronation accurately. The accuracy of the classifier of 3 channels is 5.56% higher than the classifier of 2 channels in the forearm supination. The total accuracy of the classifier of 3 channels is 5.37% higher than the classifier of 2 channels in 5 motions. Therefore,

the classifier of 3 channels is more accurate than the classifier of 2 channels in the 5 motions of subject 5.

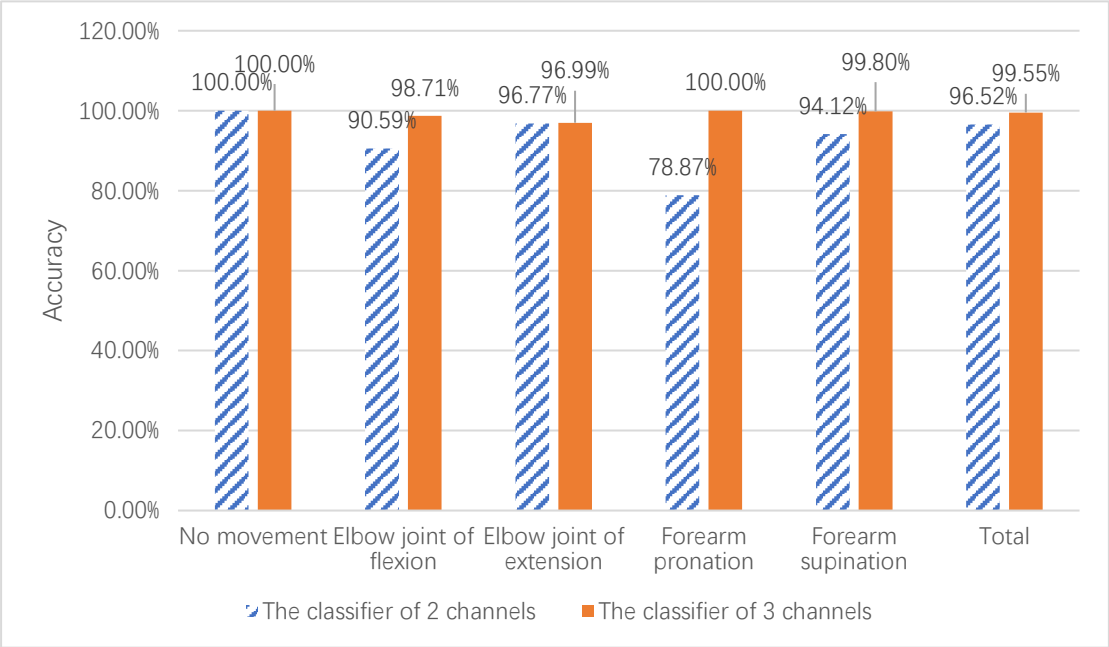

Fig. 4.17 The comparison for the classifier of 2 channels and 3 channels based the sampling window size of 256 samples from subject 6

In the Fig. 4.17, the accuracy is tested based on subject 6. The accuracy of the classifier of 3 channels is equal the classifier of 2 channels in the no movement. The accuracy of the classifier of 3 channels is 8.12% higher than the classifier of 2 channels in the elbow joint of flexion. The accuracy of the classifier of 3 channels is 0.22% higher than the classifier of 2 channels in the elbow joint of extension. The accuracy of the classifier of 3 channels is 21.13% higher than the classifier of 2 channels in the forearm pronation. The classifier of 2 channels does not detect the forearm pronation accurately. The accuracy of the classifier of 3 channels is 5.68% higher than

the classifier of 2 channels in the forearm supination. The total accuracy of the classifier of 3 channels is 3.03% higher than the classifier of 2 channels in 5 motions. Therefore, the classifier of 3 channels is more accurate than the classifier of 2 channels in the 5 motions of subject 6.

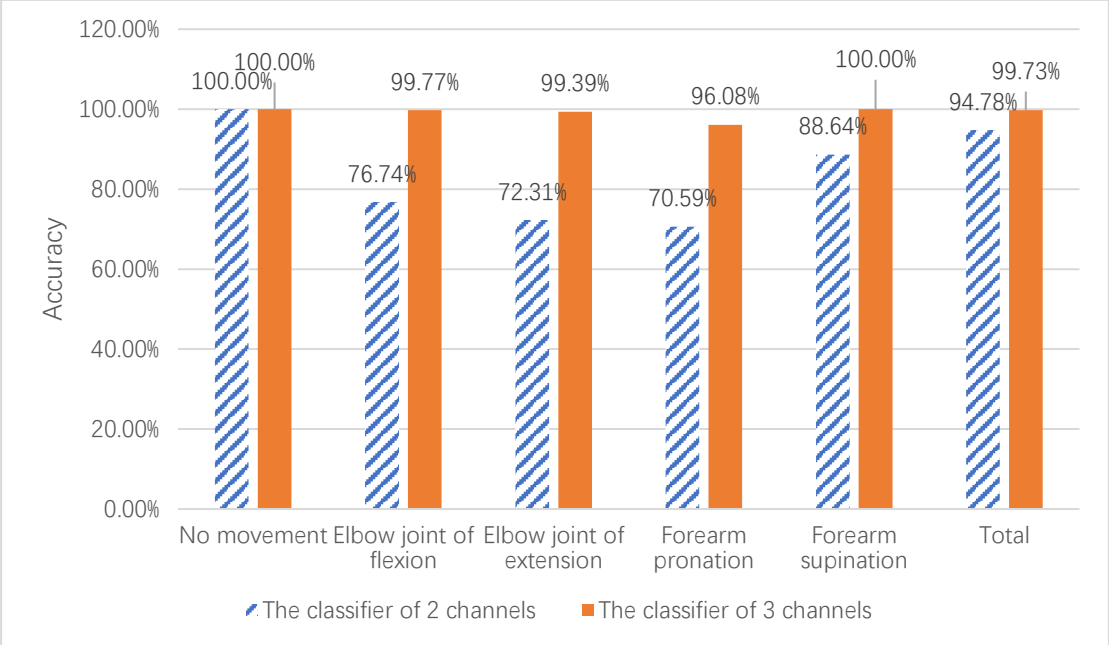

Fig. 4.18 The comparison for the classifier of 2 channels and 3 channels based the sampling window size of 256 samples from subject 7

In the Fig. 4.18, the accuracy is tested based on subject 7. The accuracy of the classifier of 3 channels is equal the classifier of 2 channels in the no movement. The accuracy of the classifier of 3 channels is 23.03% higher than the classifier of 2 channels in the elbow joint of flexion. The classifier of 2 channels does not detect the elbow joint of flexion accurately. The accuracy of the classifier of 3 channels is 27.08% higher than the classifier of 2 channels in the elbow joint of extension. The classifier of

2 channels does not detect the elbow joint of extension accurately. The accuracy of the classifier of 3 channels is 25.49% higher than the classifier of 2 channels in the forearm pronation. The classifier of 2 channels does not detect the forearm pronation accurately. The accuracy of the classifier of 3 channels is 11.36% higher than the classifier of 2 channels in the forearm supination. The classifier of 2 channels does not detect the forearm supination accurately. The total accuracy of the classifier of 3 channels is 4.95% higher than the classifier of 2 channels in 5 motions. Therefore, the classifier of 3 channels is more accurate than the classifier of 2 channels in the 5 motions of subject 7.

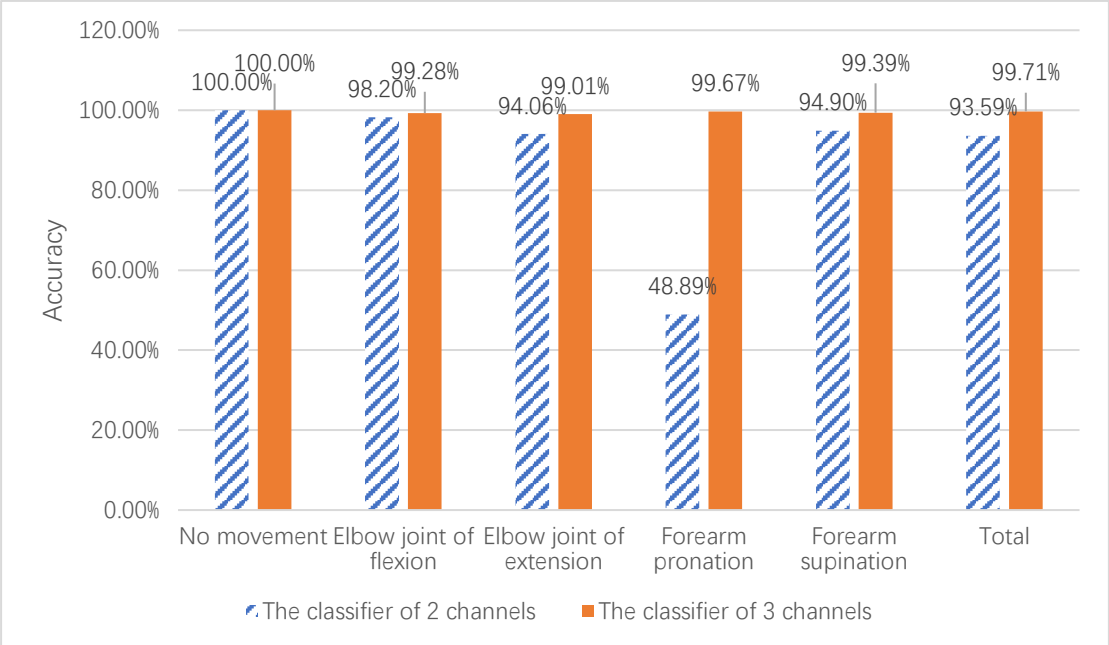

Fig. 4.19 The comparison for the classifier of 2 channels and 3 channels based the sampling window size of 256 samples from subject 8

In the Fig. 4.19, the accuracy is tested based on subject 8. The accuracy of the classifier of 3 channels is equal the classifier of 2 channels in the no movement. The accuracy of the classifier of 3 channels is 1.08% higher than the classifier of 2 channels in the elbow joint of flexion. The accuracy of the classifier of 3 channels is 4.95% higher than the classifier of 2 channels in the elbow joint of extension. The accuracy of the classifier of 3 channels is 50.78% higher than the classifier of 2 channels in the forearm pronation. The classifier of 2 channels does not detect the forearm pronation accurately. The accuracy of the classifier of 3 channels is 4.49% higher than the classifier of 2 channels in the forearm supination. The total accuracy of the classifier of 3 channels is 6.12% higher than the classifier of 2 channels in 5 motions. Therefore,

the classifier of 3 channels is more accurate than the classifier of 2 channels in the 5 motions of subject 8.

In conclusion, the sampling window size of 256 samples achieves the average accuracy 89.46% in the classifier of 2 channels based on 8 healthy subjects, but the classifier of 2 channels does not detect each motion accurately. The no movement for subject 2 is not detected accurately, the elbow joint of flexion for subject 7 is not detected accurately, the elbow joint of extension for subject 1, subject 3, subject 5 and subject 7 is not detected accurately, the forearm pronation for subject 1, subject 5, subject 6, subject 7 and subject 8 is not measured accurately, the forearm supination for subject 2, subject 3 and subject 7 is not measured accurately. Moreover, the classifier of 3 channels achieves the average accuracy of five motions up to 99.54% and it detects each motion accurately. Hence, the classifier of 3 channels is used in the thesis.

In the Fig. 4.12 to Fig. 4.19, the accuracy of the classifier of 3 channels in each motion is better than 90% for each subject. Compared to classifier of 2 channels, the 5 motions are detected accurately by the classifier of 3 channels. The comparison for the test result is shown in Fig. 4.20.

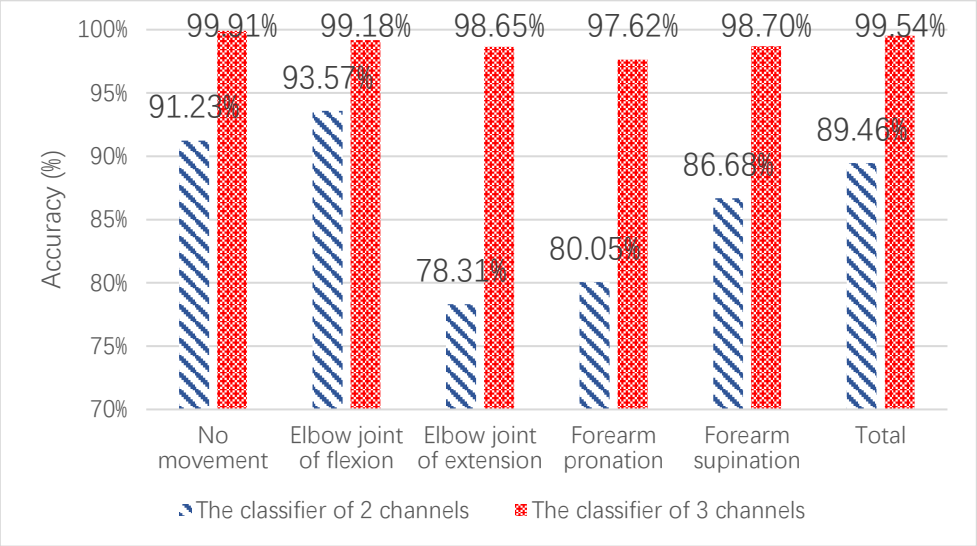

Fig. 4.20 The comparison of average accuracy for the classifier of 2 channels and 3 channels based the sampling window size of 256 samples from 8 healthy subjects

In the Fig. 4.20, the result shows that the classifier of 3 channels based on 8 healthy subjects is better than the classifier of 2 channels. Firstly, the average accuracy of no movement increases 8.68% in the classifier of 3 channels. Secondly, the average accuracy of elbow joint of flexion increases 5.61%. Thirdly, the average accuracy of elbow joint of extension increases 20.34%. Fourthly, the average accuracy of forearm pronation increases 17.57%. Fifthly, the average accuracy of forearm supination increases 12.02%. At the end, the average accuracy of 5 motions increases 10.08%. But the total delay time only increases 18.904 milliseconds that is 460.296 milliseconds. Hence, the classifier of 3 channels gives better overall accuracy than the classifier of 2 channels.

4.6 The comparisons for the experiment of the weight-bearing motions

In order to improve the system usability, the 3 healthy subjects wear the weight to test the effect of the weight for the system. All of the tests are based on the training data of the subjects without weight in the classifier of 3 channels. It means that the trained system is used to test the experiment without the weight and the experiment with the weight of 1.5 kg. The 1.5 kilogram (kg), which is the common maximum of the weight for artificial robot arm, is used in this comparison. Moreover, the comparisons shown in Table 4.10 to Table 4.12 are based on 3 subjects: subject 1, subject 5 and subject 6. In addition, the setups of system are kept in the same conditions. All results are calculated by the average of the 10 identical experiments.

Table 4.10: The result for the experiment of the weight-bearing motions from subject 1

Motion	The experiment without the weight	The experiment with the weight of 1.5 kg	%△ accuracy
No movement	100.00%	99.58%	-0.42%
Elbow joint of flexion	97.78%	100%	2.22%
Elbow joint of extension	98.33%	91.67%	-6.66%
Forearm pronation	94.44%	88.89%	-5.55%
Forearm supination	99.82%	98.21%	-1.61%
Average accuracy	99.48%	95.67%	-3.81%

In the Table 4.10, the result for subject 1 is shown. The no movement with the weight of 1.5 kg is 0.42% lower than the motion without the weight. The elbow joint of flexion with the weight of 1.5 kg increases 2.22% based on the elbow joint of flexion without the weight. The elbow joint of extension with the weight of 1.5 kg is 6.66% lower than this motion without the weight. The forearm pronation with the weight of 1.5 kg is 5.55% lower than the motion without the weight. The forearm supination with the weight of 1.5 kg reduces 1.61% based on the forearm supination without the weight. At the end, the average accuracy for 5 motions with the weight of 1.5 kg is 3.81% lower than the 5 motions without the weight.

Table 4.11: The result for the experiment of the weight-bearing motions from subject 5

Motion	The experiment without the weight	The experiment with the weight of 1.5 kg	%△ accuracy
No movement	99.89%	99.64%	-0.25%
Elbow joint of flexion	100.00%	99.01%	-0.99%
Elbow joint of extension	100.00%	91.43%	-8.57%
Forearm pronation	97.26%	98.63%	1.37%
Forearm supination	98.89%	96.67%	-2.22%
Average accuracy	99.61%	97.07%	-2.54%

In the Table 4.11, the result for subject 5 is shown. The no movement with the weight of 1.5 kg is 0.25% lower than the motion without the weight. The elbow joint of flexion with the weight of 1.5 kg reduces 0.99% based on the elbow joint of flexion without the weight. The elbow joint of extension with the weight of 1.5 kg is 8.57 % lower than this motion without the weight. The forearm pronation with the weight of 1.5 kg is 1.37% higher than the motion without the weight. The forearm supination with the weight of 1.5 kg reduces 2.22% based on the forearm supination without the weight. At the end, the average accuracy for 5 motions with the weight of 1.5 kg is 2.54% lower than the 5 motions without the weight.

Table 4.12: The result for the experiment of the weight-bearing motions from subject 6

Motion	The experiment without the weight	The experiment with the weight of 1.5 kg	%△ accuracy
No movement	100%	99.65%	-0.35%
Elbow joint of flexion	98.71%	97.65%	-1.03%
Elbow joint of extension	96.99%	96.77%	-0.22%
Forearm pronation	100.00%	95.77%	-4.23%
Forearm supination	99.80%	96.08%	-3.72%
Average accuracy	99.55%	97.18%	-2.37%

In the Table 4.12, the result for subject 6 is shown. The no movement with the weight of 1.5 kg is 0.35%, lower than the motion without the weight. The elbow joint of flexion with the weight of 1.5 kg reduces 1.03% based on the elbow joint of flexion without the weight. The elbow joint of extension with the weight of 1.5 kg is 0.22%, lower than this motion without the weight. The forearm pronation with the weight of 1.5 kg is 4.23%, lower than the motion without the weight. The forearm supination with the weight of 1.5 kg reduces 3.72% based on the forearm supination without the weight. At the end, the average accuracy for 5 motions with the weight of 1.5 kg is 2.37%, lower than the 5 motions without the weight.

In conclusion, the average accuracy for 5 motions of subject 1 with the weight of 1.5 kg is 3.81% lower than the 5 motions without the weight. The average accuracy for 5 motions of subject 5 with the weight of 1.5 kg is 2.54% lower than the 5 motions of subject 6 without the weight. The average accuracy for 5 motions with the weight of 1.5 kg is 2.37% lower than the 5 motions without the weight. Therefore, the weight of artificial robot arm does not exert the influence over the classification system.

4.7 The demonstration of the artificial robot arm for each motion detection

According to the section 3.3.7, the 10 windows of sEMG signals shown in Table 4.13 from each motion of 8 healthy subjects are used to test and the recognition results are demonstrated by the artificial robot arm. In addition, the recognition results sent to Arduino device by the Matlab support package for Arduino hardware. This support package provides the ability to set the device communication information and drive the devices function attached to Arduino hardware. Each motion of artificial robot arm is shown in Fig. 4.21 to Fig. 4.24.

Moreover, the robot arm only demonstrates that the recognition result from the classifier of 3 channels is sent to the controller correctly. Therefore, the accuracy should be the same as the previous result.

Table 4.13: The number of windows from each subject based on the sampling window size of 256 samples for system test and artificial robot arm demonstration

Test data	Number of windows
No movement	10
Elbow joint of flexion	10
Elbow joint of extension	10
Forearm pronation	10
Forearm supination	10

In the Table 4.13, the 10 windows of sEMG signals of each motion from subject 1 based on the sampling window size of 256 samples are used to test and the

recognition results are demonstrated by the artificial robot arm. Moreover, the same number of windows are used for the other subjects.

The no movement of artificial robot arm is shown in Fig. 4.21 (c). The elbow joint of flexion of artificial robot arm is shown in Fig. 4.22 (c). The elbow joint of extension of artificial robot arm is shown in Fig. 4.23 (c). The forearm pronation of artificial robot arm is shown in Fig. 4.24 (c). The forearm supination of artificial robot arm is shown in Fig. 4.25 (c).

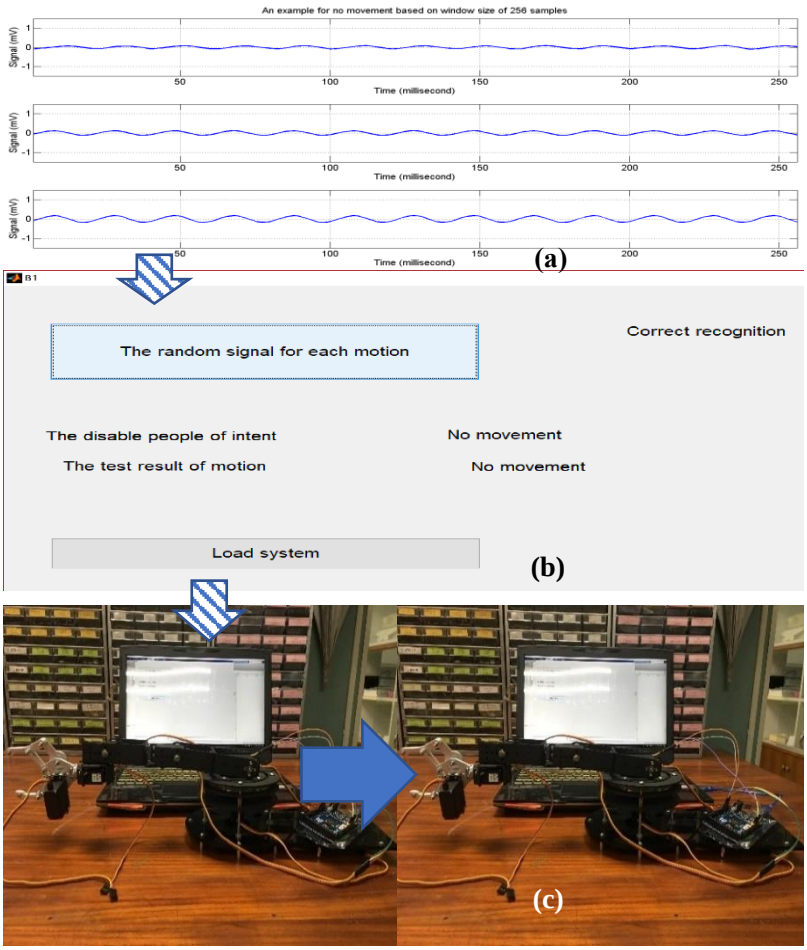

Fig. 4.21 The denoised sEMG signals of 3 channels for no movement based on the sampling window size of 256 samples (a), the recognition result of no movement on the control panel (b) and the no movement of artificial robot arm (c)

In the Fig. 4.21, an example for the no movement of denoised sEMG signals of 3 channels based on the sampling window size of 256 samples is shown in the Fig. 4.21 (a). The system processes the sEMG signals based on a window basis. After that, the recognition result of no movement on the control panel is shown in the Fig. 4.21 (b). At the end, the no movement is demonstrated by artificial robot arm and it is shown in the Fig. 4.21 (c).

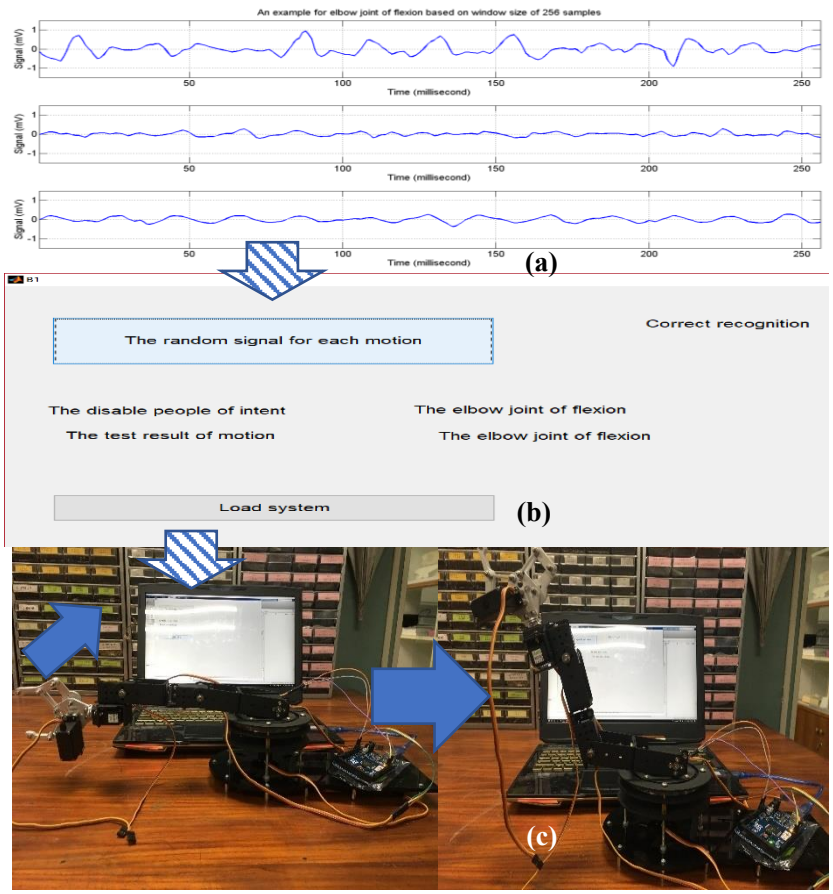

Fig. 4.22 The denoised sEMG signals of 3 channels for elbow joint of flexion based on the sampling window size of 256 samples (a), the recognition result of elbow joint of flexion on the control panel (b) and the elbow joint of flexion of artificial robot arm (c)

In the Fig. 4.22, an example for the elbow joint of flexion of denoised sEMG signals of 3 channels based on the sampling window size of 256 samples is shown in the Fig. 4.22 (a). The system processes the sEMG signals based on a window basis. After that, the recognition result of elbow joint of flexion on the control panel is shown in the Fig. 4.22 (b). At the end, the elbow joint of flexion is demonstrated by artificial robot arm and it is shown in the Fig. 4.22 (c).

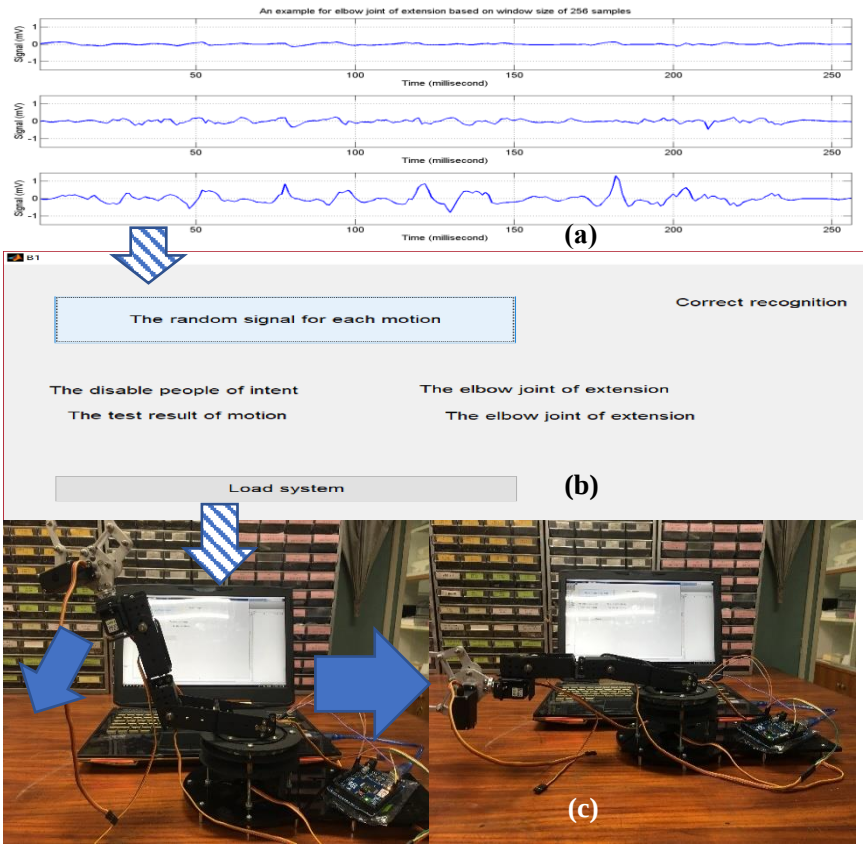

Fig. 4.23 The denoised sEMG signals of 3 channels for elbow joint of extension based on the sampling window size of 256 samples (a), the recognition result of elbow joint of extension on the control panel (b) and the elbow joint of extension of artificial robot arm (c)

In the Fig. 4.23, an example for the elbow joint of extension of denoised sEMG signals of 3 channels based on the sampling window size of 256 samples is shown in the Fig. 4.23 (a). The system processes the sEMG signals based on a window basis. After that, the recognition result of elbow joint of extension on the control panel is shown in the Fig. 4.23 (b). At the end, the elbow joint of extension is demonstrated by artificial robot arm and it is shown in the Fig. 4.23 (c).

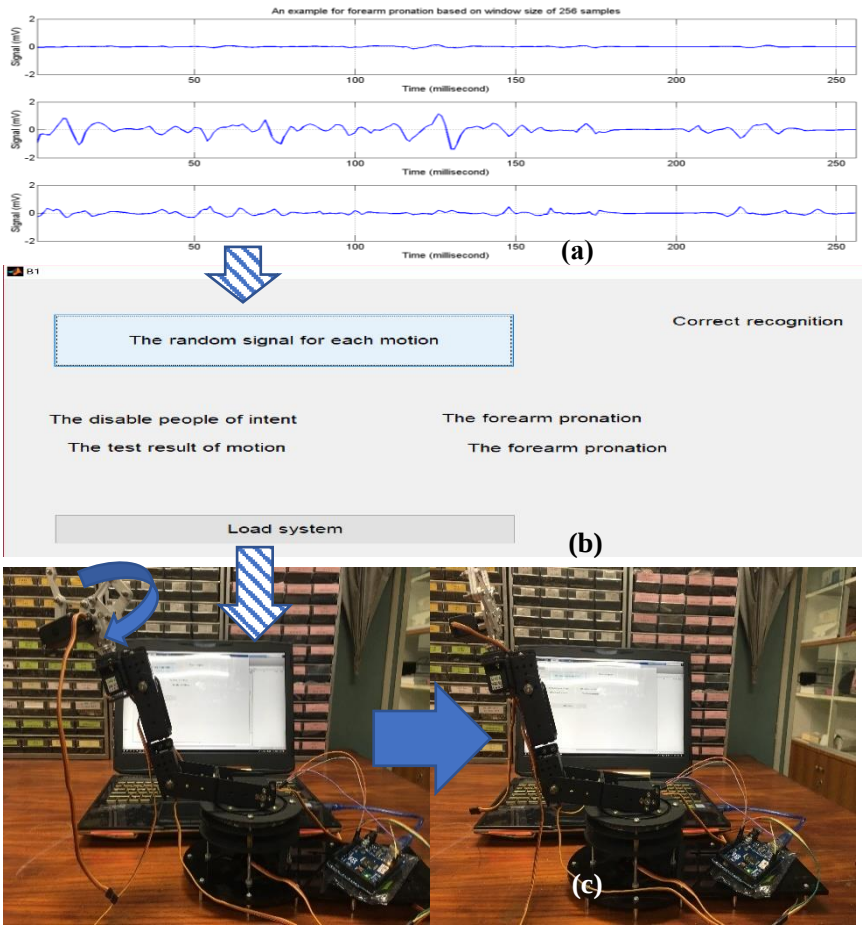

Fig. 4.24 The denoised sEMG signals of 3 channels for forearm pronation based on the sampling window size of 256 samples (a), the recognition result of forearm pronation on the control panel (b) and the forearm pronation of artificial robot arm (c)

In the Fig. 4.24, an example for the forearm pronation of denoised sEMG signals of 3 channels based on the sampling window size of 256 samples is shown in the Fig. 4.24 (a). The system processes the sEMG signals based on a window basis. After that, the recognition result of forearm pronation on the control panel is shown in the Fig. 4.24 (b). At the end, the forearm pronation is demonstrated by artificial robot arm and it is shown in the Fig. 4.24 (c).

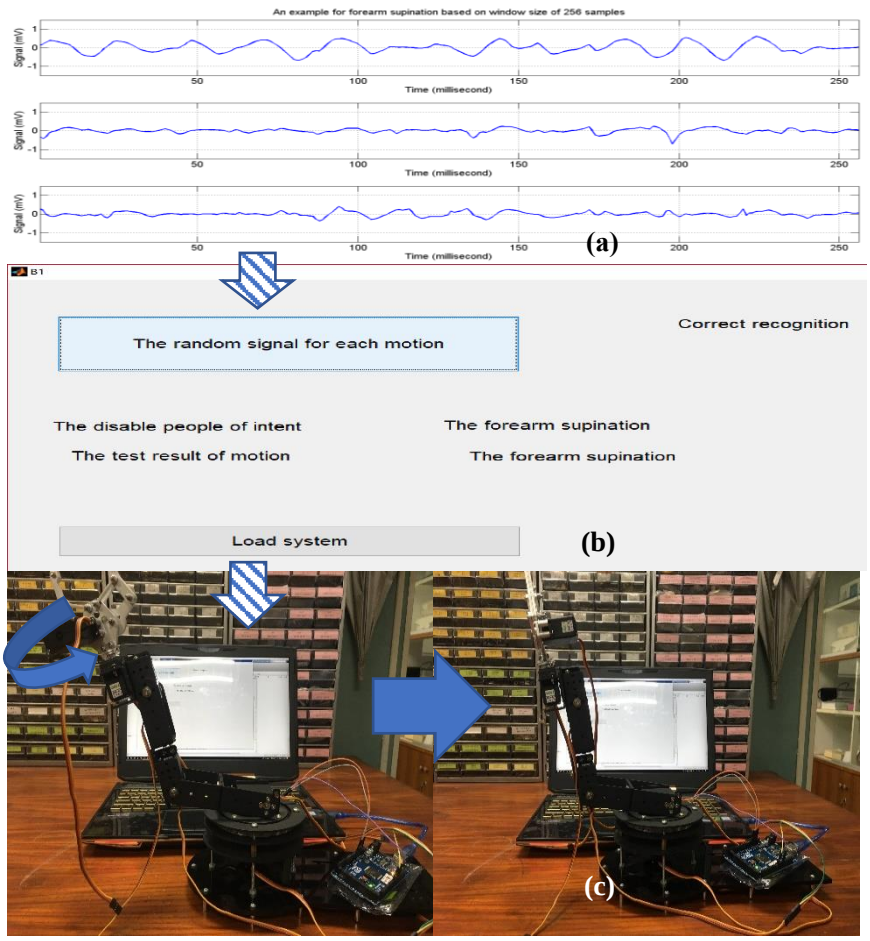

Fig. 4.25 The denoised sEMG signals of 3 channels for forearm supination based on the sampling window size of 256 samples (a), the recognition result of forearm supination on the control panel (b) and the forearm supination of artificial robot arm (c)

In the Fig. 4.25, an example for the forearm supination of denoised sEMG signals of 3 channels based on the sampling window size of 256 samples is shown in the Fig. 4.25 (a). The system processes the sEMG signals based on a window basis. After that, the recognition result of forearm supination on the control panel is shown in the Fig. 4.25 (b). At the end, the forearm supination is demonstrated by artificial robot arm and it is shown in the Fig. 4.25 (c).

CHAPTER 5

Conclusion

5.1 Conclusion

In this thesis, the proposed method solves forearm without muscle to control forearm pronation based on sEMG signal. The proposed method is friendlier, cheaper and safer than the mechanical prostheses and the targeted muscle reinnervation transform. In addition, the proposed systems which are the band-pass filter in the signal measurement system and the denoised system in the pre-processing system reduce the electrical noise by 56.68%.

After that, the class of motions is analyzed utilizing 5 features in the classification system based on BP network. Moreover, the best accuracy is produced by the sampling window size of 256 samples. The total delay time which is the time of system process and robot arm response in sampling window size of 256 samples is 460.296ms that is acceptable to use. Besides, the processing time processed on computer is reduced with the increasing of computer performance. As the result shown, the classifier of 3 channels better than the classifier of 2 channels achieves 99.54% accuracy through testing 8 healthy subjects. Moreover, the system is tested by 8 healthy subjects, including 4 males and 4 females. Hence, the system can be used for different gender. The accuracy of classifier is tested on a subject-by-subject basis. The classifier of 3 channels is that: (1) the input data is based on the sampling window size of 256

samples, (2) the classifier has 1 input layer, 1 hidden layer and 1 output layer, (3) 15 input layer nodes, 3 hidden layer nodes and 3 output layer nodes are utilized into the classifier. At the end, the 1.5 kg weight that the users wear does not exert the influence over the system accuracy.

5.2 Recommendation to the future study

In this thesis, all of the subjects are healthy. The high accuracy is achieved by the 8 healthy subjects. The disable people whose osteotomy sites for supracondylar above-elbow amputation or below-elbow amputation do not attend the experiment. In order to improve the system to be a robust, the more datasets of real patients are needed to test into this system.

Moreover, the total delay time is reduced by more powerful processer. The processer is computer in this thesis, it can be changed to the mobile processer that makes the system wearable.

In addition, the control system does not consider the torque of artificial robot arm. It is changed by the users' requirement. Moreover, the elbow joint is usually used to activate the weight-bearing motions. According to the researches, the elbow supports about 300 N (67 lb) to activate the daily motions such as wearing and eating. When people stand up with arm from the seat, 1700 N (382 lb) is used. The people use 1900 N (427 lb) to do the weight-bearing motions such as push-up [56]. So the motor needs about 300N of total torque. However, the control system does not discuss so much about the mechanical artificial robot arm, it will be considered for the mechanical study.

REFERENCES

[1] "WHO | Disability and health," *WHO*. [Online]. Available: http://www.who.int/mediacentre/factsheets/fs352/en/. [Dec-2015].

[2] K. Z. Graham, E. J. MacKenzie, P. L. Ephraim, T. G. Travison, and R. Brookmeyer, "Estimating the prevalence of limb loss in the united states: 2005 to 2050," *Arch. Phys. Med. Rehabil.*, vol. 89, no.3, pp. 422–429, 2008.

[3] A. Esquenazi, and R. H. Meier, "Rehabilitation in limb deficiency. 4. limb amputation," *Arch. Phys. Med. Rehabil.*, vol. 77, no. 3, pp. 18–28, 1996.

[4] D. R. Merrill, J. Lockhart, P. R. Troyk, R. F. Weir, and D. L. Hankin, "Development of an implantable myoelectrical sensor for advanced prosthesis control," *Artif. Organs*, vol. 35, no. 3, pp. 249–252, 2011.

[5] D. Novak, X. Omlin, R. L. Hess, et al. "Predicting targets of human reaching motions using different sensing technologies," *IEEE Trans. on Biomed. Eng.*, vol. 60, no. 9, pp. 2645-2654, 2013.

[6] M. Adrian, and J. M. Cooper, *The biomechanics of human movement*. Benchmark Press, 1995.

[7] G. Kamen, "Electromyographic Kinesiology," In *Research Methods in Biomechanics*, G. Robertson, D. Gordon., G. Caldwell, J. Hamill, G. Kamen, and S. Whittlesey, Champaign, IL: Human Kinetics Publ., pp. 455-465, 2004.

[8] Google Scholar Search: "Hand Prosthesis" OR "Prosthetic Hand" 2011 [Online]. Available: http://scholar.google.com/scholar?hl=en&q="hand+prosthesis"+OR+"prosthetic+hand"

[9] J. R. Cram, and Steger, J.C. Steger. “EMG scanning in the diagnosis of chronic pain.”. *Biofeedback Self Regul*, vol. 8, no. 2, pp. 229–241, 1983.

[10] A. C. Rothman, *Selective Insurance Company of America*, Supreme Court of New Jersey, Jan. 19, 2012.

[11] Texas Court of Appeals, *Case No. 03-10-673-CV*, Austin, April 5, 2012.

[12] Michigan Compiled Laws, *Section 333.17018*, Michigan, 2005. Available: http://legislature.mi.gov/doc.aspx?mcl-333-17018

[13] S. Ananthi, *A Text Book of Medical Instruments*. New Age International, 2005.

[14] J. G. Webster, *Medical Instrumentation Application and Design, 4th Edition*. Wiley Global Education, 2009.

[15] A. Agarwal, *Essentials of Prosthetics and Orthotics*. Jaypee Brothers Publishers, 2013.

[16] M. M. Malawer, and P. H. Sugarbaker. “Musculoskeletal cancer surgery: treatment of sarcomas and allied diseases,” *Springer Science & Business Media*, 2001.

[17] M. M. Lusardi, M. Jorge, M. Jorge, and C. C. Nielsen, *Orthotics and Prosthetics in Rehabilitation*. Elsevier Health Sciences, 2013.

[18] B. Hudgins, P. A. Parker, and R. N. Scott, “A new strategy for multifunction myoelectrical control,” *IEEE Trans. on Biomed. Eng.*, vol. 40, no.1, pp. 82–94, Jan. 1993.

[19] D. S. Childress, “Myoelectrical control of powered prostheses,” *IEEE Eng. Med. Biol. Mag.*, vol. 1, no. 4, pp. 23–25, Dec. 1982.

[20] P. A. Parker and R. N. Scott, “Myoelectrical control of prostheses,” *Crit. Rev. Biomed. Eng.*, vol. 13, no. 4, pp. 283–310, 1986.

[21] R. N. Scott, and P. A. Parker, “Myoelectrical prostheses: State of the art,” *J. Med. Eng. Technol.*, vol. 12, no. 4, pp. 143–151, Jul. 1988.

[22] T. W. Williams III, “Practical methods for controlling powered upperextremity prostheses,” *Assist. Technol.*, vol. 2, no. 1, pp. 3–18, 1990.

[23] P. A. Parker, K. B. Englehart, and B. S. Hudgins, “Control of powered upper limb prostheses,” in *Electromyography: Physiology, Engineering and Noninvasive Applications*, pp. 453–475, 2004.

[24] P. A. Parker, K. B. Englehart, and B. S. Hudgins, “Myoelectrical signal processing for control of powered limb prostheses,” *J. Electromyogr. Kines*, vol. 16, no. 6, pp. 541–548, 2006.

[25] A. Fougner, Ø. Stavdahl, P. J. Kyberd, Y. Losier, and P. A. Parker, “Control of upper limb prostheses: terminology and proportional myoelectrical control—a review,” *IEEE Trans. on Neural syst. Rehab. Eng.*, vol. 20, no. 5, pp. 663-677, 2012.

[26] T. A. Kuiken, G. Li, B. A. Lock, R. D. Lipschutz, L. A. Miller, K. A. Stubblefield, and K. B. Englehart, “Targeted muscle reinnervation for real-time myoelectrical control of multifunction artificial arms,” *J. Am. Med. Assoc.*, vol. 301, no. 6, pp. 619–628, 2009.

[27] D. R. Merrill, J. Lockhart, P. R. Troyk, R. F. Weir, and D. L. Hankin, “Development of an implantable myoelectrical sensor for advanced prosthesis control,” *Artif. Organs*, vol. 35, no. 3, pp. 249–252, 2011.

[28] D. F. Lovely, B. S. Hudgins, and R. N. Scott, “Implantable myoelectrical control system with sensory feedback,” *Med. Biol. Eng. Comput.*, vol. 23, no. 1, pp. 87–89, 1985.

[29] R. F. F. Weir, P. R. Troyk, G. DeMichele, M. Lowery, and T. Kuiken, "Implantable myoelectrical sensors (IMES)," in *Proc. Myoelectrical Controls Symp. (MEC)*, Fredericton, NB, Canada, 2005.

[30] R. F. F. Weir, P. Troyk, G. DeMichele, D. Kerns, J. Schorsch, and H. Maas, "Implantable myoelectrical sensors (IMESs) for intramuscular electromyogram recording," *IEEE Trans. on Biomed. Eng.*, vol. 56, no. 1, pp. 159–171, Jan. 2009.

[31] R. D. Alley and H. H. Sears, "Powered upper-limb prosthetics in adults," in *Powered Upper Limb Prostheses: Control, Implementation and Clinical Application*, A. Muzumdar, Ed. New York: Springer-Verlag, pp. 117–145, 2004.

[32] N. Hogan, "Impedance control: An approach to manipulation," *J. Dyn. Syst. Meas. Control*, vol. 107, no. 1, pp. 1–24, 1985.

[33] B. Lock, A. M. Simon, K. Stubblefield, and L. Hargrove, "Prosthesis guided training for practical use of pattern recognition control of prostheses," in *Proc. Myoelectrical Controls Symp. (MEC)*, Fredericton, NB, Canada, 2011.

[34] A. M. Simon, B. Lock, K. Stubblefield, and L. Hargrove, "Prosthesis-guided training increases functional wear time and improves tolerance to malfunctioning inputs of pattern recognition-controlled prostheses," in *Proc. Myoelectrical Controls Symp.*, Fredericton, NB, Canada, pp. 1-4, 2011.

[35] Y. Losier, "Shoulder complex motion based input strategies for prosthetic limb control," Ph.D. dissertation, Univ. New Brunswick, Fredericton, NB, Canada, 2009.

[36] R. W. Mann, “Efferent and afferent control of an electromyographic, proportional-rate, force sensing artificial elbow with cutaneous display of joint angle,” *In Proc. Inst. Mechan. Engineers 1847–1996*, vol. 183, no. 10, pp. 86–92, 1968.

[37] B. Hudgins, P. A. Parker, and R. N. Scott, “A new strategy for multifunction myoelectrical control,” *IEEE Trans. on Biomed. Eng.*, vol. 40, no.1, pp. 82–94, Jan. 1993.

[38] A. Fougner, E. Scheme, A. D. Chan, K. Englehart, and Ø. Stavdahl, “Resolving the limb position effect in myoelectrical pattern recognition,” *IEEE Trans. Neural Syst. Rehab. Eng.*, vol. 19, no. 6, pp. 644–651, Dec. 2011.

[39] K. Englehart, B. Hudgin, and P. A. Parker, “A wavelet-based continuous classification scheme for multifunction myoelectrical control,” *IEEE Trans. on Biomed. Eng.*, vol. 48, no. 3, pp. 302–311, Mar. 2001.

[40] T. R. Farrel, “Multifunctional Prosthesis Control: The Effect of Targeting Surface vs. Intramuscular Electrodes on Classification Accuracy, and Effect of Controller Delay on Prothesis Performance,” Ph.D. dissertation, Evanston, IL: Northwestern University, 2007.

[41] K. Englehart, and B. Hudgins, “A robust, real-time control scheme for multifunction myoelectrical control,” *IEEE Trans. on Biomed. Eng*., vol. 50, no. 7, pp. 848-854, 2003.

[42] K. Englehart, B. Hudgins, and A. D. Chan, “Continuous multifunction myoelectrical control using pattern recognition,” *Technol. Disabil*., vol. 15, no. 2, pp. 95-103, 2003.

[43] G. Hefftner, W. Zucchini, and G. G. Jaros, “The electromyogram (EMG) as a control signal for functional neuromuscular stimulation, I: autoregressive modeling as a means of EMG signature discrimination.” *IEEE Trans. on Biomed. Eng*., vol. 35, no. 4, pp. 230-237, 1988.

[44] S. J. Hall, *BASIC BIOMECHANICS, SIXTH EDITION*. McGraw-Hill press, New York, 2012.

[45] M. E. Gohary, and J. McNames, “Human Joint Angle Estimation with Inertial Sensors and Validation with A Robot Arm,” *IEEE Trans. on Biomed. Eng.*, vol. 62, no. 7, pp. 1759–1767, Jul. 2015.

[46] BIOPAC® System, Inc., “System, THE GOLD STANDARD FOR LIFE SCIENCE INSTRUCTION,” *BIOPAC System, Inc*. [Online].
Available: https://www.biopac.com/education/

[47] R. H. Chowdhury, M. B. Reaz, M. A. B. M. Ali, A. A. A. Bakar, K. Chellappan, and T. G. Chang, “Surface electromyography signal processing and classification techniques," *Sensors*, vol. 13, no. 9, pp. 12431-12466, 2013.

[48] A. Phinyomark, C. Limsakul, and P. Phukpattaranont, “A comparative study of wavelet denoising for multifunction myoelectrical control,” *Computer and Automation Engineering, 2009. ICCAE'09*, pp. 21-25, 2009.

[49] P. S. Addison, *The illustrated wavelet transform handbook: introductory theory and applications in science, engineering, medicine and finance.* CRC press, 2002.

[50] D. L. Donoho, and J. M. Johnstone, “Ideal spatial adaptation by wavelet shrinkage,” *Biometrika*, vol 81, no. 3, pp. 425–455.

[51] H. Yu, A. Lee, and Y. Choi, “Human elbow joint angle estimation using electromyogram signal processing.” *IET signal processing*, vol. 5, no. 8, pp. 767-775, 2011.

[52] D. Liu, X. Zhao, D. Ye, Y. Zhao, and Z. Wu, "sEMG Based Movement Quantitative Estimation of Joins Using SVM Method." *IFAC*, vol. 47, no. 3, pp. 12311-12316, 2014.

[53] S. Thongpanja, A. Phinyomark, P. Phukpattaranont, and C. Limsakul, "Mean and median frequency of EMG signal to determine muscle force based on time-dependent power spectrum," *Elektronika ir Elektrotechnika*, vol. 19, no. 3, pp. 51-56, 2013.

[54] A. K. Bhoi, D. Phurailatpam, and J. S. Tamang, "Evaluation of Frequency Domain Features for Myopathic EMG Signals in Mat Lab," *Int. Journal of Engineering Research and Application*, vol. 3, no. 5, pp. 622-627, 2013.

[55] "Arduino - Introduction." *arduino.cc*.

Available: https://www.arduino.cc/en/Guide/ArduinoMega2560

[56] M. Nordin, and V. H. Frankel, "Biomechanics of the elbow," In *Nordin M and Franke l VH, eds: Basic biomechanics of the musculoskeletal system (3rd ed)*, Lippincott Williams & Wilkins, Philadelphia, 2001.

Paper

Paper

J. Wang, and W. Wichakool, “Artificial elbow joint classification using upper arm based on surface-EMG signal.” *Engineering Technologies and Social Sciences (ICETSS)*, pp. 1-4, 2017.

Artificial Elbow Joint Classification Using Upper Arm Based on Surface-EMG Signal

Jicheng Wang, Warit Wichakool
Department of Electrical Engineering, Faculty of Engineering
Prince of Songkla University, Hat Yai
Songkhla 90112, Thailand
wjc623064109@126.com, warit.wi@psu.ac.th

Abstract— **This paper proposes a method of elbow joint motions recognition using surface electro-myography (sEMG) signal for disable people with below-elbow amputation. It solves the situation that forearm without muscle cannot control forearm pronation. The pre-processing system processes sEMG signal to remove noise by soft threshold method, then denoising sEMG signal is sent to artificial neural network which trains features to recognize motions. The probability of this method activating 4 motions is 91.78% that was demonstrated by experimental results of recognition motions.**

Keywords— *surface-EMG signal, soft threshold method, signal processing, artificial neural network*

I. INTRODUCTION

Disable people cannot do daily work using forearm if they had a surgery of below-elbow amputation. Some prostheses have only mechanical component [1], which only can provide fixed motion for disable people, since existing artificial prostheses may not solve the problem well. In addition, Simon's system needs a long training time and costs relatively high [2]. Therefore, improvements can be done to make artificial prosthesis more friendly and affordable.

Nowadays, many researches are applied to control artificial arm, Fougner's model and Englehart's models of these researches, however, are not adequate to help disable people who have a surgery of below-elbow amputation [3]-[5], since the forearm without muscle cannot control forearm pronation [6]. Though a new method becomes quite necessary, few researches serve for disable people with below-elbow amputation.

Therefore, this research proposes a method of elbow joint motions control using sEMG signal for an artificial arm. The sEMG is non-invasive, painless mode, low cost and high usability, which uses non-invasive electrodes on the skin. The method uses elbow joint of extension motion of high-intensity force to control artificial arm of forearm pronation motion in my research. The users experience a short delay time before forearm pronation motion activated from elbow joint of extension motion.

In this research, the proposed method of relationship between motions of elbow joint and sEMG signals is feasible by back propagation neural network (BPNN).

II. THEORY

A. Motions

The detected motions in this research contain: 1. Elbow joint of flexion; 2. Elbow joint of extension; 3. Forearm supination; 4. Forearm pronation. There are 4 motions shown in Fig. 1.

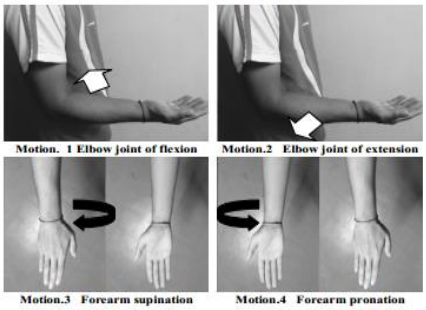

Fig. 1. Motions

In this research, the elbow joint of flexion and extension are activated by biceps of long head and triceps of long head. On the other hand, the detected muscles of forearm pronation and supination are biceps of long head and triceps of lateral head. Therefore, the detected sEMG signals have 3 channels: ch.1 biceps of long head; ch.2 triceps of lateral head; ch.3 triceps of long head. Besides, the common ground is used by the 3 channels as shown in Fig. 2.

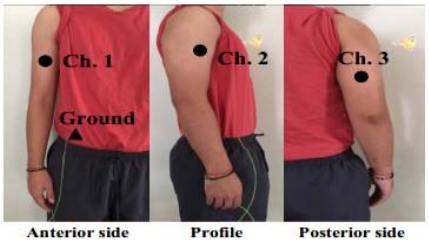

Fig. 2. Electrode position

B. Pre-processing

The structure of system, containing three components, is shown in Fig. 3. Specifically, the signal measurement acquires filtered sEMG signal. Pre-processing is used for denoising and smoothing signals. The classification is a recognition system for motion of intent interpretation.

The data of sEMG signals are acquired by Biopac MP36 Four Channel Data Acquisition System shown in Fig. 3. The setup of Biopac uses Biopac Student Lab (BSL) PRO (Version: 3.73, Build: 08.26.2008) [7]. Moreover, the sampling frequency is 1 kHz. A band-pass filter cuts noise from raw sEMG signal in the BSL PRO system. The band-pass filter is 30 Hz to 500 Hz.

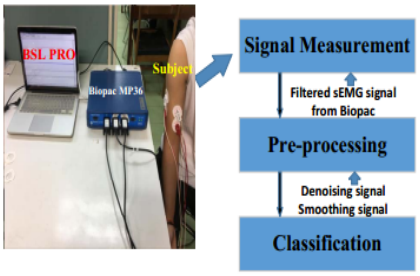

Fig. 3. System

The filtered sEMG signals are denoised and smoothed in Matlab. Denoising component utilizes soft threshold method and multi-resolution algorithm to remove noise from filtered sEMG signals. The soft threshold method recognizes the coefficients containing both signal and noise to isolate the signal by removing the noisy part from all coefficients. The soft threshold method is calculated by Eq. (1).

$$\omega_i^{Soft} = \begin{cases} 0 & |\omega_i| < \lambda \\ sign(\omega_i)(|\omega_i| - \lambda) & |\omega_i| \geq \lambda \end{cases}, \quad (1)$$

where ω_i is sequentially indexed coefficients based on multi-resolution algorithm shown in Fig. 4 and the λ is the value of threshold utilizing minimax thresholding method.

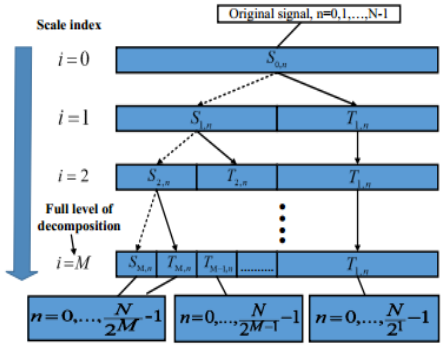

Fig. 4 The sequentially indexed coefficient ω_i

The sequentially indexed coefficient ω_i of multi-resolution algorithm has two components. They are approximation $S_{m,n}$ and detail coefficient $T_{m,n}$. The formulas are shown in Eq. (2) and Eq. (3).

$$S_{m+1,n} = \frac{1}{\sqrt{2}} \sum_k c_k S_{m,2n+k}, \quad (2)$$

$$T_{m+1,n} = \frac{1}{\sqrt{2}} \sum_k b_k S_{m,2n+k}, \quad (3)$$

where m is level of decomposition, n is number of sequence, scaling coefficient $\frac{1}{\sqrt{2}}c_k$ and wavelet function coefficient $\frac{1}{\sqrt{2}}b_k$ represents the low-pass and high-pass filter in the wavelet transform, respectively.

The minimax thresholding method outputs an extremum of minimum mean square error based on minimax algorithm. The formula in Matlab is shown in Eq. (4),

$$\lambda = 0.3936 + 0.1829 \times \frac{log(N_{smooth})}{log(2)}, \quad (4)$$

where N_{smooth} is length of coefficient ω_i.

Next, the denoised sEMG signals based on multi-resolution algorithm coefficient ω_i of backward reconstruction are smoothed by moving average algorithm. The level of smoothing is 100 for signal in1 kHz [8]. The moving average algorithm shown in Eq. (5) is used to remove abnormal value from signal.

$$x_{smoothing}(n) = \frac{1}{N} \sum_{i=0}^{N-1} x(n-i), \quad (5)$$

where N is level of smoothing.

C. Feature extraction

According to the kinesiology and the biomedical literatures [9], reports show that feature extraction is applied to recognize motion which is necessary. In order to detect each motion of sEMG signals clearly in time domain, the features of sEMG signals are analyzed as follows:

Mean absolute value of detected sEMG is used to reflect the information of a stimulated muscle of status. The formula is shown in Eq. (6),

$$x_{MAV} = \frac{1}{N} \sum_{n=1}^{N} |x_n|, \quad (6)$$

where N is the length of sEMG signal, n=1,2,3…,N, and x_n is sEMG signal of n sample.

The frequency of signal slope change is reflected by slope changes shown in Eq. (7),

$$x_{SC} = \frac{1}{N-2} \sum_{n=1}^{N-2} f_{n_{sc}}, \quad (7.1)$$

$$f_{n_{sc}} = \begin{cases} 1, & (x_n - x_{n-1})(x_n - x_{n+1}) > \lambda_{sc} \\ 0, & else \end{cases}, \quad (7.2)$$

where λ_{sc} is threshold. It is calculated with static sEMG signal.

Root mean square shown in Eq. (8) calculates the discreteness of sEMG data error,

$$x_{RMS} = \sqrt{\frac{1}{N} \sum_{n=1}^{N} x_n^2}. \quad (8)$$

Signal length shown in Eq. (9) is the signal length of N samples. This feature interprets amplitude of sEMG signal and frequency,

$$x_{SL} = \frac{1}{N-1}\sum_{n=1}^{N-1}|x_{n+1} - x_n|. \quad (9)$$

Zero crossing reflects the frequency of sEMG data through the zero,

$$x_{ZC} = \frac{1}{N-2}\sum_{n=1}^{N-2} f_{n_{zc}}, \quad (10.1)$$

$$f_{n_{zc}} = \begin{cases} 1, & x_n x_{n+1} < 0, |x_n - x_{n+1}| > \lambda_{zc} \\ 0, & else \end{cases}, \quad (10.2)$$

where λ_{zc} is threshold. It is calculated with static sEMG signal.

D. Classification

In this research, the classification recognizes four motions. Classification uses back propagation network (BP network). Steepest descent method has factor of momentum shown in Eq. (11) and it is used to find a local minimum. It takes steps proportional to the negative of the gradient or approximate gradient of the function at the current point. Error signal propagates backward in the classifier.

$$\Delta\omega(n) = -\eta(1-\alpha)\nabla e(n) + \alpha\Delta\omega(n-1), \quad (11)$$

where ∇e(n) is gradient.

In addition, it has 2 classifiers as shown in Fig. 5. The proposed method does not use the original function of muscle to activate the forearm pronation. In this case, it can be used for the daily life of disable people, however, some special motions exert a little impact on classifier 2. For example, the triceps of lateral head is also contracted while users do push-up. In classification system, the users turn on or off classifier 2, depending upon corresponding situations.

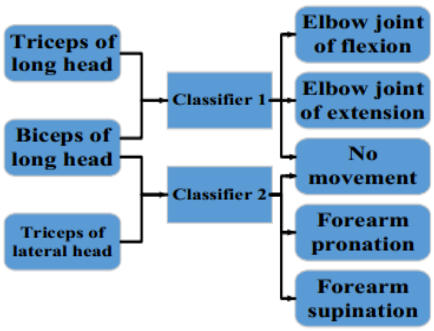

Fig. 5. Classification system

E. Experiment

The experiment is performed by 8 healthy subjects shown in Table 1. All of subjects use their right upper limb in this experiment though two of them are left handedness. The total performing times are 30 for each motions, 20 times are used to train the classifier and 10 times are utilized to test.

The 4 motions are detected as following: 1. The elbow joint of flexion is detected from 0°to 150°where the 0°is arm straight; 2. The elbow joint of extension is detected from 150°to 0°; 3. The forearm pronation is detected from 0°to 225°where the 0°is arm straight with palm up; 4. The forearm supination is detected from 180°to 0°.

Furthermore, the 8 healthy subjects are asked to perform the 4 motions following the experiment requirements within 3 seconds. It means that normally onset of motions is activated while time reaches 2 seconds and termination is activated as the time is 4 seconds.

TABLE I. SUBJECTS

Subject	Age	Gender	Height	Weight	Handedness
A	30	Female	170 cm	55 kg	L (left)
B	23	Female	150 cm	50 kg	R (right)
C	25	Female	163 cm	40 kg	R
D	28	Female	160 cm	49 kg	R
E	24	Male	175 cm	72 kg	L
F	25	Male	170 cm	65 kg	R
G	24	Male	182 cm	78 kg	R
H	25	Male	170 cm	65 kg	R

III. RESULTS AND DISCUSSIONS

The raw sEMG has a huge electric noise. The electrical noise is reduced in smoothing sEMG signals, which means that the smoothing sEMG signal is more compatible for recognition system. On the other hand, in order to compare the smoothing component shown in Table 2, average amplitudes of Fast Fourier Transform (FFT) shown in Eq. (12) of weaker muscle are utilized. Since, the forearm supination is activated by ch.1 of biceps of long head in this research, multiple of the smoothing sEMG signal between forearm supination and static state is bigger than sEMG signal without smoothing. It means that the smoothing sEMG signal of contracted muscle outputs more obvious feature set than the sEMG signal without smoothing.

$$X_{average} = X_{Amplitude}(k), \quad (12.1)$$

$$X_{Amplitude}(k) = \left|\sum_{j=1}^{N} x(j)\omega_N^{(j-1)(k-1)}\right|, \quad (12.2)$$

where $\omega_N = e^{(-2\pi i)/N}$ is N_{th} an root of unity.

TABLE II. THE COMPARISON OF SMOOTHING COMPONENT

Average amplitude of FFT for smoothing sEMG signal			
Channel	**Ch.1**	**Ch.2**	**Ch.3**
Forearm supination / static state	3.274334	1.035779	1.087946
Average amplitude of FFT for sEMG signal without smoothing			
Channel	**Ch.1**	**Ch.2**	**Ch.3**
Forearm supination / static state	2.199487	1.905546	2.282743

The accuracy results of different window size compared via the previous experiment is shown in Fig. 6.

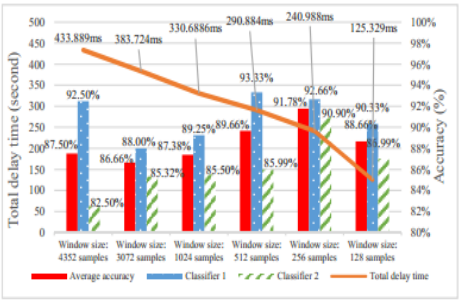

Fig. 6. The accuracy of different window size

In Fig. 6, 125ms is the best processing time when the window has 128 samples. The highest accuracy is 91.78% while window size is 256 samples. Actually, human cannot feel a time delay of less than 100 ms [10], nevertheless, the acceptable time interval of delay is up to 300 ms to 400 ms [11]-[13]. Hence it is more appropriate for disable people who just feel a very short processing time as the window size is 256 samples rather than 128 samples.

The accuracy results of each healthy subject for each motion are shown in Table 3 and the window size is 256 samples. It shows that the independent test accuracy is very high while the training dataset only comes from one healthy subject. The universal test accuracy is available for the 8 healthy subjects, which signifies that the proposed method can be applied to male and female.

TABLE III. ACCURACY RESULTS FOR EACH SUBJECT AND MOTION

Subject	Elbow joint of flexion	Elbow joint of extension	Forearm pronation	Forearm supination
A	97.63%	96.53%	96.60%	95.60%
B	95.66%	95.78%	94.03%	95.33%
C	96.25%	96.20%	95.66%	96.85%
D	96.78%	96.33%	96.25%	96.60%
E	97.78%	96.63%	97.33%	97.75%
F	97.03%	96.55%	95.98%	96.33%
G	97.93%	96.25%	94.90%	95.15%
H	96.66%	95.33%	94.25%	96.25%

Finally, the proposed method is feasible for disable people with below-elbow amputation. Furthermore, according to the result analysis, in the situation of very low force or muscle contracting time less than 100ms, motions cannot be identified, which result in failing to extract an obvious feature set. Besides, the processing time processed on computer is reduced with the increasing of computer performance. It means that users feel a very short time delay before prosthesis motion begins based on the performance of computer.

IV. CONCLUSION

In this research, the proposed method solves forearm without muscle to control forearm pronation based on sEMG signal. The proposed system reduces electric noise by pre-processing system. The class of motions is analyzed utilizing 5 features in BP network. From the experimental results, the proposed method exhibits a high accuracy through testing 8 healthy subjects in ideal condition. The system can become robust with more datasets of patients. Finally, we can improve the method for the future clinical use.

REFERENCES

[1] A. Agarwal, "Upper Limb Prosthesis," in *Essentials of Prosthetics and Orthotics*. New Delhi, India: Jaypee Brothers Publishers, 2013, pp. 57-64.

[2] A. M. Simon, B. Lock, K. Stubblefield, and L. Hargrove, "Prosthesis-guided training increases functional wear time and improves tolerance to malfunctioning inputs of pattern recognition-controlled prostheses," in *Proc. Myoelectric Controls Symp.*. Fredericton, NB, Canada, 2011.

[3] A. Fougner, Ø. Stavdahl, P. J. Kyberd, Y. G. Losier, and P. A. Parker, "Control of Upper Limb Prostheses: Terminology and Proportional Myoelectric Control—A Review," *IEEE Trans. Neural Systems and Rehabilitation Engineering*, vol. 20, no. 5, Sep. 2012, pp. 663–677.

[4] P. A. Parker, K. B. Englehart, and B. S. Hudgins, R. Merletti and P. A. Parker, Eds., "Control of powered upper limb prostheses," in *Electromyography: Physiology, Engineering and Noninvasive Applications*, vol. 11. John Wiley & Sons, 2004, pp. 453–475.

[5] P. A. Parker, K. B. Englehart, and B. S. Hudgins, "Myoelectric signal processing for control of powered limb prostheses," *J. Electromyogr. Kines*, vol. 16, no. 6, 2006, pp. 541–548.

[6] Hall, Susan. "The Biomechanics of the Human Upper Extremity," in *Basic biomechanics*, McGraw-Hill Sixth Education. New York: McGraw-Hill, 2011, pp. 185-228.

[7] *BIOPAC® System, Inc. | System, THE GOLD STANDARD FOR LIFE SCIENCE INSTRUCTION*, BIOPAC System, Inc., Goleta, CA, 2015. [Online]. Available: https://www.biopac.com/wp-content/uploads/MP36-MP35-P45.pdf

[8] *BIOPAC® System, Inc. | Application Notes, 165-Integrated EMG, ASSOCIATED FILES*, BIOPAC System, Inc., Goleta, CA, 2015. [Online]. Available: https://www.biopac.com/wp-content/uploads/app165.pdf

[9] Kamen, Gary. "Electromyographic Kinesiology," in *Research Methods in Biomechanics*, Robertson, DGE et al. Champaign, IL: Human Kinetics Publ., 2004.

[10] Farrell, Todd Richard. "Multifunctional prosthesis control: The effects of targeting surface vs. intramuscular electrodes on classification accuracy and the effect of controller delay on prosthesis performance," Diss.. Evanston, IL: NORTHWESTERN UNIVERSITY, 2007, pp. 83-84.

[11] K. Englehart and B. Hudgins. "A robust, real-time control scheme for multifunction myoelectric control," *IEEE Trans. Biomed. Eng.*, vol. 50, no. 7, Jul. 2003, pp. 848–854.

[12] Englehart K, Hudgins B, Chan AD. "Continuous multifunction myoelectric control using pattern recognition," *Technol Disabil. 15(2)*, 2003, pp. 95-103.

[13] Hefftner G, Zucchini W, Jaros GG. "The electromyogram (EMG) as a control signal for functional neuromuscular stimulation, I: autoregressive modeling as a means of EMG signature discrimination," *IEEE Trans. Biomed. Eng., 35(4)*, 1988, pp. 230-237.

VITAE

Name Jicheng Wang
Student ID 5810120003
Educational Attainment

Degree	Name of Institution	Year of Graduation
Bachelor of Engineering	Jiangxi University of Science and Technology	2014

List of Publication

1. International Publication

J. Wang, and W. Wichakool, "Artificial elbow joint classification using upper arm based on surface-EMG signal." *Engineering Technologies and Social Sciences (ICETSS)*, pp. 1-4, 2017.